BRNO UNIVERSITY OF TECHNOLOGY

VYSOKÉ UČENÍ TECHNICKÉ V BRNĚ

CENTRAL EUROPEAN INSTITUTE OF TECHNOLOGY BUT

STŘEDOEVROPSKÝ TECHNOLOGICKÝ INSTITUT VUT

ADVANCED PREPARATION OF INORGANIC (CERAMIC) PARTICLES AND NANOSTRUCTURES

POKROČILÉ PŘÍPRAVY ANORGANICKÝCH (KERAMICKÝCH) NANOČÁSTIC A NANOSTRUKTUR

DOCTORAL THESIS
DIZERTAČNÍ PRÁCE

AUTHOR — **Ing. Eva Šťastná**
AUTOR PRÁCE

SUPERVISOR — **doc. Ing. Klára Částková, Ph.D.**
ŠKOLITEL

BRNO 2021

Abstract

An electrospinning process was used for bioactive nanofibrous structures preparation. Neat polycaprolactone nanofibres and polycaprolactone nanofibres containing hydroxyapatite nanoparticles were successfully prepared via electrospinning and characterized using scanning electron microscopy. Mechanical properties of the nanofibres were analyzed using uniaxial tensile strength test. Results of the testing showed strong influence of the nanofibres direction alignment and nanoparticles presence on the mechanical properties of the prepared structures. The direction alignment contributed to higher elastic modulus and failure stress regardless the presence of the hydroxyapatite nanoparticles in the structure. However, the direction alignment considerably reduced failure strain of the structure. An interesting phenomenon occurred by the composite nanofibres – the influence of the hydroxyapatite particles was more distinct by the random fibres (they worsened failure strain and failure stress of the random composite fibres) but the hydroxyapatite particles did not have such strong effect on the parallelly aligned fibres.

The samples were then modified by surface low-temperature plasma treatment to improve biological properties of the nanofibres. Change of the nanofibres surface characteristics was examined by contact angle measurement by sessile drop method and by XPS spectroscopy. The contact angle measurement showed that the plasma treatment considerably increased structures hydrophilicity – was unmeasurable. The XPS analysis explained the effect of the plasma treatment on microscopical scale – the plasma treatment had affected only polymer constituent of the treated structure, the hydroxyapatite nanoparticles remained intact.

Selected prepared structures were biologically tested. Test in simulated body fluid proved high bioactivity of the polycaprolactone/hydroxyapatite composite nanofibres through precipitation of calcium phosphates phases on the composite structures. Following *in-vitro* tests using living cell cultures (ISO 10993-5 and WST-8 test) proved beneficial influence of the hydroxyapatite in the structure and of the surface plasma treatment when bioactivity of the plasma treated composite structures increased 1.5 times compared to the neat as-spun polycaprolactone fibres.

Key words: electrospinning, nanofibres, polycaprolactone, hydroxyapatite, plasma treatment

Abstrakt

Elektrostatické zvlákňování bylo použito pro příprvu čistě polykaprolaktonových nanovláken a kompozitních nanovláken na bázi polykaprolaktonu s hydroxyapatitovými nanočásticemi. Připravená vlákna byla analyzována za použití rastrovací elektronové mikroskopie. Mechanické vlastnosti vláken byly určeny prostřednictvím zkoušky jednoosým tahem. Testy prokázaly silnou závislost mechanických vlastností vláken na jejich směrovém uspořádání a fázovém složení (především přítomnosti hydroxyapatitových částic). Směrové uspořádání vláken přispělo k výraznému zlepšení napětí při přetržení a celkové tažnosti. Zajímavý jev byl pozorován v případě kompozitních vláken– hydroxyapatitové částice zhoršily mechanické vlastnosti neuspořádaných vláken (napětí při přetržení a celkovou tažnost), ale vliv částic nebyl tak patrný v případě směrově uspořádaných vláken.

Povrchové vlastnosti vláken byly modifikovány prostřednictvím nízkoteplotní plazmy. Změny povrchových vlastností vláken byly analyzovány pomocí měření kontaktního úhli a XPS analýzy (rentgenové fotoelektronové spektroskopie). Měření kontaktního úhlu ukázalo výrazný vliv plazmového opracování na povrchovou smáčivost vláken, kdy kontaktní úhel byl zcela neměřitelný. Výsledky analýzy ukázaly vliv plazmového opracování struktur na mikroskopické úrovni – plazmové opracování ovlivnilo pouze polymerní složku vláknitých struktur, zatímco hydroxyapatitové částice nebyly ovlivněny vůbec.

Na vybraných strukturách bylo provedeno několik biologických zkoušek. Test v simulovaném tělním roztoku prokázal bioaktivitu kompozitních (polykaprolaton/hydroxyapatit) nanovláken prostřednoctví precipitace fází na bázi fosforečnanů vápenatých na povrchu kompozitních struktur. Následné in-vitro buněčné testy (dle normy ISO 10993-5 a WST-8 test) prokázaly významný pozitivní přínos hydroxyapatitových částic ve vláknitých strukturách, stejně jako kladný vliv plazmového opracování, kdy kompozitní oplazmovaná vlákna vykazovala 1,5násobnou bioaktivitu v porovnání s neplazmovanými čistě polykaprolaktonovými vlákny.

Klíčová slova: Elektrostatické zvlákňování, nanovlákna, polykaprolakton, hydroxyapatit, plazmové opracování

Bibliographic citation

ŠŤASTNÁ, Eva. *Pokročilé přípravy anorganických (keramických) nanočástic a nanostruktur.* Brno, 2021. Dostupné také z: https://www.vutbr.cz/studenti/zav-prace/detail/136691. Dizertační práce. Vysoké učení technické v Brně, Středoevropský technologický institut VUT, Středoevropský technologický institut VUT. Vedoucí práce Klára Částková.

Declaration

I declare that this doctoral thesis was worked out on my own using mentioned literature and under supervision of above-named supervisor.

In Brno on ……

……

Ing. Eva Šťastná

Acknowledgements

I would like to thank my supervisor doc. Ing. Klára Částková, PhD. for her support, valuable advices and professional guidance. I would also like to thank all my colleagues from CEITEC and CEITEC Nano infrastructure for making a great scientific and friendly environment for my research. And least but not last, I would love to thank my husband and my whole family for their never-ending love, support and patience during my studies.

Contents

1 Introduction

Modern medicine is constantly developing every day. In the past, the only task of the doctors was saving bare life of the patient. Nowadays, also quality of the patient‘s life plays an important role in the medical treatment. Therefore, the medicine is closely connected with the latest research to implement new procedures, that are less invasive (and hence painful) and more efficient, to the common praxis. The research focuses on both new materials and new technologies.

One of the most dynamic fields of study is tissue engineering that focuses on treating large wounds (both chronic and injuries) that our body cannot heal itself. The human body has a great ability of regeneration, but it has its limits – if there is a damage larger than approximately 5 mm, our body needs help for full recovery. The implants that are used as the damaged (or missing) tissue replacement, have to provide mechanical support for the surrounding tissue and protect the wound from the surrounding environment (as protentional source of infection). The implant material also must not cause any inflammation reaction in the body.

In the past, people used for example metal plates for bone replacements and there are also known attempts to replace the damaged skin with animal (usually pig) tissue. The modern medicine tries to use implants, so called scaffolds, that are structurally and mechanically closed to the human tissues. The scaffolds must fulfill more requirements than just biocompatibility – they should actively support the healing process and they should be bioresorbable. It means that the gradually dissolve in the body environment during the healing process and they are replaced by the new tissue without any residues left in the body.

To fulfil the requirements mentioned above, the researchers are trying to mimic the natural tissues in the means of structural, chemical and phase composition. New methods of synthesis, production and post-production treatment are developed to reach the goals. Considering the fibrous structure of all the body tissues, electrospinning is a promising method for scaffold production. The process is based on the interaction of a liquid precursor with a high electrostatic voltage resulting in a continuous fiber. Since the main requirement for the electrospinning precursor are liquid state and electrical conductivity, the method is very versatile and allows production of a wide variety of fibrous structures.

This thesis is focused on preparation of a bioactive fibrous structure with potential utilization in bone tissue engineering. It describes optimization of the precursor composition, electrospinning parameters and surface treatment, analysis of the prepared structures, mechanical and biological tests.

2 Theoretical background

2.1 Human body tissues and their regeneration

The body mass is formed mostly from tissues – soft tissues (e.g. skin or muscles) and hard tissues (bones). The hard tissues mechanically support the body and the soft tissues define body shape, enable its movability and constitute all the organs. The tissues consist of from water, proteins, inorganic substances (salts) and the living cells. The ratio of the constituents differs among various tissues. Considering the topic of this thesis, this chapter will be focused mostly on the bone tissue.

2.1.1 Bone tissue

Bones are mineralized connective tissue. Their main role in the body is mechanical support and load of mechanical tension. It also protects the inner organs from mechanical damage, serves as a calcium and phosphorus deposit and finally, there is the bone marrow inside the bones where blood corpuscles are produced that are important for autoimmune system. The correct bone function is based on rather complicated macro- and microstructure as can be seen in Figure 1 where structure of a long bone is displayed. [1]

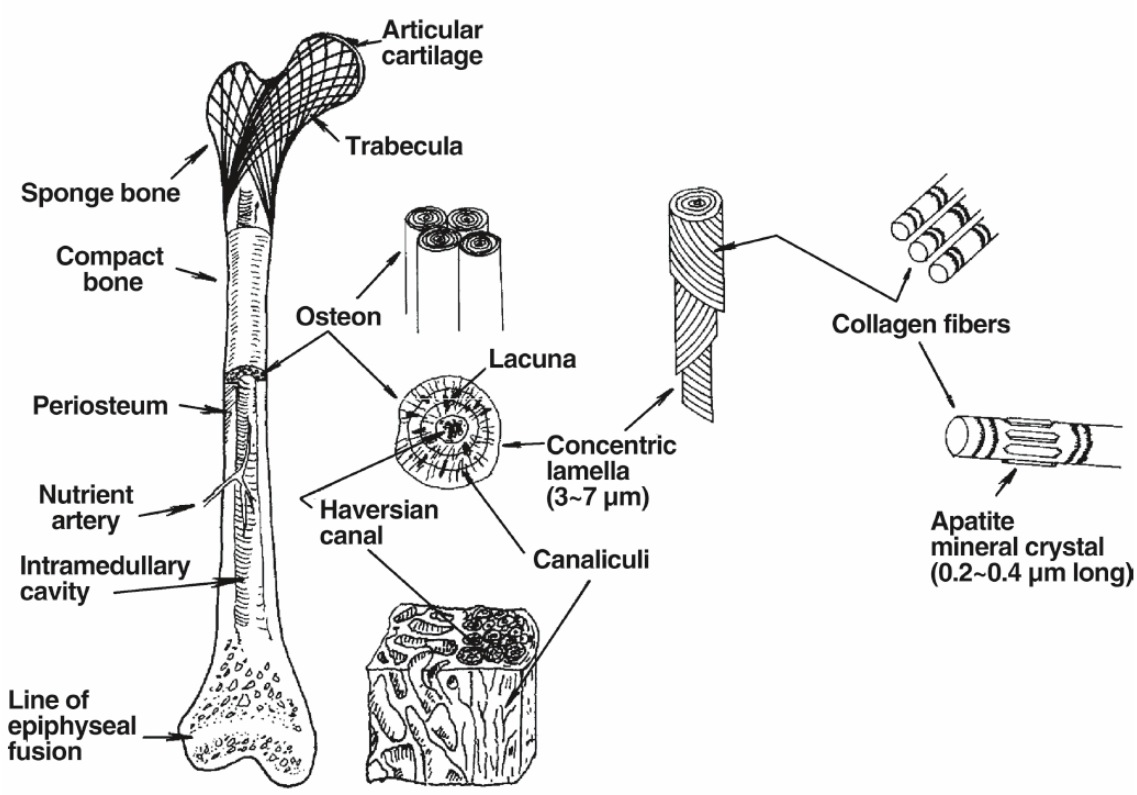

Figure 1 Structure of a long bone [1]

Bones are made from 22 wt.% of the organic (fibrous) matrix, which is formed mainly from collagen. The rest of the bone mass is created from inorganic substances (60 – 70 wt.%) and water (10 wt.%). The inorganic element content is in Table 1. [1]

Table 1 Content of inorganic elements in the bone tissue

Element	Ca	P	Na	Mg	K	F	Cl	Sr, Zn…
Wt.%	34.80	15.20	0.90	0.72	0.03	0.03	0.13	Trace amount

There are two types of bone tissue structures – lamellar and trabecular. The lamellar tissue forms the middle part of the long bones. The outer part is formed from osteons – cylindrical structures that are aligned along the bone. The osteons are formed from lamellae (from collagen fibres) arranged into circles. The collagen fibres have 1 – 4 µm in diameter and their submicroscopic structure is made from fibrils – the smallest collagen molecules bundles that are able to be distinguished under a light microscope. Submicroscopic inorganic crystals are placed among the fibrils. They are usually 20 – 40 µm long and 1 – 4 µm wide needles that form a continuous mesh in the osteons. Inorganic crystals are chemically based on calcium phosphates and their structure is close to hydroxyapatite [$Ca_{10}(PO_4)_6(OH)_2$]. There are also substitutional ions (e.g. fluorides, carbonates or hydroxyls) placed in the inorganic crystals. There is Harversian canal inside each osteon where the vessels (that transport nutrients into the bone tissue), and nerves are placed. Osteons surround the marrow cavity where the bone marrow is located. The other type of bone tissue is trabecular bone (cancellous, spongy) which is located at the ends of the long bones and is important for bone regeneration process. The spongy bone is made from 3D fibril structure based on collagen. The spongy bone can be changed into the long bone by activity of the bone cells. This process is crucial for bone regeneration and it will be further explained in the following chapters. [1]

Bone cells

Bone cells are important for regeneration of the bone tissue. The bone regeneration does not take place only after an injury, but it goes on during the whole life. Three types of cells are important for the bone regeneration – osteoblasts, osteoclasts and osteocytes. An important thing for the whole regeneration process is balance between activity of the osteoclasts and osteoblasts. [2]

Osteoclasts are large multinucleus cells (100 µm) with many protrusions on their surface that are in contact with the bone surface. The edges of the osteoclasts are attached to the bone surface and using the protrusions, they etch the inorganic constituents of the bone and hence create space for the new bone tissue. The etching is enabled by simultaneous excreting of hydrogen cations, chloride anions and some specific enzymes. The substances created by the etching are absorbed by the osteoclasts or penetrate through the cells to the surrounding body environment. The scheme of the chemical processes taking place at the osteoclast-bone interface are displayed in Figure 2. [2]

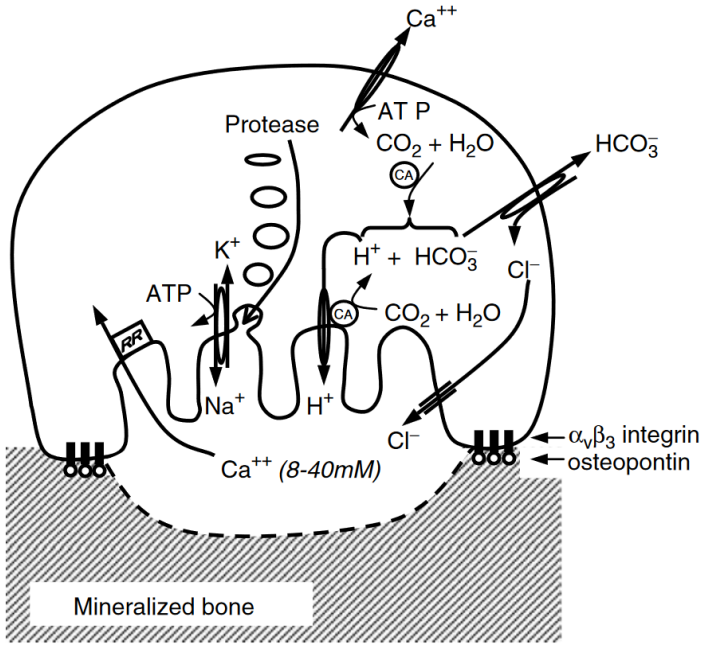

Figure 2 Activity of an osteoclast [2]

Osteoblasts create bone tissue, they have only one nucleus and they cannot proliferate. The osteoblasts are located only on the bone surface, where they are organized in a single layer. Osteoblasts secrete the substances crucial for bone matrix formation (especially collagen and other proteins) and their activity supports bone mineralization. After the bone matrix formation, some osteoblasts are left in the matrix and they change into osteocytes and further participate in the bone metabolism. This transformation can be reversible. [2]

The last (already mentioned) bone cells type are osteocytes formed from the osteoblasts, and they are the most common bone cell type. Today it is believed that the osteocytes control the activity of osteoclasts and osteoblasts by receiving mechanical and hormonal signals. The osteocytes are able to detect small bone damages caused by long time stress load (fatigue) and changes in stress load during the bone remodulation. Osteocytes react to these signals by regulation of the osteoclasts and osteoblasts activity. [2]

2.1.2 Bone regeneration and remodulation

Bleeding always occurs as a consequence of a bone injury – vessels nourishing the bones are damaged and the bone usually breaks through the skin. The first body reaction to the injury is creation of a blood clot that prevents body from further bleeding. The next step is removal of the damaged tissue – it is the role of mastocytes and histiocytes (a type of leukocytes). This phase starts already after 8 hours after the injury. Mastocytes and histiocytes focus on the damaged periosteum and the surrounding tissue at first. Then they work along the whole injured bone and after several days they are active only around the place of the injury again. [1]

At the same time, fibroblasts and osteogenic cells (from the periosteum) migrate towards the place of the injury. These cells proliferate intensively and create a callus – a tissue made from collagen fibres that fixate the damaged edges of the bone. It enables their connection and renovation. New blood vessels are created in the callus that nourish the present cells during the first phase of the bone healing and then they can be ossificated and transformed into the new bone matrix. [1]

As soon as the damaged edges of the bone are connected, the present osteoblasts start to calcify the callus and turn it into trabeculae – the basic cancellous bone unit. The osteoclasts start to create canals both in the dead and the new formed bone that enables the formation of the vessel system and then the osteon. The callus is gradually absorbed and a new bone tissue completely replaces it after approximately four weeks. Simultaneously, with the bone surface process, there is a healing process directing from the marrow cavity. The healing process of the marrow cavity is similar to the bone surface's healing process, but it is faster thanks to the naturally generous blood supply. The appearance of the bone healing process is displayed in Figure 3. [1]

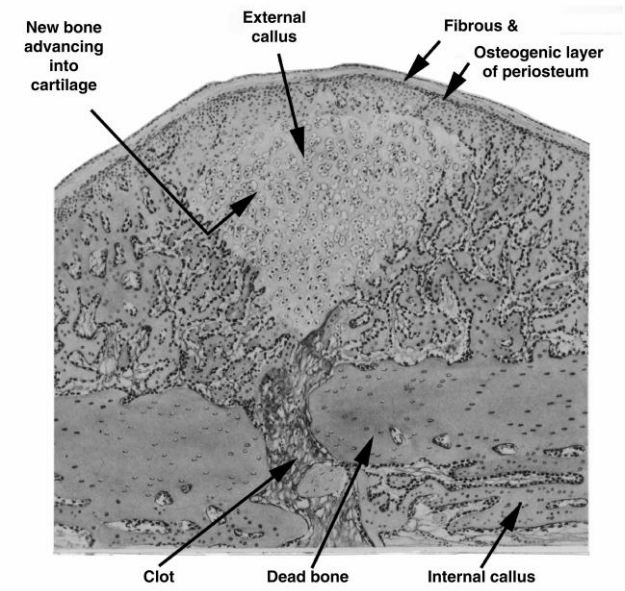

Figure 3 A bone injury during the healing process [1]

As soon as a strong connection of the damaged bone edges is ensured, the remodulation phase begins. There are several theories why the cancellous bone is transformed into the lamellar bone. The reliably proven theory is based on the cells activity's biochemical regulation by various specific proteins (bone morphogenetic proteins). The bone transformation into the lamellar type usually takes two weeks, so that the whole bone healing process is usually finished after six weeks from the injury. The timing of the bone healing process is in Figure 4. [1]

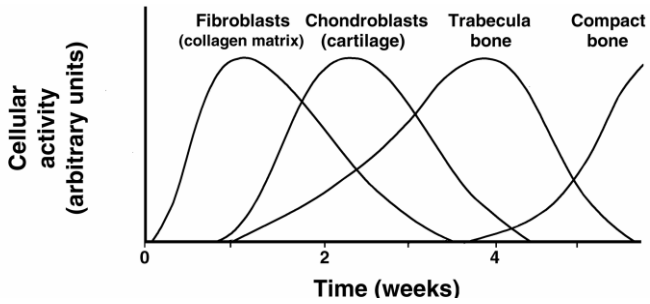

Figure 4 Timing of the bone healing process [1]

2.2 Bone implants and biocompatible materials

Sometimes the injuries are so vast that the body itself is not able to complete the healing process and it needs some outer help. Therefore, so called grafts or scaffolds are used as a healing support. The grafts are implants from the same type of tissue as the injured one. Autografts are implants that come from the patient's body, and allografts are taken from a donor. Application of the grafts is beneficious for their natural biocompatibility, but it requires additional (painful) surgery during the taking of. Moreover, in the case of allografts, there is always a risk of autoimmune reaction or disease transfer. [3] Xenografts (when the donor is another species, e.g. pig) are also known, but their long-term compatibility with the human body is speculative. [4] Therefore, artificial implants are looked for.

Artificial implants are well known for a long time – already in ancient Macedonia, Greek and Egypt the doctors used metal plates for treating large (bone) injuries. [5] Their motivation was to preserve the mechanical properties of the injured bone and (empirically found out) antibacterial properties of the metal. The modern tissue engineering (as a scientific field examining relationship between chemistry, phase composition, structure and body response) started to develop in 1970's in USA when experiments with bone implants on mice were done. Although the first experiments were unsuccessful, the field of study was established, and more and more doctors and scientists started to explore the best way for tissue healing support. [6]

There are several requirements on the modern (bone) scaffolds. Besides the biocompatibility there are characteristics supporting new bone tissue formation. Osteoinduction means a chemical stimulation of the mesenchymal stem cells to differentiate into the bone-forming osteoblast cells. This transformation is supported by a proper concentration of growth factors in the environment and the growth factors can be entrapped in the pores of the scaffold. Osteoconduction is a tendency of the new bone growth onto the scaffold surface or into the scaffold volume. The osteoconduction is given mostly by the micro- and macrostructure of the scaffold – open porosity helps a lot. Osseointegration is the material's ability to form a chemical bond with the bone tissue (without the formation of fibrous tissue). Osseointegration is given by physical properties of the implant material – wettability, nano topography, micro porosity and hemocompatibility. [7]

Mechanical properties of the scaffolds should be close to the mechanical properties of the natural tissues. Otherwise viability of the scaffold and the surrounding tissue would be endangered. A typical example of a large difference in the scaffold's mechanical properties and the surrounding tissue is metal (titanium) bone implants. The titanium is considerably tougher than natural bone, and consequently loss of inorganic substances occurs at the surrounding tissue and bone loses its mechanical properties. Hence it is prone to further mechanical damage and injury. [7]

2.2.1 Implant materials

Metals

Titanium is a typical example of a widely used material for bone and joint implants. At first it was believed that titanium is bioinert material (thanks to the passivation process on its surface) that does not cause any inflammation in the body environment. However, stress and wear can enhance the corrosion rate and cause the formation of toxic substances on the metal-tissue interface. [8]

Ceramics

One of the first widely used ceramic implant materials was pure alumina (in the 1970s). It was used mostly for the hip joint prostheses and the teeth replacements thanks to its significant friction and wear resistance. Its brittleness and low compressive strength limited wider use. [9] Zirconium oxide is an alternative for brittle alumina implants. Thanks to the possible phase transformation of the (yttrium doped) zirconia, the material is tougher and stronger than alumina. However, its wear resistance is much lower than the wear resistance of the alumina. [1]

Glass-ceramics are a special category of inorganic materials. The production process was developed already in the 1960s, but tissue engineering's potential began to be examined some decades later. The glass-ceramics' main characteristics are controlled crystal precipitation from the glass phase to reach fine and uniform grain size. The chemical composition of the glass-ceramics is more complicated than the composition of the ceramics previously mentioned. Two compositions have been proven as suitable for implantations: SiO_2–CaO–Na_2O–P_2O_5 (Bioglass®) and Li_2O–ZnO–SiO_2 (Ceravital®). [1] [10] The main advantage of glass-ceramics is their ability to chemically react with the surrounding tissue and create a chemical bond.

Calcium phosphates are inorganic materials based on calcium and phosphor oxides that try to mimic the bone inorganic phase's chemical composition. The calcium phosphate research aims to develop a scaffold that would mimic the chemical and phase composition of the bone, induce the ossification, and gradually dissolve during the new bone tissue formation. The dissolution rate is directly dependent on the Ca/P ratio – hydroxyapatite with Ca/P ratio 1.67 is less soluble than β-tricalcium phosphate with Ca/P ratio 1.5 (see the calcium phosphates commonly studied for tissue engineering in Table 2). It is obvious that the overall solubility of the scaffold can be designed by the phase composition of the scaffold. The solubility can be further influenced by some substituents such as Mg^{2+}, Si^{4+} or Sr^{2+}. [11]

Table 2 List of common calcium phosphates studied for tissue engineering utilization [11]

Calcium phosphate	**Formula**	**Ca/P molar ratio [-]**
Hydroxyapatite	$Ca_{10}(PO_4)_6(OH)_2$	1.67
α-Tricalcium phosphate	α -$Ca_3(PO_4)_2$	1.5
β-Tricalcium phosphate	β -$Ca_3(PO_4)_2$	1.5
Dicalcium phosphate dihydrate	$Ca(HPO_4).2H_2O$	1
Tetracalcium phosphate	$Ca_4(PO_4)_2O$	2

Polymers

Natural polymers are considered as renewable substances and they can be derived directly from living tissues (animal or plant) or they can be produced artificially. Their biggest advantage is their guaranteed biocompatibility and easy prognosis of their degradation rate in the human body. A typical natural polymer that is easily produced on form of fibres is for example alginate (a polysaccharide derived from ocean algae). Fibrous structures from alginate are promising materials for tissue engineering or targeted drug release. Another natural polysaccharide suitable for fibrous structures preparation is chitosan, promising for skin and bone scaffolds or targeted drug release. Last but not least from natural polymers are hyaluronic acid and collagen. Both materials seem to be suitable for tissue engineering (hyaluronic acid is intended especially for skin regeneration), targeted drug release, or designed timing of the scaffold resorption in the human body. [12] [13] [14]

Polycaprolactone (PCL), poly(lactic-co-glycolic) acid (PLGA) or polyvinyl alcohol (PVA) are typical examples of artificial polymers examined as candidates for tissue engineering. PCL has the lowest

degradation rate in the human body from named polymers. It can be beneficial in the mean of gradual scaffold degradation or gradual release of molecules bond to the PCL chain. Vice versa, PVA has a high degradation rate in the human body that can be used in targeted drug release or designed timing of the scaffold degradation rate. The low contact angle is one of the most significant disadvantages of artificial polymers (especially PCL and PLGA). Hydrophobicity of the material limits cells from adhesion (and further proliferation). It can be compensated by presence of a natural polymer in the structure (for example easily available gelatin). On the contrary, their price is much lower compared to the natural polymers. [14]

2.2.2 Implant structures

Dense materials

The first generation of bone implants was based on metals and ceramics in their dense state. The main motivation was to replace the missing tissue and handle its mechanical support role. The only requirement on their properties was long-term biocompatibility (no toxic substances were produced on the implant-tissue interface). However, the development of the implant materials went forward and materials able to make a chemical bond with the surrounding tissues were found.

Porous materials

Effective performance of the biocompatible and bioactive materials is not conditioned only by their chemical and phase composition but also by their microstructure and morphology. The scaffold surface must be rough enough to enable movement, adhesion and proliferation of the cells. Open porosity of the scaffold is crucial for the successful ingrowth of the cells. The pores should be at least 100 µm, optimum is 200 – 350 µm. The pores should be interconnected by windows with diameter of 100 µm. The described structure can be prepared by various methods suitable for different materials. [15] [16]

There are several production techniques of porous ceramic materials – selective etching of a dense material [17], foaming of a ceramic suspension [15], stereolithography rapid prototyping (3D printing) [18] or emulsion freeze-drying. [19]

Fibrous materials

One of the biggest advantages of the fibrous structures is their similarity to the living tissues' natural structure. Another advantage is the penetrability of the fibrous structure for the cells and chemical substances. The most suitable materials for fibres production are polymers (regardless of the production technology).

Polymer fibres seem suitable for the regeneration of all types of the tissues, and inorganic fibres are perspective for hard tissues regeneration. Typical inorganic materials for bone scaffolds are substances based on calcium phosphates, bioactive glasses (bioglasses) and ceramic glasses. Nowadays production technology of glass nanofibres based on silicon is well described. [20] The bioglass nanofibres support cell proliferation that is (according to in-vitro tests) faster than on PCL fibres or dense bioglass. Fabrication of fibres based on hydroxyapatite, fluorohydroxyapatite or silicon oxide is already also known. When a fibrous inorganic material is produced, a polymer must be added to the initial solution as a carrier. It is typically polyvinyl pyrrolidone or polyvinyl butyral. The carrying polymer is removed from the resulting structure by heat treatment and pure inorganic fibres are prepared. Inorganic nanofibres can support cell proliferation and migration into the scaffold, but they are brittle,

limiting their utilization in tissue engineering. Therefore, new approaches for combination of bioactivity of the inorganic materials and mechanical properties of the polymers are searched nowadays. [14]

Very promising are composite fibres with polymer matrix and inorganic (ceramic) filling. Besides the suitable mechanical properties, the composite fibrous scaffold mimics the structure of ECM that consists of collagen fibres with hydroxyapatite nanoparticles. Another effect of the composite fibrous structure can be acceleration of new vessels creation during the tissue regeneration. The biggest challenge of composite fibres preparation is complicated production process. Considering planned fibres thickness of $10^2 – 10^3$ nm, the ceramic particles can have dimensions in the range of 10^2 nm maximum. Such small particles tend to agglomerate that are nearly impossible to disperse in a polymer solution. The presence of the inorganic agglomerates in an organic precursor can complicate preparation of a uniform fibrous organic matrix and cause large defects in the structure. [21] [22]

There are three most common production methods for fibres preparation – electrospinning, phase separation and self-assembly method. A whole chapter (2.3 Electrospinning) is dedicated to the electrospinning, therefore only the last two techniques will be described in the following paragraphs.

Phase separation is a production method for preparation of (mostly) polymer fibres, porous membranes and thin films. Apparatus for this technology is not complicated and the formed fibres are easy to be macroscopically aligned. However, the process is time consuming and optimization for various polymers is difficult. The resulting product morphology is influenced by the type of the polymer and the initial concentration of the precursor. The whole process consists of the following steps:

- Dissolution of the polymer
- Liquid phases separation
- Gelation (solidification) of the polymer
- Removal of the solvent
- Drying

The most common type of the phase separation used for fibres preparation is thermally induced separation. The polymer is derived from the solution by change of the solution temperature. [23]

Self-assembly method requires specific characteristics of the initial precursor. The process is time and money consuming, but it is versatile, and many various structures can be prepared using this method (fibres, lamellar structures etc.). The most suitable materials for the self-assembly are amphiphilic peptides. These substances contain hydrophilic sequences (with bond lipid chain) and hydrophobic (aliphatic) sequences. The aliphatic parts have the key role during aggregation of the molecules in water-based solutions which enables the fibres preparation. The hydrophobic sequence creates a “core” of the molecule during the aggregation (the hydrophobic part reduces its surface area in the water environment) with hydrophilic sequence on its surface. Interactions of the aliphatic parts of the molecules enable formation of the fibres. [24]

The self-assembly process is influenced by pH of the precursor and its chemical composition – for example, presence of multivalent cations. The whole process can be accelerated by electrostatic voltage, according to recent research. Utilization of the electrostatic voltage makes the process more versatile – the amphiphilic character of the initial material is no longer required, and even polysaccharides can be treated. [25]

2.3 Electrospinning

Fibrous structures with various structural characteristics can be prepared via electrospinning method. Two most usual electrospinning setups (vertical and horizontal) are displayed in Figure 5 and b, respectively.

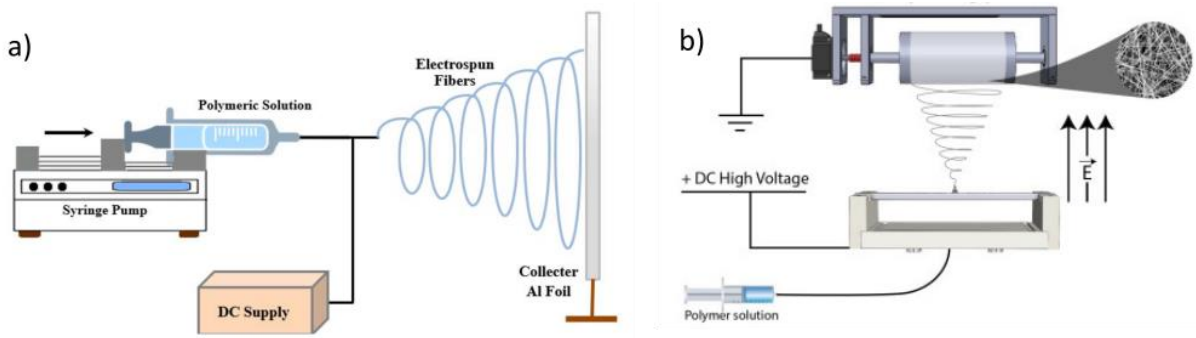

Figure 5 Two most common electrospinning setups: a) horizontal, [26] b) vertical [27]

The electrospinning process is based on the interaction of a liquid precursor with electrostatic voltage. The liquid precursor is attracted to the collector. During its way to the collector, the precursor's solvent is evaporated and then solid fibres reach the collector. The quality of the prepared structures depends on the precursor characteristics (mostly viscosity and electrical conductivity), parameters of the electrospinning (e.g. voltage, emitter-collector distance) and on the external conditions (air humidity, temperature etc.). [21]

2.3.1 Precursor characteristics and their influence on the fibres quality

The key requirement for the electrospinning precursor is its liquid state. Electrospinning is typically used for the processing of polymer materials. Therefore, this chapter is focused mostly on them.

Solvent of the precursor

Dissolution of polymers with high molecular weight is more difficult process than dissolution of organic substances with short molecular chains or inorganic materials. The solvent molecules at first diffuse into the polymer structure, the material expands, and a gel is created. After that, the structure of the organic chain is broken, and the liquid solution is formed. [21]

Molecular weight (length of the polymer chain) is important during dissolution of the polymers. Generally, the longer is the chain, the more time takes the dissolution process (the forces among the single monomers are stronger and the solvent cannot diffuse into the structure easily). Polymers with high crystallinity are nearly impossible to dissolute due to the polymers' closely packed structure – the solvent cannot reach the inner structure of the polymer and hence cannot break its bonds. [21]

The solvent must disappear from the precursor during its transport from the emitter to the collector. Otherwise, the originating fibres stick together, or a uniform polymer layer is formed on the collector and no homogenous fibres are produced. The time needed for complete removal of the solvent is dependent on its melting point, pressure of its vapors, rate of removing the vapors or interactions between solvent molecules and the polymer chains. [21]

Surface tension

Surface tension is a consequence of a difference between the liquid molecules' attractive forces on the precursor surface and the repulsive forces caused by collisions with molecules from the solution's interior.

The surface tension of the polymer solutions is influenced by the molecular weight of the dissolved polymer and the solvent's surface tension. This characteristic influences before all morphology of the fibres – too high surface tension can cause beads formation on the fibres or it causes flattening of the fibres into ribbons (ribbon formation is caused by synergic effect of more influences mentioned below). In a case of extremely high surface tension, drops are created instead of fibres and electrospraying occurs. [21] [28]

Viscosity

Viscosity of the material is defined as resistance of the material to flow. Before all the polymer chain length and its complexity influence (increase) the polymer solutions' viscosity value.

If the viscosity is too low, the electrospraying can occur instead of electrospinning – the precursor is formed into droplets and no fibres are produced. In the case of too high precursor viscosity, the solution can be electrospun, but there will be drops and other inhomogeneities on the fibres instead of a smooth uniform surface. Another problem of the viscous materials is precursor drying on the tip of the emitter's needle and its clogging. [21] [28]

In the case of an ideal viscosity, one Taylor cone is formed on the top of the precursor drop. The morphology of the fibres (e.g. diameter) can be then changed by control of the electrospinning parameters. In a precursor with low viscosity that still can be electrospun, more than one Taylor cone is formed and thin fibres are produced. [21] [28]

Electrical conductivity of the precursor

The electrical conductivity of the precursor is crucial for a successful electrospinning process. Sufficient charge must be accumulated on the emitter needle tip to overcome the surface tension of the precursor. The electrospinning precursors usually have low electrical conductivity (typically between 10^{-3} and 10^{-9} $ohm^{-1}m^{-1}$). The conductivity is higher when acids, bases or salts are present in the precursor. Therefore, these substances are added to the precursor (e.g. NaCl to water-based solutions). In the case of organic acid solvents, a small amount of water significantly increases the precursor conductivity by ionization of the solvent molecules. [21] [28]

2.3.2 Electrospinning parameters

Accelerating voltage

The accelerating voltage between the emitter needle and the collector is probably the most important electrospinning parameter. The accelerating voltage induces the electrical charge that enables the fibres formation. When enough charge is accumulated on the emitter needle's top, the Taylor cone is created that is the first stadium of the electrospinning process. The fibre is then pulled from the Taylor cone within the further impact of the accelerated voltage. The minimum voltage required for the creation of the fibres is usually 6 kV. [21] [28]

The voltage and the induced electrical field influence the final morphology of the fibres, before all their thickness – with increasing voltage the thickness decreases. It is caused by shrinking of the precursor during the fibres formation when large columbic forces are present on the emitter needle's tip. However, using high accelerating voltage may cause beads formation. The value of the voltage also influences the shape of the beads (from elongated to spherical). [21] [28]

The accelerating voltage influences also the inner structure of the fibres – under the electrical field, the polymer molecules tend to directionally arrange and hence increase the crystallinity of the fibres. However, with increasing voltage decreases the flight time of the fibres. Since the flight time also strongly influences the crystallinity of the polymer, the greater emitter-collector distances are recommended for reaching the lowest thickness of the fibres. [21] [28]

Feeding rate

The feeding rate strongly influences the quality of the fibres. For every combination of the electrospinning parameters exists a suitable range of the feeding rate that has an impact on the fibres morphology (especially thickness of the fibres) – with increasing feeding rate grows the thickness of the fibres. However, with increasing fibres thickness the time needed for solvent removal is prolonged and therefore the emitter-collector distance must be widened. If the feeding rate crosses the maximum border when all the precursor can be consumed, beads are formed on the fibres. [21] [28]

Apparatus arrangement

Besides the physical conditions of the electrospinning process, the apparatus's arrangement influences the prepared structure's quality. The first important thing is the diameter of the emitter needle. The thin needle reduces the size of the precursor drop on its top. It means that the precursor's surface tension that must be overcome is higher, which requires stronger electric field. Consequently, the time of the fibres creation is prolonged, the precursor molecules has more time for their arrangement and the resulting fibres are thinner. Small needle diameter also reduces the tendencies of the precursor to form beads on the fibres. [21] [28]

Another important parameter is the emitter-collector distance. The emitter-collector distance influences the flight time of the originating fibres and the electric field – with increasing emitter-collector distance, the flight time grows and the electric field is weakened (that further prolongs the flight time), which results in thinning of the fibres. However, if the emitter-collector distance reaches a critical value, the electric field is too weak to induce the fibre creation and electrospinning is impossible. On the other hand, if the emitter-collector distance is too low, the precursor solvent does not have enough time to evaporate and the solid fibres cannot be created (the fibres connect to each other on the collector or even a continuous layer of the polymer is created). [21] [28]

The last important part of the electrospinning equipment that influences the morphology of the fibres as well as the morphology of the whole structure is the collector where the solid fibres are deposited. The collector is usually made from an electrically conductive material (typically aluminum). The electrically conductive collector is electrically grounded to lead away charge collected on the fibres surface to keep the electrical field between the emitter and the collector stable. Such an arrangement enables collecting large amount of the electrospun material. If an electrically nonconductive collector is used, the electrical charge is accumulated on the fibres surface and the resulting fibrous mash is thinner. It is beneficial for 3D structures preparation. Such an effect can also be reached with the

conductive collector after deposition of a thick fibres layer when the charge cannot be led away anymore and is accumulated on the structure surface. [21] [28]

Directionally aligned fibres can be produced by the proper choice of the collector type. The first possibility of reaching the fibres alignment is high rotations per minute (in the range of 10^3) of the cylindrical collector (see Figure 6a). This method is easy and versatile, but the alignment level is sometimes low. Another choice is the specially designed shape of the collector. In the Figure 6b there is a collector with wires arranged into a cylinder. If this collector rotates slowly (10^0 rpm), the fibres organize themselves along the wires. The second suitable type of collector is a quickly (10^3 rpm) rotating disk (see Figure 6c). The resulting structure is highly aligned, but the collecting area is very small, so the process's effectivity is lower compared to other types of the collectors. [21] [28]

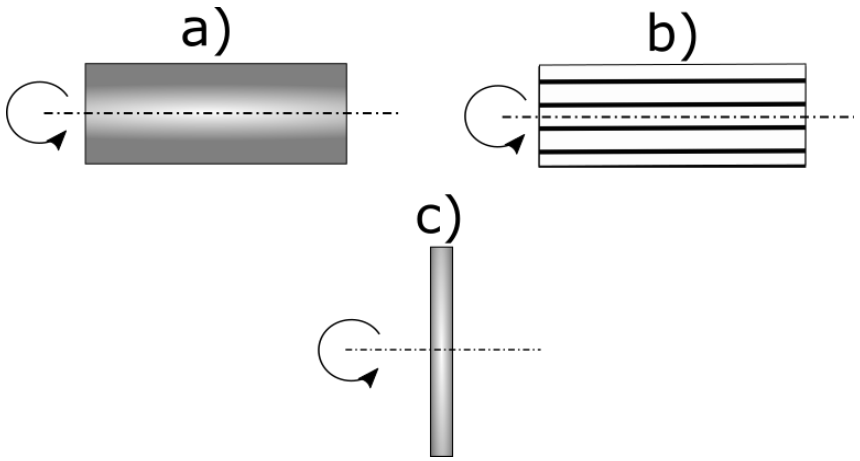

Figure 6 Collectors for harvesting of parallel aligned fibres: a) rotating cylinder, b) cylinder consisting of parallel wires, c) rotating disc

Outer conditions

The outer conditions have a crucial impact on the electrospinning process. Air temperature influences the solvent's evaporation rate, the precursor's viscosity, solubility of the polymer in the precursor and mobility of the molecules in the precursor (that further enhances the columbic forces). All these parameters grow with increasing temperature, which results in fibres thinning. [28]

Air humidity is another important characteristic of the environment because most polymer solutions are sensitive to water. If the relative air humidity is up to 50 %, the electrospinning process is usually not influenced. However, if the relative air humidity grows higher, the water condenses on the fibres surface and creates defects in the electrospun structure. A typical example of such defects are pores on the fibres surface are shown in Figure 7 where polysulphone nanofibres spun at different air humidity are depicted. Sometimes even too low humidity can be harmful – the precursor solvent evaporates too quickly, and the emitter needle is clogged. [28] [29]

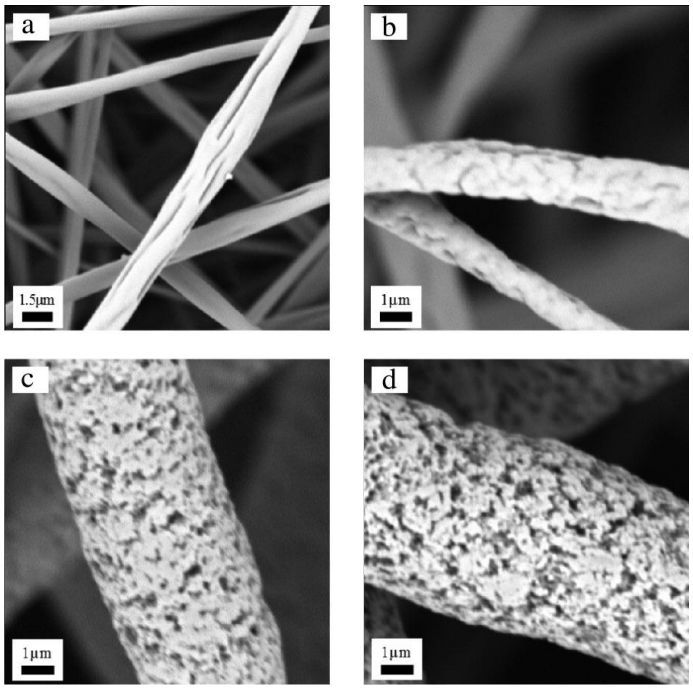

Figure 7 Nanofibres which were spun at different air humidity: a) 0 %, b) 10 %, c) 30 %, d) 50 % [29]

2.3.3 Fibres morphologies

The usual fibres morphology that can be prepared via electrospinning are dense fibres. However, this method offers more options – porous, flat or hollow fibres. Production process of such fibres is difficult to optimize but sometimes the fibres morphology is crucial for their utilization and looking for the proper electrospinning parameters is beneficial.

Type of the solvent and its vapors pressure in the surrounding atmosphere is important for porous polymer fibres preparation. The pores creation is based on phase separation of the precursor components during the solidification process. When the solvent starts to evaporate, the precursor is thermodynamically unstable, and the phase separation occurs at this moment. Places rich in the polymer quickly solidifies and a fibrous mash is formed. The solvent evaporates from places depleted of the polymer and pores are created. A typical system for porous fibres preparation is a poly-lactic acid dissolved in dichloromethane. Preparation of porous ceramic fibres requires a controlled heat treatment. The temperature must be higher than the solvent evaporation point but low enough to prevent sintering of the ceramic fibres. [28]

Origin of the flat fibres (they are also called as ribbons in literature) is not precisely described yet. It is probably connected with polymer molecular weight or solution concentration and different solvent evaporation rate on the fibres surface and their inner part. When the solvent evaporates off the surface considerably faster, the fibres core still contains the original liquid precursor. The air pressure from the surrounding atmosphere presses on the solid envelope of the fibres and the fibres are flattened. An example of changing fibres morphology with different molecular weight can be seen in Figure 8. [28] [30]

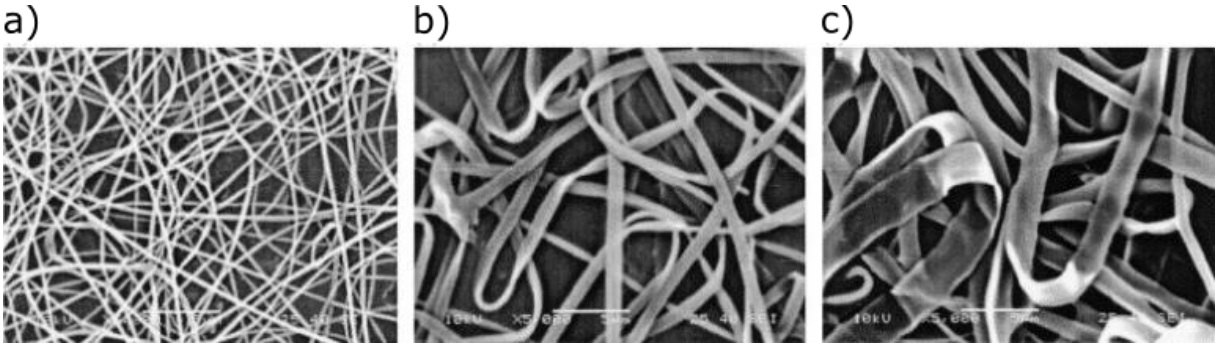

Figure 8 Influence of precursor concentration on polyvinyl alcohol (Mw = 50 000 – 89 000 g/mol) nanofibres morphology: a) 9 wt.%, b) 13 wt.%, c) 21 wt.% [30]

Helical fibres can be also prepared via electrospinning. The preparation of such fibres was described only for few combinations of precursor compositions and electrospinning parameters. It is believed (but it was not confirmed yet) that the helical morphology is created by combination of the electrostatic repulsive forces on the fibres surface and viscoelastic restoring force in the electrospun polymer. [28] [31]

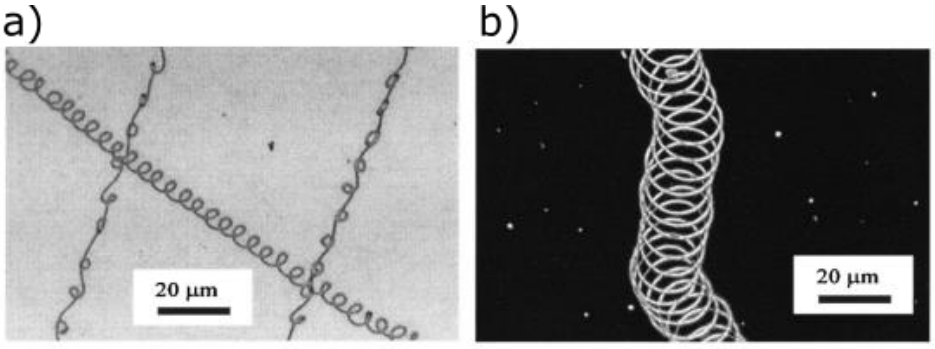

Figure 9 Helical nanofibres prepared from poly(ethylene oxide) dissolved in poly(aniline sulfonic acid) prepared via electrospinning [31]

Hollow nanotubes or nanofibres are required in energetic industry. There are two ways how to prepare hollow nanofibres using the electrospinning process. The first method is based on the preparation of polymer fibres (with thickness corresponding with future hollow diameter) and subsequent chemical vapor deposition (CVD) of the actual nanofibre/nanotube material. [32] The polymer is then removed during the subsequent heat treatment. The second method for hollow fibres preparation is coaxial electrospinning, when the temporary core and permanent envelope are created during one step. This process was described already in 2005 on poly(vinyl) pyrrolidone (core) – titanium propoxide (shell) system. After heat treatment of the fibres, TiO_2 hollow fibres were obtained. [33]

Coaxial electrospinning can also be used to prepare composite fibres but it is very sensitive to the geometrical arrangement of the setup (see Figure 10a) and choice of the precursors. Another option for composite fibres preparation is side-by-side electrospinning when two different solutions are pumped into one emitter needle (Figure 10b). The resulting fibres are made from two different materials and the chemical and phase composition differs along the fibres. The basic requirement for such setup is that no reaction can occur between the present substances. If the two chosen precursors react with each other, using two different emitter needles is a possibility (Figure 10c). The single fibres

are made from one material, but the resulting structure is made from two types of fibres and hence can combine (chemical or physical) properties of both.

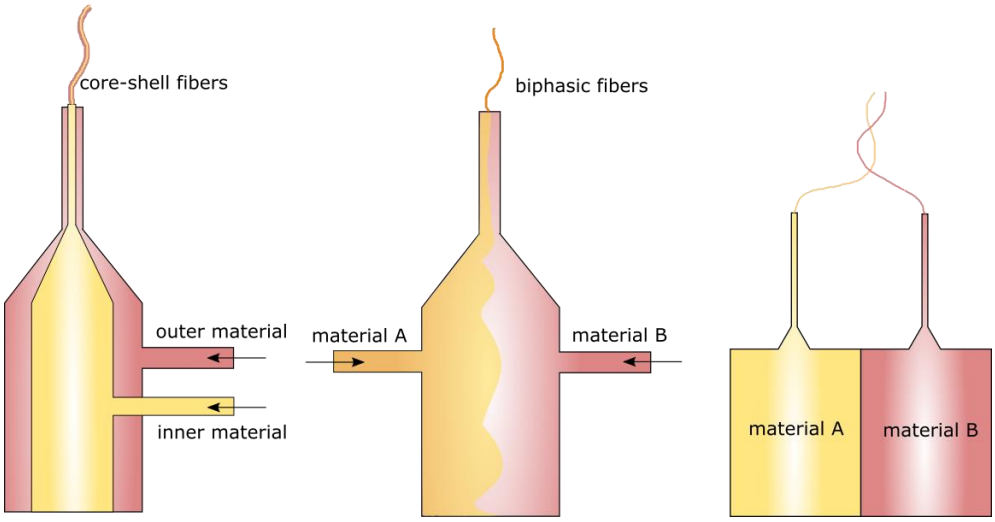

Figure 10 Emitters used for electrospinning of a) core-shell fibres, b) biphasic fibres, c) fibres from different materials

Sometimes macroporosity of the whole electrospun structure is engineered. The macroporosity should allow better chemical substances transport and easier cell migration into the electrospun structure. There are more ways how to increase the electrospun structure porosity. The first possibility is incorporating a soluble phase into the electrospun structure – e.g. sodium chloride crystals incorporated into a polycaprolactone fibrous structure will dissolve after rinsing in water and create macropores, as can be seen in Figure 11. The key to achieving such structure is modification of the electrospinning setup to ensure NaCl (or other material soluble in water) to be incorporated among the fibres – see Figure 12 where an example of such equipment is displayed. Therefore, this method is limited by the construction of the electrospinning machine and space available around the emitter and collector. [34] [35]

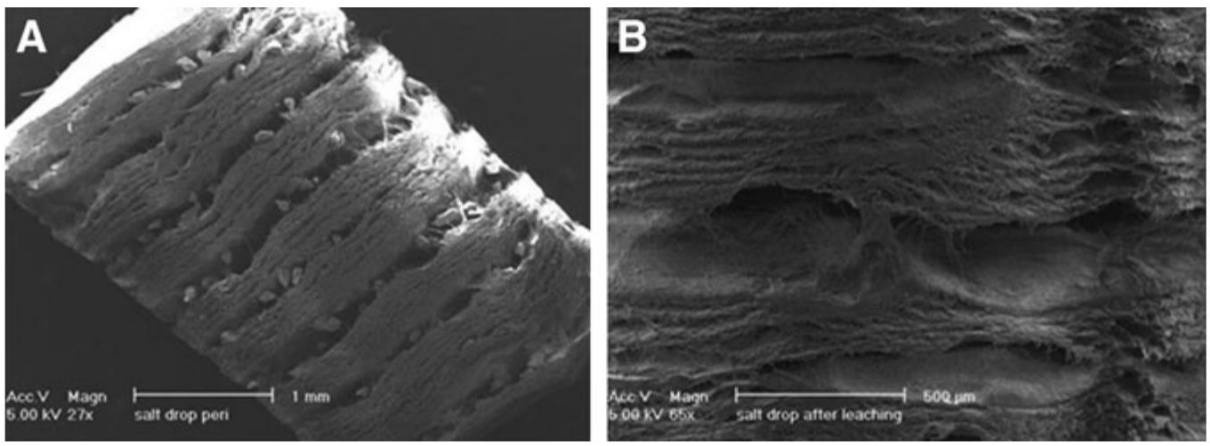

Figure 11 Electrospun structure with NaCl crystals a) as-spun structure, b) after the salt leaching [34]

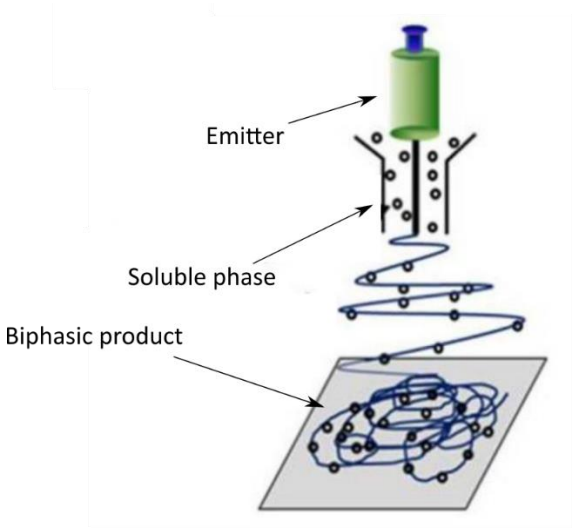

Figure 12 A setup for incorporation of soluble particles into the electrospun structure [34]

Other way of preparing microporous structure is using a physical approach, e.g. ultrasonication after the electrospinning process. The principle of this technique is displayed in Figure 13 and the resulting microstructure before and after the treatment is in Figure 14a and b, respectively. The effect of the ultrasonication is visible with the naked eye, as can be seen in Figure 14c-f where cross and top view of the electrospun structure before and after the treatment is displayed. The ultrasonication method requires and additional equipment to the structure preparation and prolongs the structure production process. However, the prepared materials have a homogenous structure and the process is highly reliable and reproducible. [36] [37]

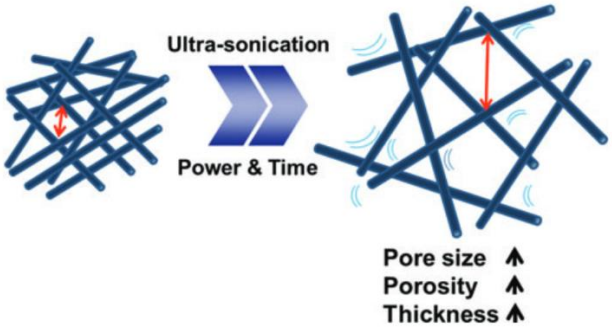

Figure 13 Principle of increasing fibrous mesh porosity via ultrasonication [37]

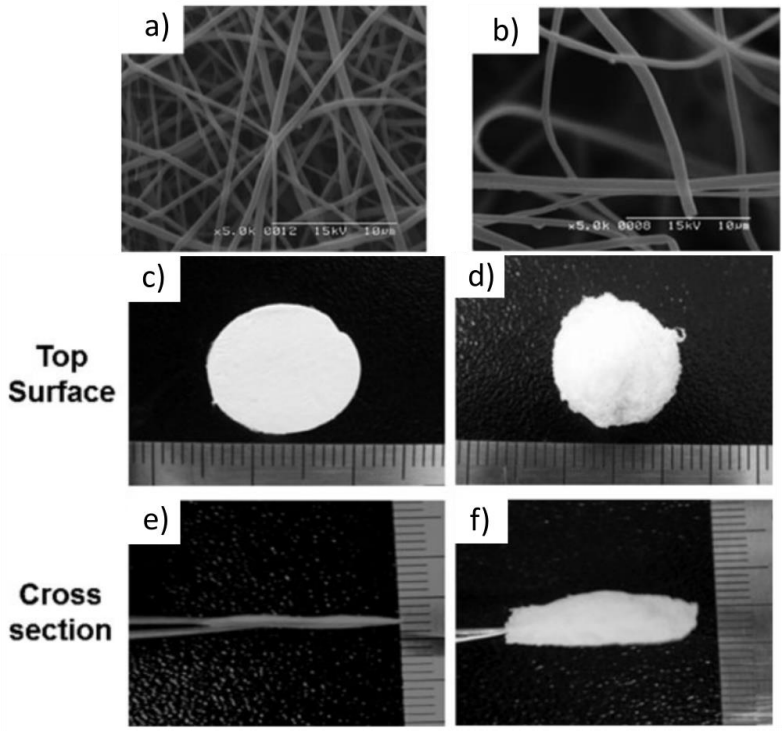

Figure 14 Microstructure of a) as-spun fibres, b) fibres after the ultrasonification; top overview of c) as-spun structure, d) ultrasonificated structure; cross view of e) as-spun structure, f) ultrasonicated structure [37]

2.3.4 Surface treatment of the fibres

Sometimes it is beneficial to modify the surface properties of the electrospun fibres. There are several possibilities for how to reach required physical or chemical surface properties. Widely used physical treatment is using plasma to increase hydrophilicity of the polymer (usually hydrophobic) fibres. Plasma does not modify directly the material of the fibres, but it initiates cascade of dissociative reactions with molecules adsorbed on the fibres surface (typically water, CO_2, O_2, N_2). The formed radicals react with the material of the fibres and create some functional groups (e.g. –COOH, –C=O, -NH_2) that support the hydrophilicity of the fibres. The formation of the functional groups (that is not easy to be predicted) can be controlled by the surrounding atmosphere – for example nitrogen atmosphere support formation of amine groups. [38] [39] [40]

UV irradiation can be used as an alternative to plasma treatment. Carboxylic functional groups are immobilized on the fibres surface as a result of the process. It can be done as a treatment improving the surface characteristics of the fibres (although for example the resulting contact angle is higher than after plasma treatment) or as the first step of further coating of the fibres with a bioactive layer. [41] Gamma ray radiation is another technique of the fibres surface treatment. The gamma ray radiation has greater penetration depth than the plasma treatment. The radiation process is effective and does not require any additional chemicals or catalysts. However, when the process is not carefully designed, some structural changes or even degradation can occur at the structure. [13]

Surface functionalization with biomolecules and protein immobilization are another surface treatment methods used for artificial polymers. For example, combination of polycaprolactone and silk fibroin has been studied recently as a promising material combination. Silk fibroin considerably supports cells attachment and their proliferation that was proven both *in-vitro* [41] and *in-vivo*. [42]

Another physical process used for fibres surface modifications is laser treatment. Laser treatment is used for modification of fibrous mesh macrostructure. For example in [43] a pulse Nd:YAG laser was used for artificial porosity creation which resulted in increased biocompatibility and better proliferation (tested *in-vitro*).

Coating of the fibres is a different approach of the fibres surface modification. The coating increases biocompatibility of the electrospun structures, which then have a role of biomaterials carriers. The coating can be ceramic (typically for bone scaffolds) or polymer (suitable for skin tissue engineering). The ceramic coatings are usually based on calcium phosphates. The calcium phosphate coating provides chemical as well as physical changes of the surface properties of the structure. The ceramic coating of the polymer structures also slows down the polymer structure's degradation (for example, collagen structures). The easiest way of providing such coating is using simulated body fluid (SBF) presented by Kokubo in 1990. [44] The SBF was at first intended for biocompatibility material testing (see chapter 2.5), but today is used for coating of titanium implants [45] and is considered as a promising method for collagen or silk structures. [46] Nowadays, the effect of various morphologies of SBF induced calcium phosphate coating on the cell behaviour is examined. [47] The polymer coatings modify the surface chemistry of the scaffold structure, too. A typical example of polymer fibres coating is collagen [48] or silk fibroin. [41] Polymer coating of scaffolds usually requires multistep dip coating, which means it is more complicated than surface mineralization of the structures, but it can crucially improve skin implants' bioactivity. [41]

2.3.5 Electrospinning of PCL

Polycaprolactone has been explored for some time and many solvent systems and corresponding electrospinning parameters were described. In Table 3 there are some combinations of precursor composition, PCL concentration and resulting fibres morphology. As can be seen, the fibres morphology changes considerably with the precursor composition and the electrospinning parameters.

Thanks to wide variety of the PCL solvents, polycaprolactone fibres can be used for many modern technological purposes. Non-toxic solvents, namely acetic and formic acid, are interesting for future medical utilization. Besides the standard laboratory requirements, acetic and formic acid utilization does not require any special precautions and there is no possible ecological danger.

Table 3 Common PCL electrospinning systems and resulting fibres morphology

PCL concentration	Solvent composition	Electrospinning voltage [kV]	Fibres diameter [nm]	Citation
8 wt.%	Chloroform	13	3100 ± 450	[49]
10 wt.%	Chloroform	13	400 ± 200	[50]
12 wt.%	Chloroform	20	200-500	[51]
7.5-11 wt.%	Dichloromethane	15	615-4000	[52]
11 wt.%	Methylene chloride	15	4000 ± 2000	[52]
20 wt.%	Acetic acid	20	1000-2000	[53]
20 wt.%	Acetic acid	6	1360 ± 330	[49]
23 wt.%	Acetic acid	12	1833	[54]
14 wt.%	Acetic/formic acid (1:9)	18	364	[55]

Besides the controllable parameters, PCL is sensitive to the relative humidity of the surrounding atmosphere. Nezarati et al. described the influence of the relative humidity on the resulting fibres morphology. At low relative humidity (up to 35%) there was a high percentage of broken fibres in the electrospun structure. When the relative humidity was increased to 50%, a homogeneous and nearly defect-free structure was electrospun. According to the authors, the porosity was formed at even higher relative humidity (up to 75%) porous nanofibres due to a phase separation caused by interaction between the hydrophobic polymer and water absorbed into the electrospinning jet. [56]

All the described structure changes can be seen in Figure 15. However, the low air humidity effect can be compensated by appropriate accelerating voltage (decrease of the voltage lowers content of the broken fibres percentage). [56]

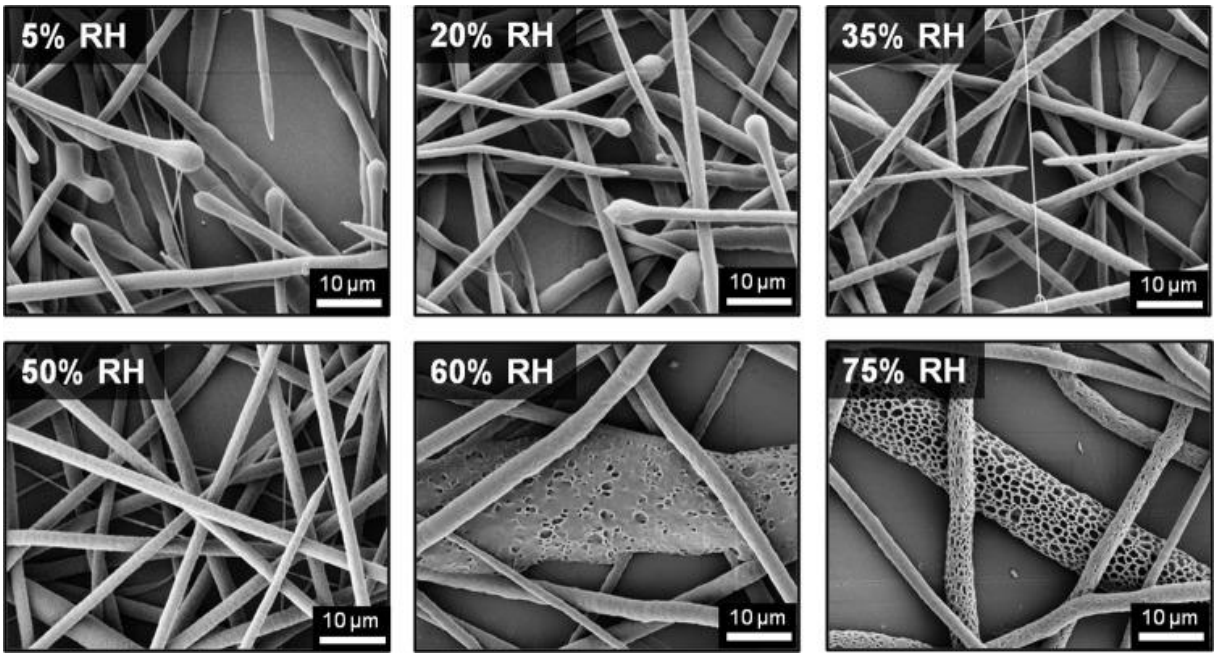

Figure 15 Influence of the relative humidity on PCL electrospun fibres [56]

2.4 Fibres in medicine

Fibrous structures have already been proven as beneficial for cell adhesion and proliferation and several studies have shown their great ability to act as carriers of drugs and other substances supporting wound healing. Moreover, polycaprolactone, which is the core material in this thesis, was approved by Food and Drug Administration (USA) for medical applications. [57]

2.4.1 Skin tissue engineering

The main reason for research of nanofibres as potential scaffolds is similarity of their structure to the natural tissue structure. The (not only fibrous) scaffolds must be structurally and chemically compatible with the treated tissue. The chemical compatibility is reached by choose of a proper material and the surface treatment. The structure compatibility means that the scaffold can support cell adhesion and migration. Other specific scaffold requirements were discussed in chapter 2.2.

The skin scaffolds must reflect the type and severity of the wound – there are different requirements for treating damaged epidermis (surface layer of the skin) and deep injuries affecting dermis. The skin scaffolds can (bud does not have to) contain living cells to accelerate the regeneration process. The key process conditions for successful skin regeneration are early excision of the damaged tissue

(typically burns) and fast closure of the wound. Moreover, skin healing process is highly prone to post-treatment complications (infection, immune reactions etc.). [58] It means that there is a high demand for scaffolds to be easily disinfected and to be produced in advance and storage. [59]

The fibrous scaffolds are still not widely used in the medicine praxis. However, many different structures are considered as promising for future utilization in medicine. The first choice for skin scaffolds would be collagen, but it is expensive and has high degradation rate (the material degradation is faster than new tissue formation). Therefore, different fibrous structures have been recently tested. From natural polymers, silk fibroin (polymer produced by *Bombyx mori* larvae, the domestic silk moth) seem very promising – it is biocompatible, non-toxic, non-carcinogenic and induces minimal immunologic response. Park et al. proved electrospinning as a very promising method for skin scaffolds – it considerably supported fibroblasts and keratinocytes proliferation compared to silk fibroin porous structures produced by freeze-drying or salt leaching. [60]

Chitosan is another natural polymer widely discussed as a promising material for skin scaffolds. To improve its bioactivity, additional natural polymer or bioactive agents are added to the structure. Bakhsheshi-Rad et al. tested *in-vitro* and *in-vivo* chitosan scaffolds loaded with alginate and gentamicin (to improve bioactivity and antibacterial performance, respectively). The *in-vivo* tests on a mouse model showed a successful healing process, including blood vessels, hair follicles, and sebaceous glands. [61]

Yao et al. described the positive influence of gelatin-poly vinyl alcohol nanofibres containing *Centella asiatica* extract (an Asian herb used as antibacterial agent) on skin wound healing. The structure considerably accelerated the healing process, which was proven *in-vivo* on a rat model. [62]

Last but not least, from the natural polymers, hyaluronic acid must be mentioned. Hyaluronic acid is a natural polysaccharide well known for its antibacterial performance and support of scar-less wound healing. Nowadays it is commonly used in medicine in the form of liquid serums or gel films on solid carriers (e.g. gauze). Shin et al. produced hyaluronic-poly(lactic-*co*-glycolic) acid core-shell nanofibres loaded with epigallocatechin-3-O-gallate (as an antibacterial agent). The prepared scaffolds were tested on a rat model and showed accelerated wound healing in the entire depth of the wound. A positive influence of such structure was achieved also on diabetic rats which suggests further research of the scaffold for diabetic wound healing. [63]

Natural polymers are usually cost demanding and require rather toxic solvents to be dissolved. Therefore, artificial polymers are also examined as possible scaffold materials. Zhang et al. prepared poly vinyl alcohol (PVA) nanofibres doped with graphene oxide. The bioactivity of the PVA-graphene oxide scaffolds was tested both *in-vitro* and *in-vivo* on a rat model and the results were consistent. The graphene oxide in the specific concentration of 0.25 wt.% supported bioactivity of the scaffolds and improved mechanical properties of the scaffolds. [64]

Polycaprolactone (PCL) is widely investigated as a possible scaffold material – it is cheap, soluble in non-toxic solvents and biocompatible. However, it has a low degradability rate, and it is hydrophobic. Agnes Mary et al. showed improvement of the PCL properties by incorporating aloe vera extract. The aloe vera increased hydrophilicity and supported the scaffold's bioactivity (which was tested *in-vitro*) but it worsened the mechanical properties. Therefore, the utilization of PCL/aloe vera composite structure as a skin scaffold is disputable. [65] Augustine et al. presented PCL nanofibres filled with ZnO nanoparticles. The ZnO nanoparticles induced no inflammatory response and moreover, they considerably improved the fibrous structure's bioactivity (it was shown on a guinea pig model) and reduced formation of scar fibrotic tissue. The effectivity of the wound healing process (displayed as healed area) can be seen in Figure 16. The PCL/ZnO fibrous scaffold accelerated the healing process by

five days and moreover, the healing process was also more effective (the healed area reached 100%). Also, the pure PCL fibres accelerated the healing process, but the effect was not so significant compared to the positive control. [66]

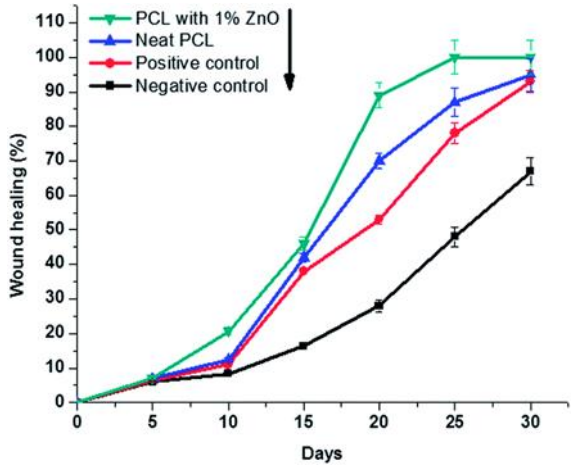

Figure 16 Skin wound healing process while using PCL and PCL/ZnO scaffolds [66]

Another possibility of PCL fibres modification is adding a specific protein naturally present in the human body. Kim et al. doped PCL nanofibres with mussel adhesive protein resulting in improved bioactivity proved both *in-vitro* and *in-vivo* (on a rat model). According to the conclusion of the authors, the PCL/mussel adhesive protein (MAP) can be used beside the skin tissue engineering for treatment of various tissues injuries. In Figure 17 there can be seen the healing process of the artificial injury comparing untreated injury, PCL scaffold and PCL/MAP scaffold. [67]

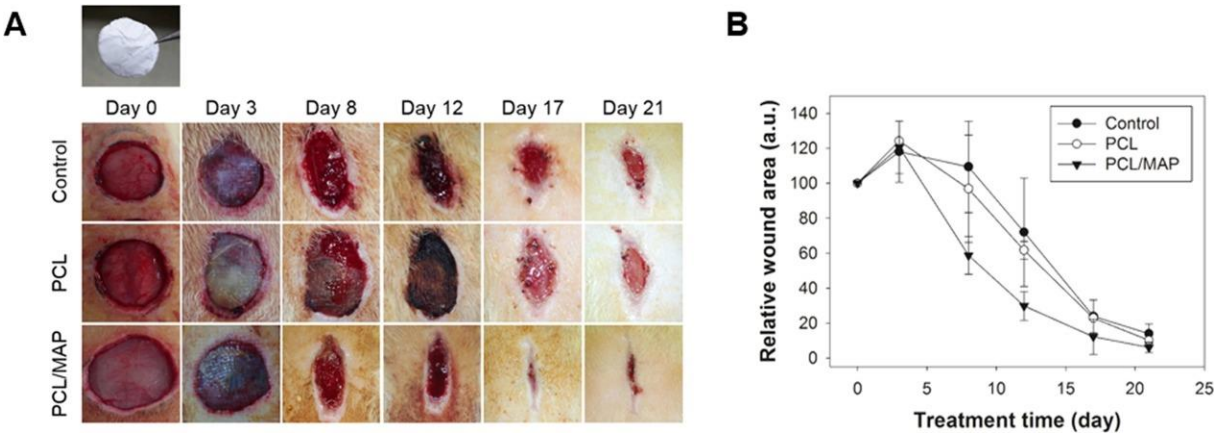

Figure 17 In-vivo test of PCL and PCL/MAP) scaffolds, a) macroscopical observation of an artificial skin wound, b) measured wound area during the treatment time [67]

2.4.2 Bone scaffolds

Structures for bone scaffolds have higher demands on the materials' mechanical properties (e.g. toughness and stiffness), which makes natural polymers unsuitable for such utilization. Therefore, research is focused on artificial polymers. [68]

PCL has been studied as a potential bone scaffold material, too. Since its performance as a bone scaffold is not sufficient, it is often combined with other polymers or ceramic phases to improve the bioactivity and mechanical properties. [69] A typical example of ceramic phase used for improving PCL's properties is β-tricalcium phosphate (β-TCP) and hydroxyapatite. Patolla and col. combined PCL fibrous mesh with βTCP/hydroxyapatite particles with promising results. It was proven that the

bioactivity depends on the homogeneity of the composite structure (e.g. uniform dispersion of the ceramic particles in the polymer fibres). The homogenous structures showed higher osteogenic activity and occurred as potential bone scaffold material. [70]

Suganya et al. prepared electrospun PCL fibres combined with hydroxyapatite nanoparticles and ether from *Cissus quadrangularis*, a herb with proven osteogenic effect. Performance of the composite structure was examined *in-vitro* using human fetal osteoblasts. The composite fibrous structure strongly supported cell proliferation suggesting its increased bioactivity compared to plain PCL fibres. [71]

Binulal et al. combined PCL with gelatin, a natural polymer. Both polymers were dissolved and electrospun together in various ratios. The structures were tested *in-vitro* using human mesenchymal stem cells, their proliferation and osteogenic differentiation was evaluated. It was shown that the best results were achieved within 30 wt.% of gelatin in the PCL nanofibres (a further increase of gelatin content worsened the structure performance). [72]

A functionalization of polymer nanofibres via bioactive coating is a popular method for bone scaffolds preparation. For example, Pereira et al. prepared co-axial PCL/gelatin nanofibres which were immersed into simulated body fluid (SBF) with 10 multiple concentration compared to the usually used SBF. Calcium-phosphates precipitated on the nanofibres surface, which increased the bioactivity of the structure (examined *in-vitro*). [73]

Poly (l-lactide) (PLLA) is considered as a bone scaffold material especially for its good mechanical properties. Cai et al. showed a promising concept of 3D macroporous nanofibrous scaffold based on PLLA/PCL electrospun nanofibres. Bioactivity of the structure was proven both *in-vitro* and *in-vivo*. The 3D structure strongly supported proliferation and cell differentiation compared to similar 2D structures. The histology results of the in-vivo test suggested support of proper cortical bone formation after six weeks from implantation. [74]

Sometimes an additional source of cells is needed for successful scaffold implantation and further healing process. There are various types of stem cells (adult, embryonic etc.) and the most suitable type for tissue engineering still has been searched for. There are several requirements for the stem cells for tissue engineering: they must be available in a sufficient amount; the harvesting procedure must be minimally invasive, and they must differentiate along multiple cell lineage pathways in a reproducible manner. However, there are also many limitations, such as limited stem cells' limited availability, potential immune response, or a disease transfer. Therefore, there is still much work to be done before the stem cells will be fully implemented into medical practice. [75]

For example, Ardeshirylajimi et al. examined several stem cells types on bioceramic dip coated PLLA nanofibres. Cell seeded scaffolds were evaluated using MTT assay for proliferation rate assessment and osteogenic differentiation was determined via calcium content, alizarin red staining and alkaline phosphatase (ALP) activity. Bone marrow mesenchymal stem cells and buccal fat pad derived mesenchymal stem cells showed the best performance promising further use in bone tissue engineering. [76]

2.4.3 Vascular scaffolds

Vascular scaffolds are designed to replace damaged blood vessels. The natural blood vessels have layer structure containing several types of cells. The outer layer (adventitia) consists of a collagenous extracellular matrix with fibroblasts and perivascular nerve cells. The middle layer, media, consists of

concentrically organized smooth muscle cells with bands of elastic fibres. The inner layer intima contains a monolayer of endothelial cells attached to a connective tissue membrane. Besides the biocompatibility and bioactivity, the scaffolds replacing the vascular tissue must withstand the blood pressure, and the blood leakage has to be avoided immediately after the implantation. [77]

Abdal-hay et al. presented a biphasic vascular scaffold consisting of an inner dense PCL tube and outer polyurethane (PU) fibrous membrane (the support was thermally cross-linked to ensure the connection of the both phases). The PCL tube serves as mechanical support of the scaffold (and immediately prevents blood leakage), and the PU fibres supported the proliferation of the cell culture during an *in-vitro* test. Moreover, the production process was rather simple and economically affordable. Therefore, this type of scaffold is a promising approach to vascular tissue engineering. [78]

Parallel aligned fibres are advantageous for the vascular grafts – the parallel fibres help the cells to get aligned, which simulates the natural vascular tissue. Zhu et al. prepared aligned PCL nanofibres coated with fibrin induced *in-vitro* human smooth muscle cells elongation and fibrin also strongly supported the cells survival and biological function. [79]

Vaz et al. prepared a tubular layered PLA/PCL scaffold. The prepared structures were evaluated *in-vitro* using 3T3 mouse fibroblasts and human venous myofibroblasts. The scaffold strongly supported the proliferation of the mouse cell culture. The human venous myofibroblasts also successfully proliferated and produced a natural extracellular matrix, although analyzed proteins content (collagen and glycosaminoglycans) did not reach the natural tissue's values. Moreover, the mechanical properties showing elastic anisotropic behaviour also promised further usage in vascular tissue engineering. [80]

Zhikai et al. prepared a bilayer PCL/poly ethylene glycol (PEG) scaffold consisting of an inner PCL layer with thin, parallel aligned fibres and an PCL/PEG outer layer. The outer layer was prepared by co-electrospinning of PCL and PEG and subsequent dissolving of the PEG fibres to increase the outer layer's pore size. The scaffold was tested both *in-vitro* and *in-vivo*. The bilayer structure had suitable mechanical properties, it supported endothelial cell migration and proliferation and nutrient infiltration and tissue growth. [81]

2.4.4 Nerve scaffolds

Peripheral nerve damage is a common injury in medical practice. It can be caused by for example, by tumor or trauma. Compared to the central nervous system injuries, the peripheral nerves can be healed under certain medical treatment. Nowadays, the most common option for such treatment is an autologous graft which means an additional invasive surgery for the patient. Moreover, only 50 % of patients regain an acceptable function level of the damaged area. Therefore, there has been intensive research on nerve scaffolds. [82] [83]

The first generation of the nerve scaffolds (also known as nerve conduits) were hollow tubes made from a biocompatible material that provides a mechanical support for the new tissue, prevents surrounding connective tissue from infiltration and induces functional rehabilitation of the damaged tissue. The second generation was made from an advanced material – it was porous (to ensure the cell and nutrition transport) and bioresorbable. The second generation of nerve conduits is currently used in medical practice, but it does not reach autografts efficiency. The nowadays researched third generation consists of an advanced structure (e.g. inner and outer micropatterning, electrical conductivity) and seeded cell culture supporting the nerve regeneration. [82] [83]

A typical example of the second-generation nerve conduits were polyglycolic acid tubes. They have been showing a great performance in the treatment of sensory and motor nerve defects and peripheral nerve injuries up to 3 cm long. [82]

Collagen conduits have a good performance, especially while treating small defects (maximally 2 cm long), but there is a problem with short degradation time – some studies suggest that the conduit disappears before the new neural tissue is formed. [82] [84]

Considering controlled porosity and surface pattering of the conduits third generation, the electrospinning seems like an appropriate production method. Electrospun structures provide patterned surface and high area-to-volume ratio suitable for adsorbance of bioactive molecules. [82] [85] [86]

Neal and et al. showed conduits with fibrous filling from polycaprolactone/laminin parallel aligned fibres. The efficiency of such conduit was examined by an *in-vivo* test on a rat model. It was proven that both alignments of the fibres and bioactive protein content were beneficial for nerve regeneration. [87]

Costa et al. compared a standard polyglycolic acid conduit, a conduit filled with bone marrow stem cells and Schamm-like cells (previously differentiated from the bone marrow mesenchymal cells). The in-vivo test results on a rat model showed accelerated facial nerve regeneration by samples using pre-seeded cell culture inside the conduit. [88]

2.4.5 Drug delivery

The nanofibrous structures' large surface area provides a great space for bioactive molecules or drugs that could further help the wound healing and the regeneration process. The available surface does not consist only of the outer surface of the fibres, but also the nanopores present in the nanofibres which considerably enlarges the available area. Another advantage of fibrous drug carrier is controllable drug release that ensures more effective drug influence, decreasing the danger of affecting non-diseased areas and reducing the number of drug applications. The drug-loaded nanofibres can be applied either orally in a form of tablets or the drug can penetrate the body through skin. [12] [89]

To make the drug release process controllable and effective, the medicaments must be immobilized in the fibrous structure. Two processes – entrapment or binding, can achieve the immobilization. The entrapment is a physical process ensuring the medicament to be contained in the structure. One of such methods is core-shell electrospinning of a polymer with a defined degradation rate and the drug. This technique was used by Jiang et al. (2006) to place BSA-dextran into polycaprolactone fibres. Another way to entrap the molecules into the structure is crosslinking the fibres when the drug is added to the structure during the crosslinking reaction. [90] Another way is the addition of the drug directly to the electrospinning precursor. However, there is a danger of chemical reaction between the medicament and the precursor solvent. The binding can be realized by hydrogen bonds, hydrophobicity, electrostatic interaction etc. [12]

There are three mechanisms of drug release from the fibres: desorption from the fibre surface, solid-state diffusion through the fibres and *in-vivo* degradation. The drugs attached to the fibres are mostly soluble in aqueous solutions, and therefore, the drugs start to release when the structure is immersed into a water-based solution. At first, the medicine is released from the fibrous structure and then diffuses into the surrounding aqueous environment. The fastest mechanism of drug release is

desorption from the fibre surface. However, there is a danger of a rapid release at the beginning of the release process. Therefore, the drug-bearing fibres can be surrounded by a shell from a water-soluble polymer that slows the drug release. [91] The *in-vivo* fibre degradation process takes place when the medicine is loaded in a structure from a fast-degradable polymer (typically poly vinyl alcohol). [92] It is obvious that the drug release rate can be designed by using various polymers, drug-loading mechanisms and potentially by coating of the drug-loaded structure.

The nanofibres drug release can be used in many various medical fields. The fibrous mats from L-lactide-caprolactone have been proven to reduce neurodegradation and scar formation after brain surgery. [93] A biodegradable fibrous mat loaded with an antibiotic can prevent a medical device and other implants from an inflammation response. [94] Nanofibres are tested as possible biosensors for a level of blood glucose detection that would improve diabetes treatment. [95] Xu et al. also presented an oral mean of insulin application via gelatin/insulin fibres which would considerably improve diabetes treatment. [96] Nanofibrous drug carriers seem to be promising even in cancer treatment – the anticancer medicine would be released at a controlled rate and directly in the place of the tumor so other body areas (typically liver and kidneys) remain unaffected. Both *in-vitro* and *in-vivo* tests have been already done, examining various drug-carrier systems. The results show a considerable decrease of tumour growth. [97] [98]

2.5 In-vitro scaffolds testing

For further utilization in medicine, a careful testing process must be carried out. Before *in-vivo* tests in living bodies can be done, *in-vitro* tests are carried out. The *in-vitro* tests gain information from cell cultivation on the tested material.

A crucial property of a tissue engineering material is its bioactivity. The first test indicating bioactivity of a material intended for bone scaffolds is soaking in the simulated body fluid (SBF), which has been already mentioned. The chemical composition of the SBF, mimics composition of human blood plasma, the ion concentration of the SBF can be seen in Table 4. [44] The SBF indicates suitable phase composition of the tested material by precipitation of hydroxyapatite on the structure surface. The SBF test is usually the very first test of the material or structure because it does not have any special demands for the laboratory equipment.

Cell culture tests are the second step of the *in-vitro* testing. The cell culture tests require a high hygienic standard of the laboratory and carefully trained staff. At first, a suitable cell line is chosen. Further material utilization is usually considered (e.g. osteoblasts for bone tissue engineering or dermal fibroblasts for skin tissue engineering). There are several methods of the execution of the *in-vitro* tests. The international ISO 10993-5 standard evaluates real number of cells on the tested material during specified time frame. [99] This type of test has high requirements on the laboratory equipment – each evaluated sample needs an optical microscope with precise positioning to observe several view fields. It makes the test slow and rather inefficient. However, there are tests that allow testing of high number of samples. These tests do not measure an absolute number of the cells, but the amount of cells activity products (metabolic substances) is determined. The cell activity's evaluation is provided by specific chemical reaction with cells metabolic products, resulting in a colour indication of the seeding solution. The colour change is then precisely measured by spectrophotometry. This type of test allows the evaluation of a large number of samples simultaneously, reducing the risk of changes in the cell line and accelerating the whole testing process. An example of such test is MTT assay (testing kit is produced by Abcam, USA) or WST-8 assay (testing kit is produced by PromoCell, Germany). [100] [101]

Table 4 Comparison of ion concentration in blood plasma and SBF [44]

Ion	Ion concentration (mM/l)	
	Blood plasma	SBF
Na^+	142.0	142.0
K^+	5.0	5.0
Mg^{2+}	1.5	1.5
Ca^{2+}	2.5	2.5
Cl^-	103.0	147.8
HCO^{3-}	27.0	4.2
HPO_4^{2-}	1.0	1.0
SO_4^{2-}	0.5	0.5
pH	7.2-7.4	7.40

The polycaprolactone has been widely examined as a promising bioscaffold material. However, polycaprolactone itself lacks sufficient bioactivity, considerably improving and accelerating the healing process. Therefore, many various morphologies, additive constituents and ways of surface treatment has been studied and tested.

Fibrous morphology seems ideal for tissue engineering since it mimics the structure of the natural tissues. For bone tissue engineering, calcium phosphates are beneficial for successful bone regeneration, which can be further accelerated by a proper surface treatment, for example, by plasma treatment. However, there has not been done much work exploring the synergic effect of ceramic (calcium phosphate) particles into polycaprolactone nanofibres and subsequent plasma treatment. Therefore, this work focuses on the combination of these two improvements to design a biocompatible and bioactive structure for further bone tissue engineering.

3 Aims of the thesis

The motivation for the presented research is preparation and description of a novel biocompatible and bioactive material for bone tissue engineering using electrospinning method. The prepared structure should actively support the healing process and support the cells activity on the place of the injury by optimized chemical and phase composition and subsequent surface modification of the structure.

The research was divided into several tasks for successful achievement of the desired structure:

1) Development of polycaprolactone/hydroxyapatite composite nanofibres
2) Fibre surface characteristics optimization by plasma treatment
3) Biocompatibility and bioactivity testing of the prepared structures

The preparation of the polycaprolactone and the composite nanofibres required optimization of the electrospinning precursors, their analysis and optimization of the electrospinning process. The research focusing on the fibres preparation also contained experiments aiming to prepare neat ceramic or hollow nanofibres that promised interesting biological properties.

Optimization of the fibres biological properties was done by fibres surface plasma treatment on structures that were selected as promising for the future biological test and possible bone engineering utilization.

The biological tests were divided into two phases of *in-vitro* tests. The first test examined bioactivity through hydroxyapatite formation on the structure surface in the simulated body fluid. In the second phase, biocompatibility and bioactivity were tested by living cells cultivation on the structure surface.

4 Experiments and methods

4.1 Materials

All the materials used for the experiments are listed in Table 5.

Table 5 List of chemicals used for the experiments

Chemical	Specification	Producer	Country of origin
Acetic acid	98%, p.a. purity	Penta	Czech Republic
Chloroform	p.a. purity, stabilized with amylene	Lach-ner	Czech Republic
Ethanol	96%, p.a. purity	Lach-ner	Czech Republic
Formic acid	for synthesis	Merck	Germany
Polycaprolactone	Mw = 80000 g/mol	Sigma Aldrich	Germany
Polyvinyl pyrrolidone	K 90	Fluka	Germany
Titanium isopropoxide	For synthesis	Merck	Germany
$Ca(NO_3)_2 . 6H_2O$	p.a. purity	Lach-ner	Czech Republic
NH_4OH	25-29%, p.a.	Penta	Czech Republic
$(NH_4)_2HPO_4$	p.a. purity	Lach-ner	Czech Republic
$Ca(NO_3)_2 . 4H_2O$	p.a. purity	Lach-ner	Czech Republic
$(C_2H_5O)_3P$	95%	Fluka	Germany
NaCl	p.a.	Lach-ner	Czech Republic
$NaHCO_3$	p.a.	Lach-ner	Czech Republic
KCl	p.a.	Penta	Czech Republic
$K_2HPO_4 \cdot 3H_2O$	p.a.	Penta	Czech Republic
$MgCl_2 \cdot 6H_2O$	p.a.	Lach-ner	Czech Republic
HCl	35%, p.a.	Penta	Czech Republic
$CaCl_2$	p.a.	Lach-ner	Czech Republic
Na_2SO_4	p.a.	Lach-ner	Czech Republic
Tris(hydroxymethyl)-aminomethane	Pure	Penta	Czech Republic

Hydroxyapatite particles used for the preparation of composite polycaprolactone/hydroxyapatite fibres were prepared as follows. The nanoparticles were prepared via co-precipitation method followed by hydrothermal treatment. The co-precipitation was achieved by mixture of two solutions. The first solution was prepared by dissolution of calcium nitrate hexahydrate in distilled water to obtain 14.5 wt.% solution. The basicity of the solution was modified by adding ammonium hydroxide to achieve pH = 10. The second solution was 6 wt.% solution of diammonium hydrogen phosphate in distilled water. Continuously stirred at room temperature, the diammonium hydrogen phosphate solution was drop added into the calcium nitrate solution to obtain Ca/P molar ratio precisely equal 1.67. The resulting suspension was then stirred for one hour. The suspension was then hydrothermally treated at 200 °C for 5 hours (described in detail in [102]). After the treatment, the suspension was washed in distilled water to reach neutral pH and finally in isopropyl alcohol. The obtained powder was characterized by X-Ray diffraction analysis (XRD, SmartLab 3 kW, Rigaku, Japan) and the morphology of the particles was analyzed by scanning electron microscope (SEM, Verios, FEI, Czech Republic).

4.2 Precursors preparation and characterization

4.2.1 Polycaprolactone and polycaprolactone/hydroxyapatite precursors

To obtain a uniform fibrous structure, an appropriate polymer-solvent system suitable for electrospinning had to be chosen. The examined solvents are listed in Table 6. The solvents were chosen according to the literature sources. The final solvent selection was based on the spinnability of the precursor and morphology of the resulting fibres. Another considered criteria was also (non)toxicity of the chemicals.

Table 6 Examined basic precursor systems for electrospinning

Solution name	PCL concentration [wt.%]	Dissolution agent	Dissolution agent ratio
10Cl	10	$CHCl_3$	-
13AAFA	13	Acetic acid	1
		Formic acid	1
10AA	10	Acetic acid	-
10FA	10	Formic acid	-
10AAFA	10	Acetic acid	1
		Formic acid	1
10AAFA2	10	Acetic acid	1
		Formic acid	3
10AAFA3	10	Acetic acid	3
		Formic acid	1

The composite precursor contained hydroxyapatite nanoparticles that were intended to improve the biocompatibility and bioactivity of the electrospun structure. The precursor for the composite nanofibres contained 6 wt.% of polycaprolactone and 5 wt.% of hydroxyapatite nanoparticles in acetic and formic acid in weight ratio 3:1 (the solvent system was based on the precursor system for the neat polycaprolactone fibres that was evaluated as the best considering morphology of the prepared nanofibers and minimum amount of defects present at the electrospun structure). At first, the acetic and formic acid were mixed, then the hydroxyapatite particles were added, and the solution was dispersed by ultrasound probe Sonopuls 2450 (Bandelin, Germany) for 3 minutes. Finally, the polycaprolactone was added to the dispersion, and the solution was mixed for 5 hours.

The best precursor from Table 6 – 10AAFA3, which was chosen according to the uniformity of the resulting fibres morphology – and the precursor for the composite fibres were characterized via dynamic viscosity measurement on a rotational rheometer (HAKE MARS II, Thermo Scientific, Karlsruhe, Germany) equipped with parallel plate geometry. The measurement was provided at the temperature of 25 °C in the shear rate range from 1000 to 1 Hz. To map time changes of the precursor quality, the neat polycaprolactone precursor measurement was done after 5 hours, 1 day, 3 days, 5 days and 7 days of the solution preparation. The precursor for composite fibres was analyzed after 5 hours after the preparation.

4.2.2 Artificially porous polycaprolactone nanofibres

The artificial porosity of the PCL fibres could not be achieved in the same way as in [34] because of the 4SPIN (Contipro, Czech Republic) setup used for nanofibres preparation in this work. The equipment does not allow the placing of NaCl reservoir above the collector (due to the lack of space and potential

disrupting of the air flow in the electrospinning chamber). Therefore, the PCL nanofibres' artificial porosity was meant to be achieved by incorporating of the NaCl crystals directly into the PCL precursor and subsequent electrospinning.

A saturated aqueous solution (36 wt.%) was prepared from 5 g of NaCl. Then the solution was rapidly dried at 100 °C to prevent the growth of large NaCl crystals. After that, the NaCl powder was crushed and added to the standard PCL precursor to obtain PCL : NaCl weight ratio 1 : 1. The precursor was then stirred for 1 hour to ensure dispersion of the NaCl particles in the solution.

4.2.3 Ceramic nanofibres precursor

Neat ceramic nanofibers would be an interesting structure for the bone tissue engineering as an individual constituent of a scaffold or as one of the structures in a more complex composite.

The precursor was prepared by a process based on sol-gel technique, according to Lee et al. [37], who described a process of hydroxyapatite nanofibres preparation via the electrospinning. At first, the calcium-phosphate sol had to be prepared. Ethanol based solutions were prepared from $Ca(NO_3)_2 \cdot 4H_2O$ and $(C_2H_5O)_3P$. After three hours of stirring, the $Ca(NO_3)_2 \cdot 4H_2O$ solution was dropwise added to the $(C_2H_5O)_3P$ solution to obtain molar ratio Ca/P = 1.67. The solution was then mixed at 40 °C for 24 hours and another 1 hour at 60 °C to partly evaporate the ethanol and increase viscosity of the solution.

20 wt.% solution of polyvinyl pyrrolidone (PVP) in ethanol was used as a polymer carrier for the ceramic fibres. The PVP and hydroxyapatite solutions were mixed in weight ratio 1:1 for at least 2 hours before the electrospinning.

4.2.4 Hollow nanofibres precursor

A system similar to [33] based on titanium oxide and polyvinyl pyrrolidone was proposed to verify the ability of the 4SPIN machine to prepare the hollow fibres. The polyvinyl pyrrolidone served as the core (which was intended to be burned out during subsequent calcination) and titanium oxide served as the shell. Polyvinyl pyrrolidone was dissolved in ethanol to obtain 15wt% solution used as the core precursor and as the polymer carrier for titanium oxide nanofibres.

To prepare the titanium oxide nanofibres, titanium propoxide was mixed with ethanol and stabilized by acetylacetone. This solution was then mixed with 15wt% solution of polyvinyl pyrrolidone in ethanol in weight ratio 1:1. The final solution was then mixed for 1 hour at the room temperature.

4.3 Fibres electrospinning and analysis

4.3.1 Polymer and composite nanofibres

4SPIN was utilized for electrospinning of the nanofibres. The rotating cylinder was chosen as the collector, and single syringe with an inner diameter of 0.686 mm (19 gauge in hypodermic needles sizing) was used as the emitter. The electrospinning setup, including detailed view of the emitter, can be seen in Figure 18.

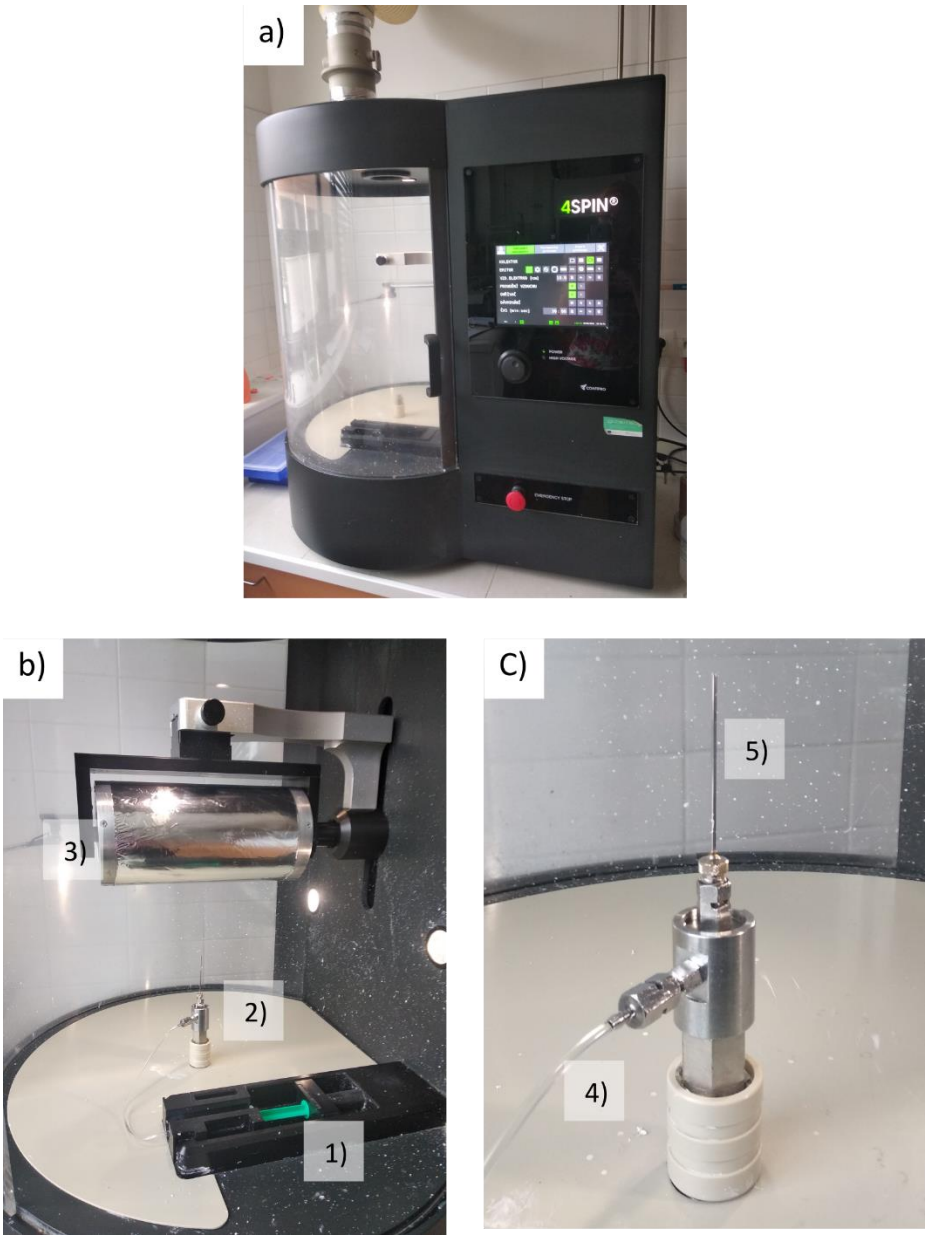

Figure 18 a) 4Spin (Contipro, Czech Republic); b) electrospinning setup: 1) syringe with the precursor, 2) emitter, 3) collector; c) detail of the emitter: 4) precursor supply tube, 5) needle

Electrospinning parameters varied depending on the precursor composition. The accelerating voltage varied from 15 to 25 kV and the feeding rate was set to obtain a visually stable electrospinning process. The parameters listed in Table 7 were set for all the precursors based on the acetic-formic acid system. The rotation speed of the collector varied according to intended fibres alignment – random fibres were collected at 100 rpm, parallel aligned fibres at 2000 rpm.

The fibres were collected for 30 minutes on aluminum foil for further analysis or a non-woven textile for further plasma treatment. If the samples were intended for biological testing according to ISO 10993-5 standard, the fibres were collected for 1 minute on thin glass plates with a diameter of 12 mm that were placed on the collector using duct tape. Such short electrospinning time ensured transparent samples suitable for the further *in-vitro* biological test.

Table 7 Electrospinning parameters for preparation of the neat polycaprolactone and the composite nanofibres

Accelerating voltage [kV]	Feeding rate [µl/min]	Emitter-collector distance [mm]	Temperature [°C]	Air flow [l/min]
20	28	100	35	25

The electrospun fibres were analyzed using SEM (Verios, FEI, Czech Republic). Several photos of each sample were taken for fibres diameter measurement. At least 100 values of the fibre diameters were measured from the photos for each sample. Then values of average diameter and standard deviation were calculated.

Types of the prepared sample structures are listed in Table 8. The marking of the samples is then used for all the tests and analysis done on the structures.

Table 8 Marking of the samples used for subsequent analysis and testing

Marking	Material	Structure	Plasma surface treatment
PCL-1	Polycaprolactone	Continuous layer	No
PCL-2	Polycaprolactone	Random fibres	No
PCL-3	Polycaprolactone	Random fibres	Yes
PCL-4	Polycaprolactone	Parallel fibres	Yes
PCL/HA-1	Polycaprolactone + hydroxyapatite particles	Continuous layer	No
PCL/HA-2	Polycaprolactone + hydroxyapatite particles	Random fibres	No
PCL/HA-3	Polycaprolactone + hydroxyapatite particles	Parallel fibres	No
PCL/HA-4	Polycaprolactone + hydroxyapatite particles	Random fibres	Yes
PCL/HA-5	Polycaprolactone + hydroxyapatite particles	Parallel fibres	Yes

4.3.2 Artificially porous polycaprolactone nanofibres

The artificially porous nanofibres were electrospun using the parameters listed in Table 9. The parameters are similar to the neat PCL and PCL/HA composite fibres, but the precursor's feeding rate had to be increased due to increased viscosity of the precursor and occasional clogging of the emitter needle.

After the electrospinning, part of the product was rinsed into distilled water to dissolve the NaCl crystals to achieve the desired porosity. Then the as-spun and water-rinsed fibres were analyzed using SEM (Verios, FEI, Czech Republic).

Table 9 Electrospinning parameters of PCL nanofibres with artificial porosity

Accelerating voltage [kV]	Feeding rate [µl/min]	Emitter-collector distance [mm]	Rotation rate [rpm]	Temperature [°C]	Air flow [l/min]
20	45	150	100	35	25

4.3.3 Ceramic nanofibres

The hydroxyapatite precursor (the sol) was electrospun using 10 ml syringe, emitter needle with 1.14 mm inner diameter (17 gauge in hypodermic needles sizing) and rotating cylindrical collector. The optimum electrospinning parameters (based on the analyzed structures) are listed in Table 10. The fibres were collected for 30 minutes on the aluminum foil at room temperature.

Table 10 Electrospinning parameters for preparation of the hydroxyapatite nanofibres

Accelerating voltage [kV]	Feeding rate [µl/min]	Emitter-collector distance [mm]	Rotation rate [rpm]
25	36	200	100

The as-spun nanofibres were analyzed using thermogravimetric analysis (TGA, TG 96 CS Evol., Setaram Instrumentation, France) to set proper calcination temperature to obtain ceramic nanofibers (750 °C and 1050 °C). Both as-spun and calcined nanofibres were analyzed using SEM (Verios, FEI, Czech Republic). The calcined nanofibres were also analyzed by XRD analysis (SmartLab 3 kW, Rigaku, Japan) to specify the resulting phase composition.

4.3.4 Hollow fibres

The core-shell arrangement of the emitter (mentioned in chapter 2.3.2) was used for preparation of the hollow fibres. The titanium oxide precursor served as the shell solution and it was pumped through the outer needle with diameter 1.372 (15 gauge in hypodermic needles sizing). The neat polyvinyl pyrrolidone was used as the core precursor and diameter of the inner (core) needle was 0.686 mm (19 gauge in hypodermic needles sizing). The fibres were collected on the cylindrical collector covered with aluminum foil. The electrospinning parameters are listed in Table 11. After the electrospinning, the fibres were peeled off the aluminum foil for further calcination in a furnace (Furnace Classic 1150M-f).

Table 11 Electrospinning parameters for preparation of the hollow ceramic fibres

Accelerating voltage [kV]	Feeding rate [µl/min]	Emitter-collector distance [mm]	Rotation rate [rpm]
40	70	170	100

Pure PVP was analyzed by TGA (TG 96 CS Evol., Setaram Instrumentation, France) to find the optimum calcination temperature – the polymer had to be removed completely from the structure, but ceramic grain growth had to be prevented. Therefore, the calcination temperature was stated at 50 °C above the PVP degradation temperature (750 °C).

4.4 Mechanical testing

The mechanical testing was done at the Friedrich-Alexander University of Erlangen-Nuremberg. The as-spun neat polycaprolactone and composite structures were examined by uniaxial tensile strength test using a universal testing machine (K. Frank GmbH, Germany). Samples PCL-2, PCL-3, PCL/HA-2 and PCL/HA-3 were mechanically tested (the parallel aligned fibres were tested along the fibres' longitudinal direction). The tested area of the samples was a rectangle 5 mm wide and 20 mm long. To ensure correct placement of the sample in the testing machine's jaws and avoid any pre-stress, the tested material was cut into 5 x 40 mm rectangle and placed into a paper frame (see Figure 19). The sample in the paper frame was placed to the testing equipment, the paper was cut, and the measurement was provided.

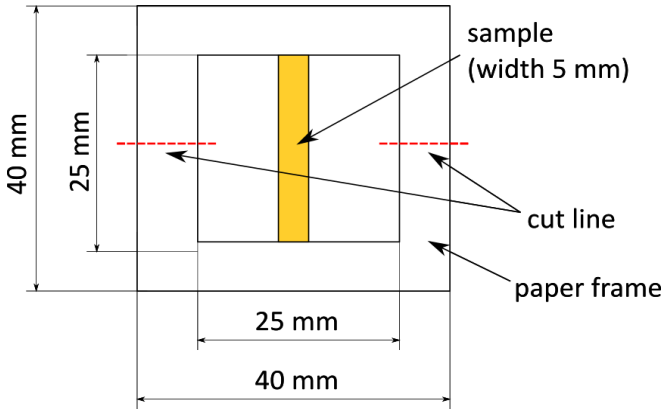

Figure 19 Scheme of a paper frame for mechanical testing

Always at least 10 pieces of each sample were tested to obtain enough values for estimation of Young modulus, tensile strength and relative elongation. The highest and the lowest values were always removed from the assessment of the mean values to avoid some statistical errors. Number of tested samples is listed in Table 12.

Table 12 Samples tested by uniaxial tensile test

Samples marking	Fibres composition	Fibres alignment	Number of tested samples
PCL-2	PCL	Random	15
PCL-3	PCL	Parallel	12
PCL/HA-2	PCL/HA	Random	15
PCL/HA-3	PCL/HA	Parallel	11

4.5 Surface treatment

The surface treatment process was designed in respect to the thermal sensibility of polycaprolactone (the meting point of polycaprolactone is 60 °C). Therefore, argon plasma generated by diffuse coplanar surface barrier discharge was chosen as a suitable treatment. The process was held in flowing argon (3 sccm) at the pressure of one atmosphere. Both polycaprolactone and composite random fibres were plasma-treated, as well as the hydroxyapatite nanoparticles.

The DCSBD electrode system consists of a pair of coplanar comb-like energizing electrodes with linear strips of 1.5 mm width and 1 mm lateral separation, screen-printed on the transformer oil insulated

face of 0.6 mm thick 96% Al_2O_3 dielectric plate. Upon energizing by 15 kHz sinusoidal high voltage at an input power of 90 W, a thin 0.3 mm layer of argon plasma was generated over the Al_2O_3 dielectric plate, covering an area of 8 × 20 cm^2. The treated samples were fixed at a height of approx. 0.1 mm above the discharge electrode, by a fine PET mesh (SEFAR PET 1500, 32/83-70 PW) inserted between the sample and the discharge electrode (see Figure 20). All the samples were treated for 30 s.

The effect of the plasma treatment lays in dissociative reactions of molecules adhered on the substrate surface. The argon atoms are excited to reach e.g. Ar $1s_5$ or one of the metastable states and they transfer their energy towards the atoms and molecules on the substrate surface (for example, water steam or adhered gases from the surrounding environment). New functional polar groups improving hydrophilicity are formed on the substrate surface.

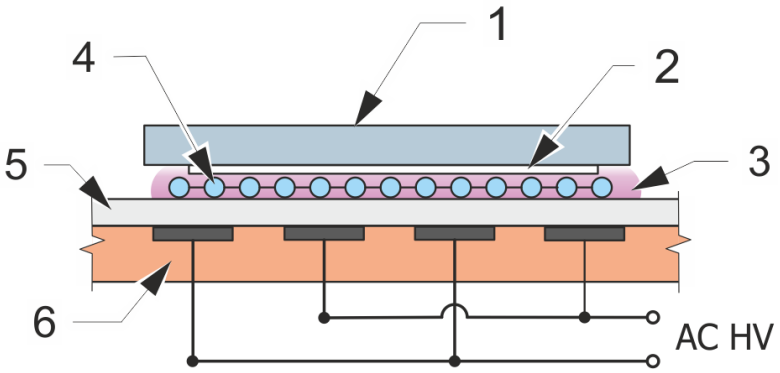

Figure 20 Scheme of plasma treatment set-up: (1) PP textile substrate; (2) treated PCL sample; (3) Ar discharge plasma; (4) spacer from PET mesh; (5) Al2O3 electrode; (6) cooling medium.

Both microscopical and macroscopical effect of the plasma treatment was evaluated. The microscopical effect was analyzed by X-ray photoelectron spectroscopy (XPS) by AXIS SupraTM (Kratos Analytical, United Kingdom). The analysis was done on the samples (hydroxyapatite particles, polycaprolactone and composite fibres) before and after the plasma treatment.

The macroscopical influence of the plasma treatment was evaluated by contact angle measurement by the sessile drop method.

4.6 Biological testing

Three types of biological tests were done on the electrospun structures. At first, the bioactivity of the structures was examined by immersion in simulated body fluid. To accelerate the bioactivity test, 1.5 multiple SBF was used. The amount of the chemicals was the same as it is listed in Table 4 for standard SBF, but the deionized water amount was reduced from 1000 ml to 666 ml to achieve the required concentration. The SBF was mixed according to the Kokubo protocol [44] including careful temperature and pH control. To provide the SBF test correctly, unique polyurethane filament holders were 3D printed (see Figure 21). 15 mm x 15 mm pieces were cut from the fibrous samples (neat polycaprolactone, composite and plasma treated random composite fibres), detached from the substrate (aluminum foil or non-woven fabric), placed onto the holders and the loose edges of the samples were cut away. The samples were then immersed into 15.6 ml of the 1.5 SBF. 4 samples of each structure were tested for mapping gradual hydroxyapatite formation on the surface of the fibres

after 1, 3 and 7 days of the immersion. During the SBF test, the pH value was measured to observe changes of the solution during the hydroxyapatite precipitation.

Figure 21 Sample holder for the SBF test, a) empty holder; b) holder with a sample

The second biological test was provided according to ISO 10993-5 standard in a certified laboratory at the University of South Bohemia, Faculty of Fisheries and Protection of Waters, Department of Complex systems. The test principle lays in cell cultivation on the examined material and establishing the specific growth rate (a relative increase of the cell number in time) during 3 days of the test. Samples PCL-1, PCL-2, PCL/HA-1, PCL/HA-2, PCK/HA-4 and PCL/HA-5 were tested. Mouse fibroblasts of L9292 cell line were utilized for the test. Samples consisting of a thin material layer on the glass plate were used for this test. At first, the samples were disinfected under UV light for 30 minutes. Then they were placed into a plastic well, fixed using a carbon tape (see Figure 22). Then nutrient solution with the cell culture was spilt on the sample surface. The sample was then placed under a confocal microscope (Zeiss, Germany) and observed for three days. At least five view fields were observed for each sample, and an image was taken every two minutes. Then the cell number was estimated on the images after 30 minutes, 24, 48 and 72 hours. Specific growth rate (SGR, growth of the cell number during a time interval) was then estimated from the received results and then the SGR was compared with the SGR of the baseline sample.

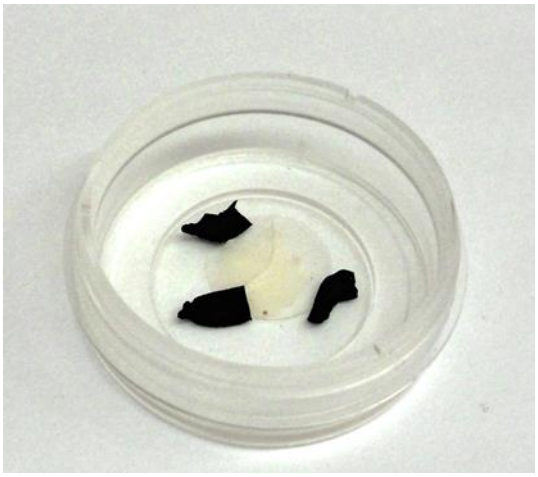

Figure 22 A sample prepared for ISO 10993-5 biological test

However, this method is rather time-consuming, and another disadvantage are high equipment device – each sample needs its own microscope with camera, meaning that all the samples cannot be tested simultaneously. It does not only prolong the test duration, but it can also slightly deform results of the test – the cells are living organisms which are continuously proliferating and, hence changing the

existing colony. Therefore, only results obtained in a short time range can be compared with each other and the longer it takes to test all the samples, the higher is the risk of the cell colony change and obtaining misrepresenting results.

Therefore, another biological test – WST-8 assay (PromoCell, Germany) was done at Friedrich-Alexander University of Erlangen-Nuremberg, Faculty of Engineering, Institute of Biomaterials. The WST-8 test allows simultaneous examination of many samples – the number of tested samples is limited only by number of wells in the testing plate, usually 96-well plate is used. Therefore, all the samples listed in Table 8 could be tested at the same time, including negative control (the contrast medium without any cell culture in the dish). Always three pieces of each sample were cultured. The samples were placed to the cylindrical holders (same as for the SBF test) and densified under UV light for 30 minutes. MG 63 cells, human osteoblast-like cells, European Collection of Authenticated Cell Cultures (Sigma Aldrich, Germany), were used for the test. The cell colony was maintained in Dulbecco's Modified Eagle Medium (Gibco®, Thermo Fisher Scientific, USA) containing 10% v/v of fetal bovine serum (Sigma Aldrich®, Germany) and 1.0% v/v penicillin streptomycin (Thermo Scientific, Germany). The cell cultivation was performed in a humidified atmosphere of 95% air and 5% CO_2 at 37 °C and approximately 25 000 cells were seeded on each sample.

The WST-8 test was done on the samples after 1, 3 and 7 days of the test – the cultivation medium was removed from the samples, the samples were rinsed with PBS (phosphate buffer saline, Gibco®, Thermo Fisher Scientific, USA) and 10 v/v% WST-8 solution in DMEM was added to the samples in the cultivation wells. After 4 hours of cultivation, the solution was removed from the cultivation dish and placed into wells suitable for the absorbance measurement. The wells with the samples were then filled with the DMEM/fetal bovine serum/ penicillin streptomycin solution again. The absorbance of the contrast medium was measured at 450 nm using PHOmo Elisa reader (Autobio Diagnostics Co. Ltd., China). Always three samples of the contrast medium were taken from each sample and therefore nine values of the absorbance were obtained for each type of tested structure. The highest and the lowest absorbance value was deleted from the evaluation and the average value with standard deviation was stated from the data.

The cell culture was also analyzed qualitatively after the cultivation test using SEM (Verios, FEI, Cyech Republic). The preparation of the cultured samples was held as follows. At first, the cultivation medium was removed from the cultivation wells. Then the samples were rinsed with PBS twice. The samples were then immersed in a fixation buffer composed of glutaraldehyde, paraformaldehyde, sucrose, and sodium cacodylate trihydrate (Sigma Aldrich, Germany) for 2x 15 minutes. After that, the samples were gradually dehydrated in water/ethanol solutions with ethanol fraction ranging from 30 % in the first step to 98 % in the last step.

5 Results and discussion

5.1 Fibres preparation and characterization

5.1.1 Polycaprolactone and polycaprolactone/hydroxyapatite nanofibres

At first, the most suitable precursor was chosen to achieve the most uniform and defect-free fibrous structure. Optimization of precursor electrospinning included systems listed in Table 6. All the obtained structures are displayed in Figure 23. Fibres produced by electrospinning of precursor 10Cl (10 wt.% PCL in chloroform) were thick, and the structure was uniform (see Figure 23a). A better result was obtained from precursor 13AAFA (13 wt.% PCL in acetic and formic acid in ratio 1:1) when the thickness of the fibres was more uniform, but the structure contained many defects such as beads and balls of polycaprolactone (see Figure 23b). All the precursors based on 10 wt.% PCL solution in acetic and/or formic acid were more uniform compare to systems based on methanol or 13 wt.% PCL solution and the present defects were rare (see Figure 23c-g). Thus, precursor 10AAFA3 (10 wt.% solution of PCL in acetic and formic acid in ratio 3:1) was chosen as the best candidate and uniformity of the obtained structure was supported by heated air blowing during the electrospinning (resulting structure is in Figure 23h). The heated air helped solvent evaporation from the arising fibres and hence prevented the bead formation.

Further, the hydroxyapatite nanoparticles were synthesized by the precipitation synthesis with the hydrothermal treatment. Figure 24a and b show a microstructure of the as-synthetized hydroxyapatite powder consisting of highly agglomerated ball-like particles. After the hydrothermal treatment, the hydroxyapatite morphology changed into needle-like particles approximately 500 nm long and 30 nm thick (see Figure 24c and d). Such morphology promises a good possibility to incorporate the particles into the electrospun fibres to prepare a composite fibrous structure. The XRD analysis confirmed the synthetized powder's phase composition – see Figure 25 XRD analysis of the hytrothermally treated hydroxyapatite powder, the star-marked peaks correspond to peaks typical for hydroxyapatite. The relatively wide peaks of the hydroxyapatite are caused by diffraction of the X-rays on the nanometric particles. The EDX analysis of the powder confirmed chemical composition typical for hydroxyapatite – the measured Ca/P ratio was 1.67 which corresponds to the stoichiometric composition of the neat hydroxyapatite.

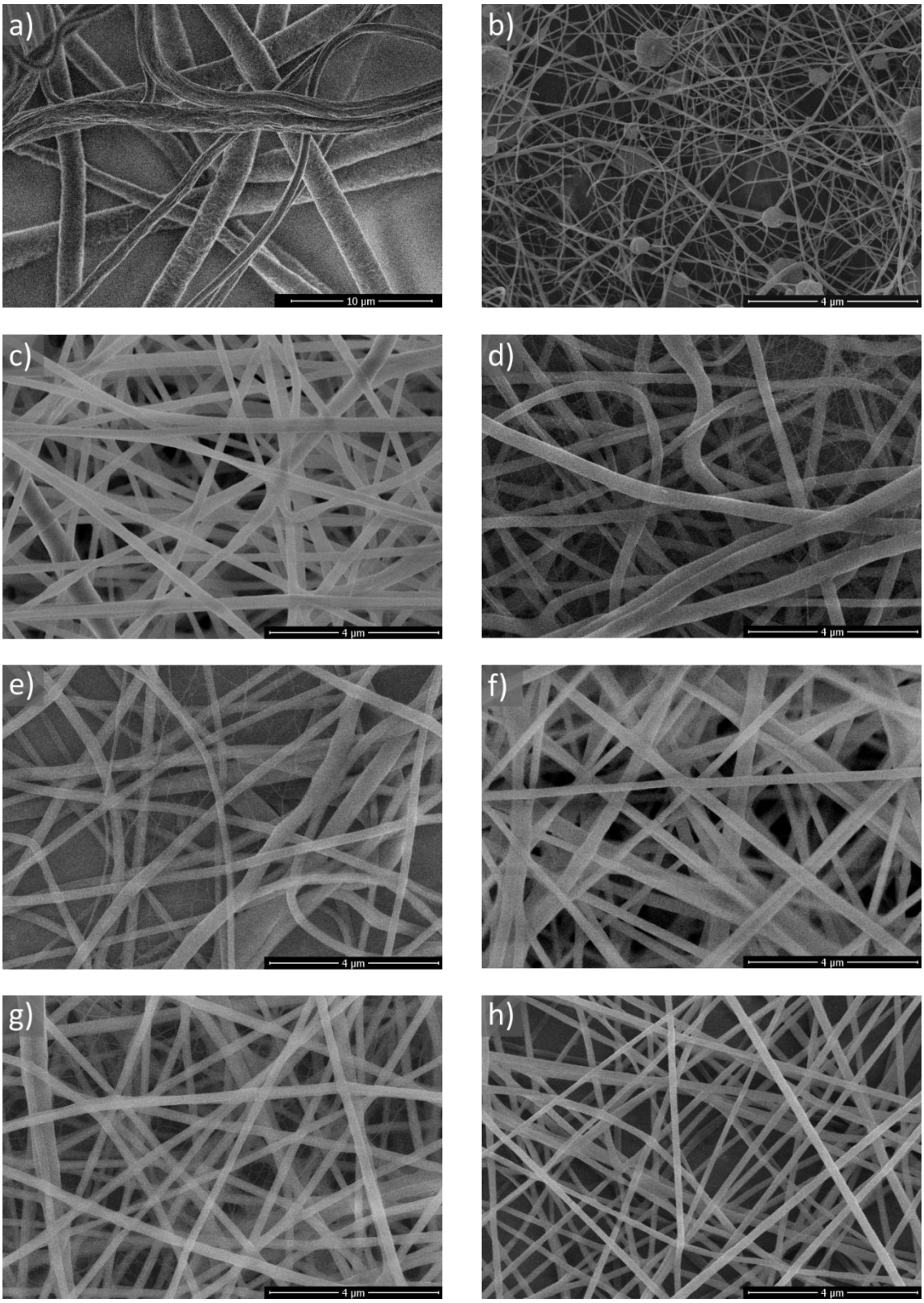

Figure 23 Structures obtained by electrospinning of various precursors, a) 10Cl, b) 13AAFA, c) 10AA, d) 10FA, e) 10AAFA, f) 10AAFA2, g) 10AAFA3, h) 10AAFA3 with heated air blowing during the electrospinning process

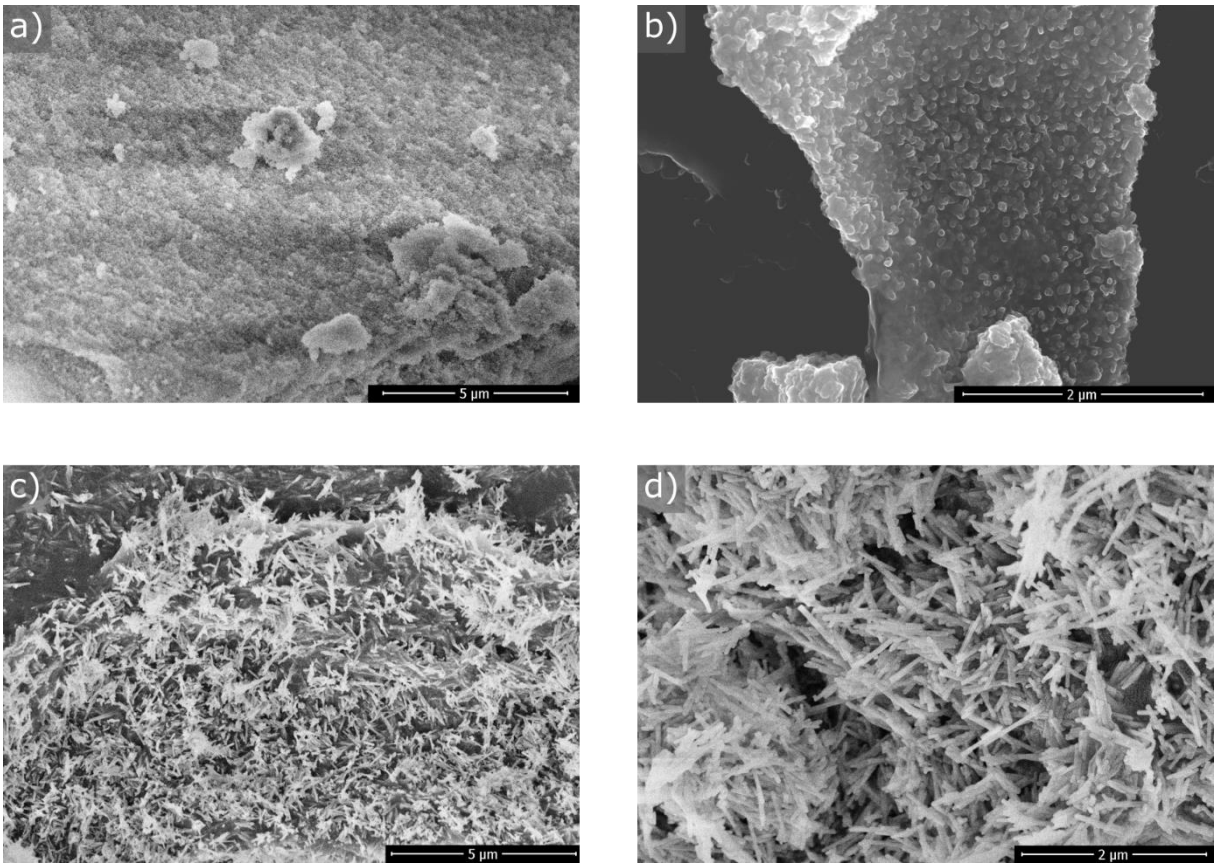

Figure 24 a), b) As-synthetized hydroxyapatite particles; c), d) hydroxyapatite particles after the hydrothermal treatment

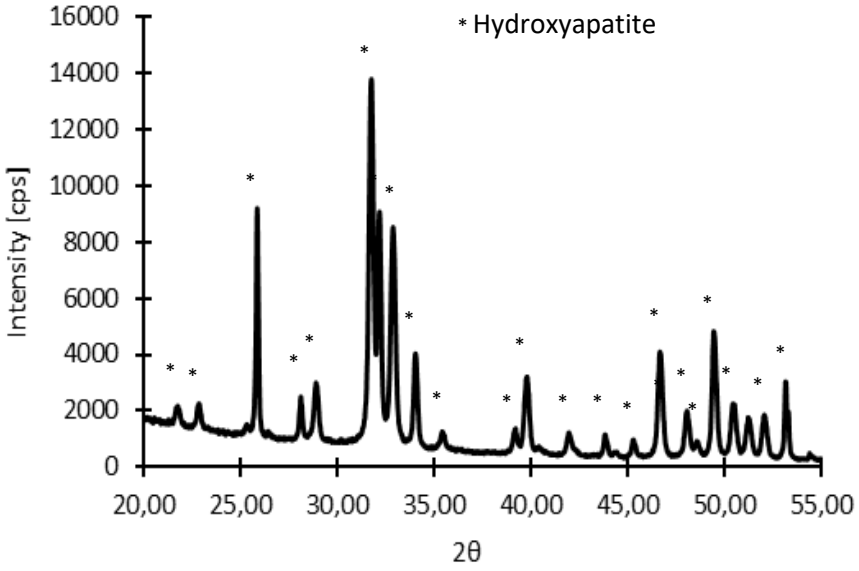

Figure 25 XRD analysis of the hytrothermally treated hydroxyapatite powder

The dynamical viscosity of 10AAFA3 (further named as PCL precursor) and the composite precursor was measured to describe and also compare the precursors properties. The dynamic viscosity η and

inner shear stress τ of the PCL precursor can be seen in Figure 26. Both dynamic viscosity and inner shear stress showed hysteresis probably caused by the polymer chains' organization under applied stress. The polymer chains' arrangement under the stress could help fibres formation during the electrospinning, especially during the parallel fibres formation. [103] The dynamic viscosity remained nearly constant during the measurement suggesting that PCL precursor behaves nearly as a Newtonian solution.

Behaviour of the composite (PCL/HA) precursor during the viscosity measurement was different, as shown in Figure 27. The shear stress hysteresis was nearly suppressed, probably caused by the hydroxyapatite particles preventing the polymer chains from the mutual arrangement. The dynamic viscosity showed so-called shear thinning, which is typical for suspensions. Under the applied shear rate, the phase separation occurs, making more space between the suspension components and resulting in considerable viscosity decrease. [104] The precursor viscosity changes under a mechanical stress can cause some fluctuations during the electrospinning process resulting in defects in the fibrous structure – e.g. areas lacking the hydroxyapatite particles and places rich on the ceramic phase.

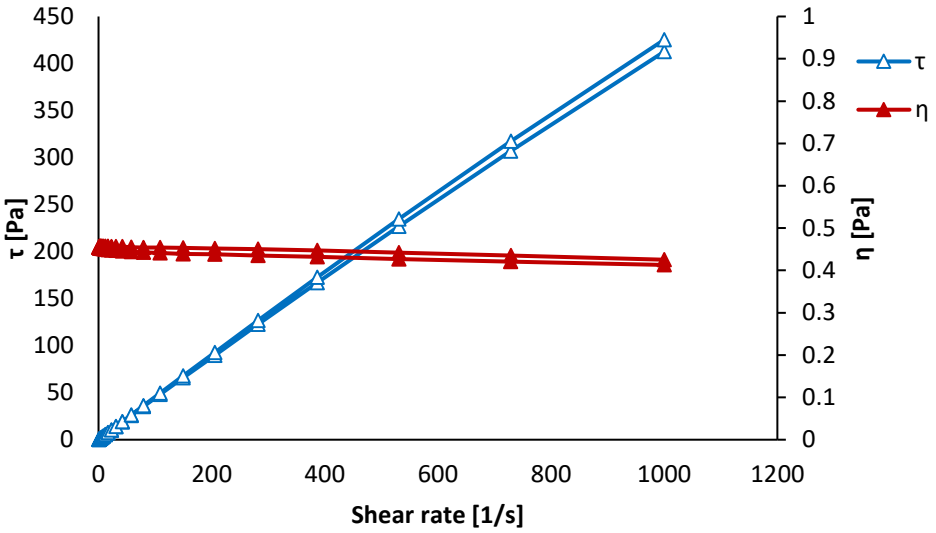

Figure 26 Dynamic viscosity η and inner shear stress τ of the PCL precursor

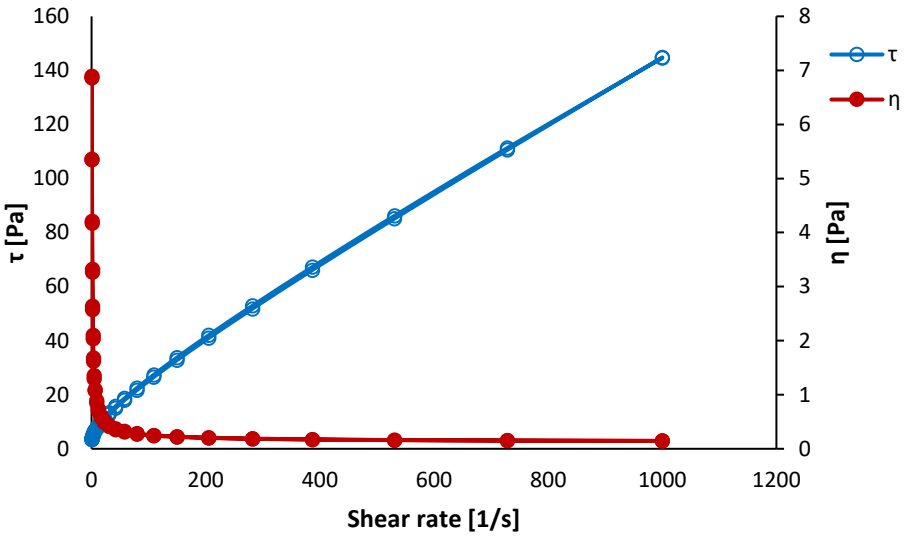

Figure 27 Dynamic viscosity η and inner shear stress τ of the composite precursor

The structures of as-spun neat polycaprolactone and composite nanofibres are shown in Figure 28 where the measured diameters' histograms are also displayed. The mean diameters and standard deviation of the fibres are listed in Table 13. It is evident that random polycaprolactone (PCL-2, Figure 28a) and composite fibres (PCL/HA-2Figure 28c) have the same diameter but the standard deviation of the composite fibres is approximately twice larger (172 ± 60 nm and 171 ± 107 nm, respectively). It is caused by hydroxyapatite particles agglomerates making inhomogeneities in the structure. However, even the composite random structure did not contain any beads or drops of the precursor, suggesting instability of the process.

The higher rotation rate of the collector caused thinning of both polycaprolactone and composite fibres, see Figure 28b for parallel PCL fibres and Figure 28d for parallel composite fibres, the fibre thickness are summarized in Table 13. The fibres' thinning was more distinct by the polycaprolactone fibres – the diameter fell from 172 ± 60 nm (random fibres) to 124 ± 66 nm (parallel fibres). The decrease of the fibres thickness was not so distinct in the case of the composite fibres (from 171 ± 107 nm to 151 ± 75 nm). It was probably caused by the presence of the ceramic particles and their agglomerates which were not influenced by higher rotation speed of the collector. Therefore, the composite fibres are forced to have larger diameter to be able to carry the ceramic particles towards the collector. In other words, the thinner fibres cannot be formed which is visible in Figure 28d – the thinnest fibres do not contain the ceramic particles.

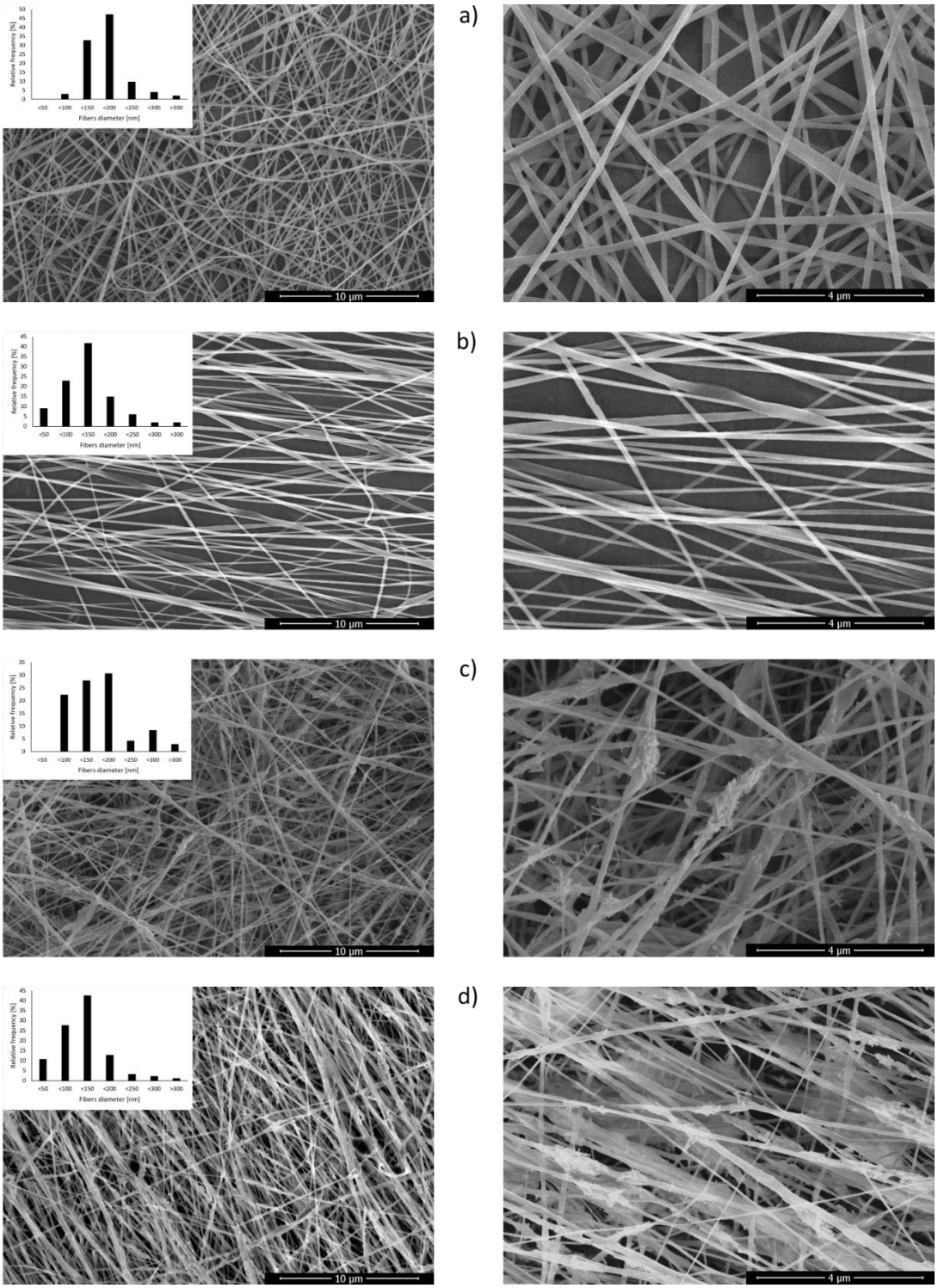

Figure 28 As-spun nanostructures, a) PCL random fibres (PCL-2), b) PCL parallel fibres (PCL-3), c) composite random fibres (PCL/HA-2), d) composite parallel firers (PCL/HA-3)

Table 13 Average diameter of the as-spun fibrous structures

Sample	Diameter [nm]
PCL-2	172 ± 60
PCL-3	124 ± 66
PCL/HA-2	171 ± 107
PCL/HA-3	151 ± 75

The plasma-treated samples did not show any structural changes as can be seen in Figure 29 and Table 13, where the average diameters of the samples are listed. The random plasma-treated PCL fibres (sample PCL-4, Figure 29a) had diameter 199 ± 64 nm, which is slightly higher than the untreated PCL-2 fibres but considering the standard deviation, the difference is not significant. The parallel plasma-treated PCL fibres had a diameter of 188 ± 49 nm. The decrease in the diameter was smaller than the difference between samples PCL-2 and PCL-3. Moreover, in Figure 29b there can be seen a wavy shape of the fibres in the longitudinal direction. The explanation of this phenomena lays in the substrate under the fibres – the non-woven textile used as the substrate for the plasma-treated fibres is not adhesive enough for the fibres. Therefore, the fibres can slide a little bit on the textile's surface and loose its straight direction (and hence loose the inner stress of the parallel fibres).

The plasma treated composite samples showed smaller diameter of the fibres (114 ± 60 for random plasma treated composite fibres - Figure 29c, sample PCL/HA-4 and 127 ± 41 for parallel composite fibres, sample PCL/HA-5 - Figure 29d), the difference between the diameters of as-spun and plasma-treated fibres was not significant. The substrate under the fibres did not play an important role in the morphology of the fibres – the higher surface roughness of the composite fibres probably prevented the fibres from sliding on the substrate.

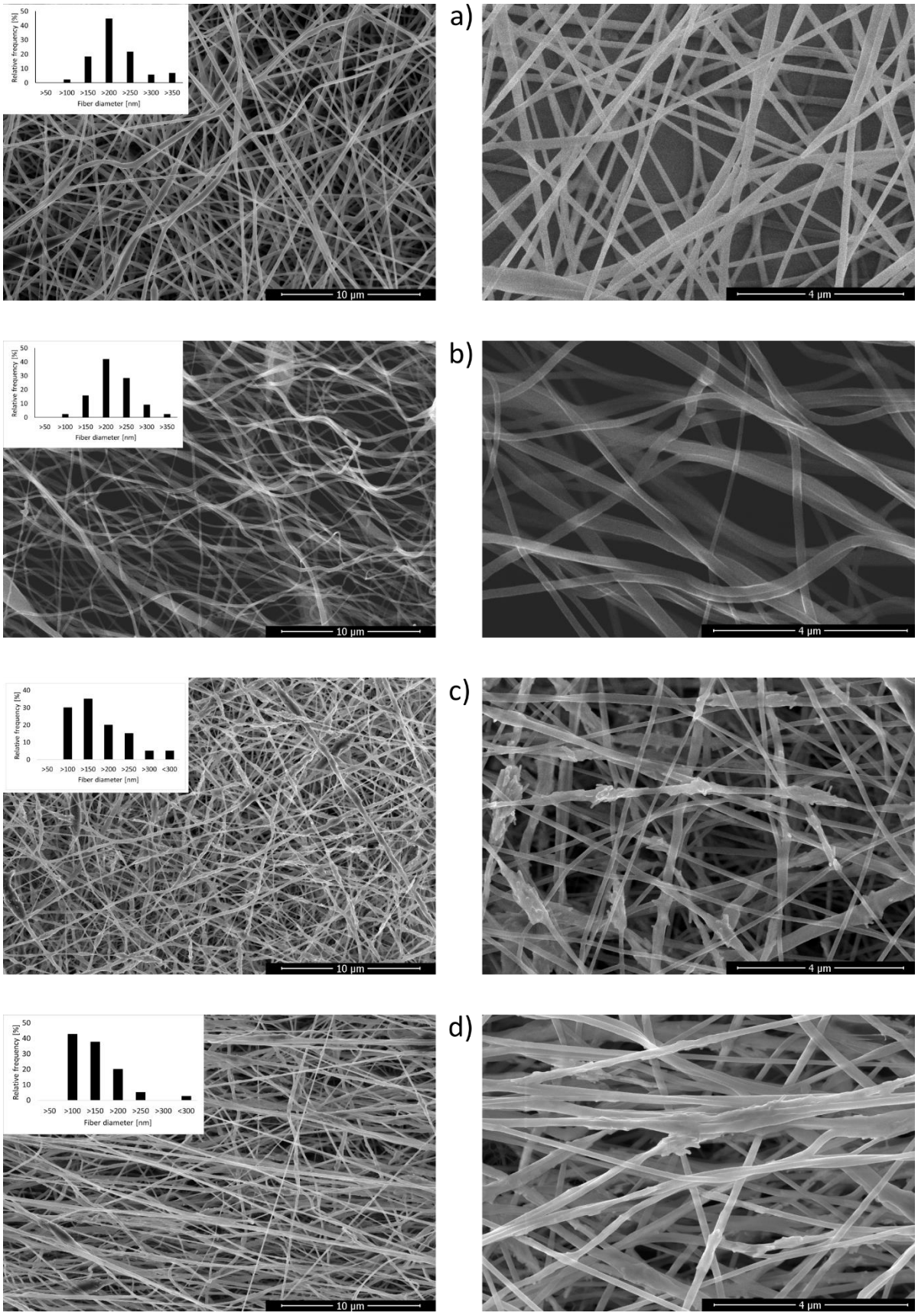

Figure 29 Plasma treated fibres, a) PCL-4 (random plasma treated PCL fibres), b) PCL-5 (parallel plasma treated PCL fibres), c) PCL/HA-4 (random plasma treated composite fibres), d) PCL/HA-5 (parallel plasma treated PCL/HA fibres)

Table 14 Average diameter of the plasma treated fibrous structures

Sample	Diameter [nm]
PCL-4	199 ± 64
PCL-5	188 ± 49
PCL/HA-4	114 ± 60
PCL/HA-5	127 ± 41

Mechanical tests

It is generally difficult to compare the measured data to literature since the morphology (mainly fibres thickness) of the neat polycaprolactone meshes varies according to the electrospinning parameters and precursor composition. Mubyana et al. [105] proved dependence of the polycaprolactone fibres mechanical properties on the specimen geometry – most of the characteristics (maximum stress, toughness, Young modulus) were growing with increased specimen thickness (meaning length of the electrospinning process) and this dependence is more distinct by the aligned fibres. The only more or less constant characteristic was failure strain, which depended only on the organization of the fibres (random/parallel). Results of the mechanical tests of the structures prepared and analyzed by Mubyana et al. are displayed in Figure 30 (unfortunately, raw measured data was not available). Thickness of the analyzed fibrous meshes are listed in Table 15. [105]

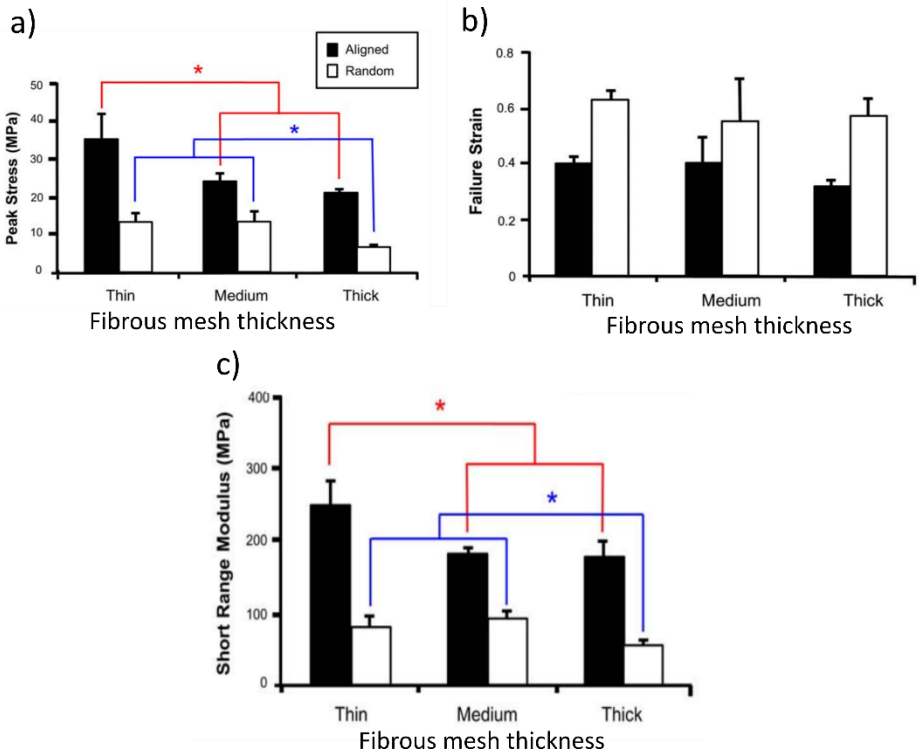

*Figure 30 Mechanical characteristics of the PCL fibers with different directional alignment and thickness of the fibrous meshes; a) peak (failure) stress, b) failure strain, c) short range (elastic) modulus; * means p < 0.05 [105]*

Table 15 Thickness of the fibrous meshes from [105]

Mesh thickness	Parallel [μm]	Random [μm]
Thin	18.64 ± 1.96	17.88 ± 2.14
Medium	52.18 ± 1.43	36.18 ± 1.30
Thick	75.63 ± 4.88	164.52 ± 10.21

Results of the mechanical tests provided for this thesis are in Table 16. The fibres parallel alignment (for both neat polycaprolactone and composite fibres) increased the elastic modulus and failure strain, but it considerably decreased the failure strain. The failure strain's difference can be explained by gradual alignment of the random fibres along the direction of the mechanical load, whereas the parallelly aligned fibres do not have any possibility to react to the applied load. The failure strain of the neat polycaprolactone random fibres (PCL-2) was considerably higher than value measured by Mubyana et al. that can be explained by different rotation speed of the collector during the electrospinning. In contrast, for this thesis only 100 rpm was used, Mubyana et al. collected the random fibres at 500 rpm. From our experience, already 300 rpm of the collector slightly organizes the fibres direction, which influences the structure's mechanical properties. [105]

Elastic modulus was significantly higher by the parallelly aligned fibres which was again in agreement with Mubyana et al. It can be explained by higher tension needed to reach the same elongation as the elongation of the random fibres. The reason for this phenomenon is the same as for the elongation difference – since the parallel fibres are already aligned along the direction of the mechanical load; it is the material itself that is stretched. The difference of the values listed in Table 15 and Table 16 probably lay in the different rotation speed (random fibres, sample PCL-2) and different thickness of the fibrous mesh (for parallel fibres, sample PCL-3).

The failure stress also increased with the alignment of the fibres. The measured values were higher than values from the literature, which can be again explained by the different thickness of the tested samples.

Table 16 Mechanical tests results of the selected samples

Sample	Elastic modulus [MPa]	Failure strain [%]	Failure stress [MPa]
PCL-2	20 ± 9	130 ± 19	19 ± 6
PCL-3	354 ± 47	32 ± 3	67 ± 9
PCL/HA-2	24 ± 5	81 ± 10	8 ± 1
PCL/HA-3	307 ± 13	33 ± 5	42 ± 8

The ceramic particles incorporated into the polymer matrix influenced the mechanical properties of the tested structures. The most significant difference was observed by the tensile stress – the ceramic particles behaved as stress concentrators and weakened the fibrous structure, and hence lower stress was needed for the sample collapse. The influence of the ceramic particles was more distinct for the random fibres (samples PCL-2 and PCL/HA-2), when the failure stress of the sample PCL/HA-2 was approximately 2.4x lower than failure stress of the sample PCL-2. The sample PCL-3 (parallel polycaprolactone fibres) failure stress was approximately 1.6x higher than failure stress of the sample PCL/HA-3 (parallel composite fibres).

Two phenomena can explain the difference. First, the fibres and the ceramic particles are aligned during collecting of the parallel fibres and hence the ceramic particles are placed mostly inside the

fibres. This arrangement is more effective for the mechanical loading because the fibre walls are not damaged by the particles randomly sticking out from the fibres. However, this theory was not confirmed by the SEM and EDX analysis (the analysis was not sensitive enough to distinguish the precise particles' positions in the thin fibres).

Second explanation relates to the collapse of the mechanically stressed fibres – when a composite fibre is torn, the damage is most probably near a ceramic particle. When the fibre collapses, the ceramic particle is exposed. It can damage the surrounding fibres, mostly in the direction of the mechanical load, meaning that in the random structure, there is a higher probability of damaging other fibres than in the parallelly aligned structure. This process would explain the stronger effect of the ceramic particles on the failure stress as well. For a better image of the described situation, see Figure 31. In Figure 31a and b there is a random composite structure during a tensile stress – the structure can react to the applied mechanical load, but when some fibres collapse, the ceramic particles are partly freed. The green lines suggest a further trajectory of the loose ends of the ceramic particles, disrupting other fibres and accelerating the whole structure's damage. In Figure 31c and d there is a parallel fibrous structure before and during the tensile stress, respectively. When a fibre is damaged in the parallel structure, disrupting neighboring fibres is smaller thanks to the direction alignment.

The already mentioned principles can also explain the influence of the ceramic particles on the failure strain when the parallel fibres are not affected by the presence of the particles, but there is a considerable decrease of the failure strain by the random fibres (the sample PCL-2 has 1.6x higher failure strain than the sample PCL/HA-2).

However, the situation is different by the elastic modulus, which is (also considering the deviations) independent from the presence of the ceramic particles. Apparently, the mechanical properties depend on the matrix material at the first phase of the tensile test and are not affected by any filling of the fibres. This information confirms the theory mentioned above that the already broken fibres (specifically the loose ends of the ceramic particles) influence the surrounding fibres' behaviour.

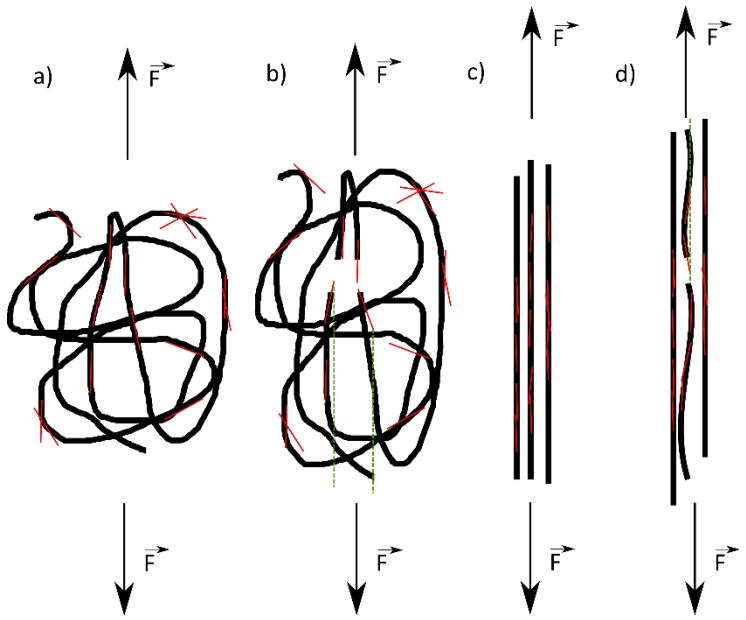

Figure 31 Influence of ceramic particles during the fibres collapse on the surrounding structure, a) random composite fibres before test, b) random composite fibres after a fibre collapse, c) parallel composite fibres before test, d) parallel composite fibres after a fibre collapse; green lines suggest further area to be influenced by a freed ceramic particle

Wettability

The samples' contact angle values (before and after the plasma treatment) are listed in Table 17. Three factors are influencing the contact angle of the samples – sample morphology (layer/fibres), presence of the hydroxyapatite and the surface treatment. The fibrous structures have considerably higher contact angle – see for example 75.5° ± 3.5° of PCL continuous layer (sample PCL-1) and 127.2° ± 4.1° of PCL random fibres (sample PCL-2). A similar situation happens also by the composite samples PCL/HA-1 and PCL/HA-2. The increase of the fibrous samples' contact angle is caused by so called lotus effect when the fine surface topography lowers the wettability even by hydrophilic materials. [106] The basic principle of the lotus effect is high energetic demands for the liquid to overcome the surface elements, and it is more beneficial for the liquid to create a liquid-gas interface.

The hydroxyapatite has considerably lower contact angle than the polycaprolactone (approximately 10° and 86°, respectively) [107], [108] therefore there is a rather large difference on the contact angle between samples PCL-1 and PCL/HA-1 (continuous layers) – from 75.5° ± 3.5° of PCL layer to 44.9° ± 1.7° of PCL/HA layer. Interestingly, the material influence disappears by the fibrous samples (PCL-2, PCL-3, PCL/HA-2, PCL/HA-3) when the topography effect overcomes the samples' surface chemistry. The fibres alignment did not affect the surface properties at all (sample PCL/HA-2 had contact angle 128.3 ± 3.6), which agrees with literature sources. [109] The largest influence on the wettability had the plasma treatment. The contact angle of the plasma-treated samples was unmeasurable. The water drop immediately spilt all over the sample surface, proving high effectivity of the surface treatment.

Table 17 Values of measured contact angle on the prepared samples

Sample	Contact angle [°]
PCL-1	75.5 ± 3.5
PCL-2	127.2 ± 4.1
PCL/HA-1	44.9 ± 1.7
PCL/HA-2	128.3 ± 3.6
PCL/HA-3	125.3 ± 5.1
PCL/HA-4	complete wetting
PCL/HA-5	complete wetting

The XPS analysis of the neat polycaprolactone fibres before the plasma treatment is displayed in Figure 32a, the results of the XPS analysis of the plasma-treated polycaprolactone fibers is in Figure 32b. The overall content of oxygen atoms increased by approximately 2 percentage points after the plasma treatment. From the deconvoluted O1s XPS spectra, it is evident that plasma broke C=O bonds by the simultaneous formation of new C-O and H-O-C bonds.

The XPS analysis of the composite fibres before and after the plasma treatment was done, but very low relative atomic content of Ca an P atoms prevented the analysis from any valid evidence. Therefore, the results of the XPS analysis of the ceramic particles alone were evaluated. As can be seen in Figure 33, there was no detected change of the XPS spectra of the ceramic particles constituents. There is two information emerging from this result – the low-temperature argon plasma energy is too low to anyhow affect the bonding in the ceramics, and the macroscopic change of the wettability is related to the changes on the polycaprolactone surface.

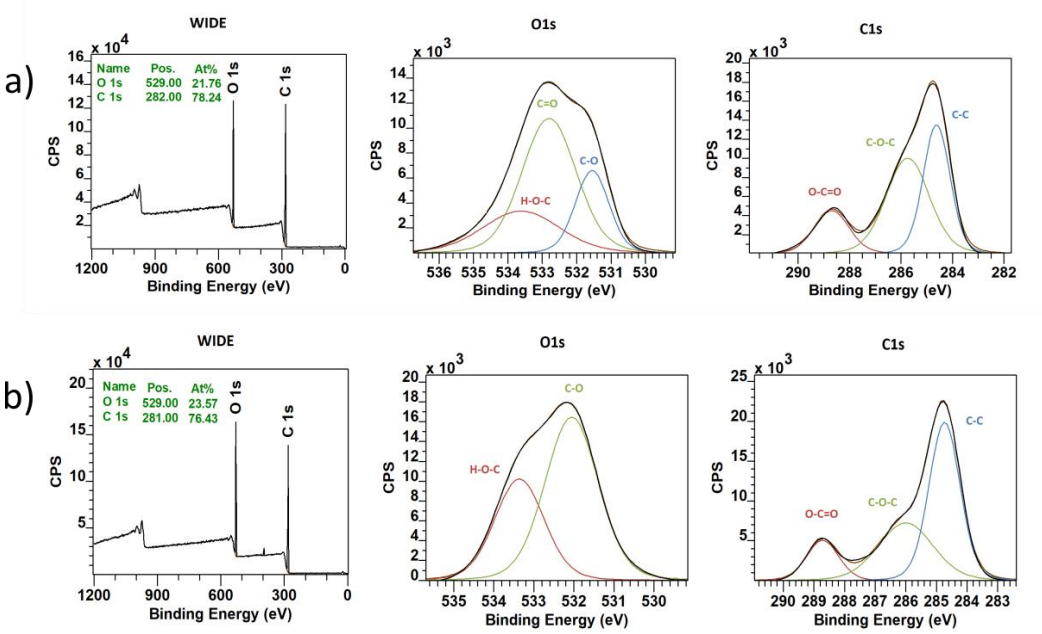

Figure 32 XPS analysis of the polycaprolactone fibres a) before, b) after the plasma treatment

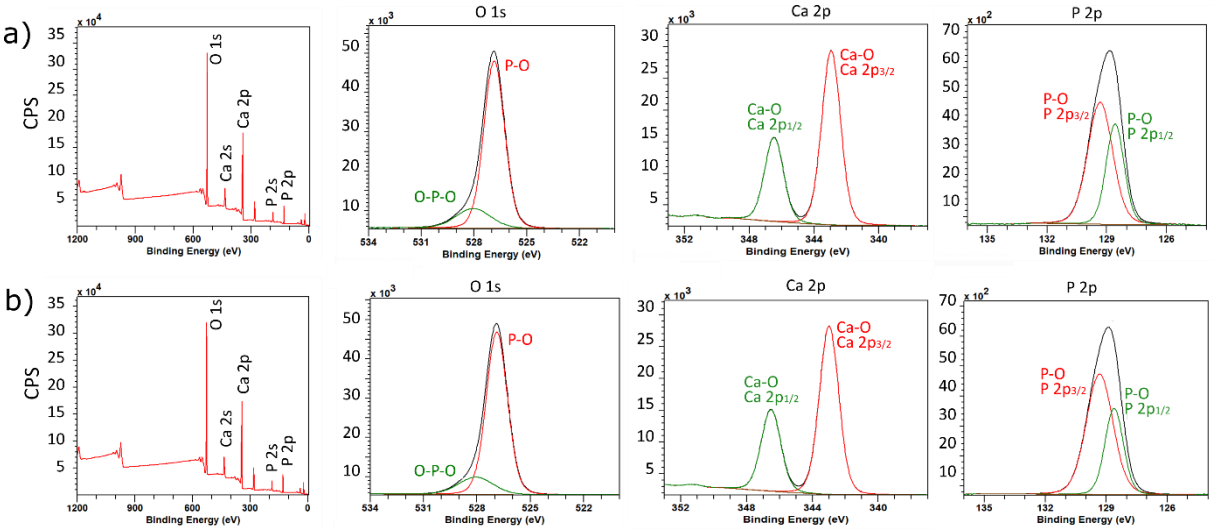

Figure 33 XPS analysis of the hydroxyapatite particles a) before, b) after the plasma treatment

5.1.2 Artificially porous nanofibres

In Figure 34, there is a photo of the NaCl crystals after the rapid drying. As can be seen, the precipitated crystals have a clearly cubic crystallographic structure. However, the size of the crystals was rather inhomogeneous, ranging from 10^1 nm to 10^0 μm.

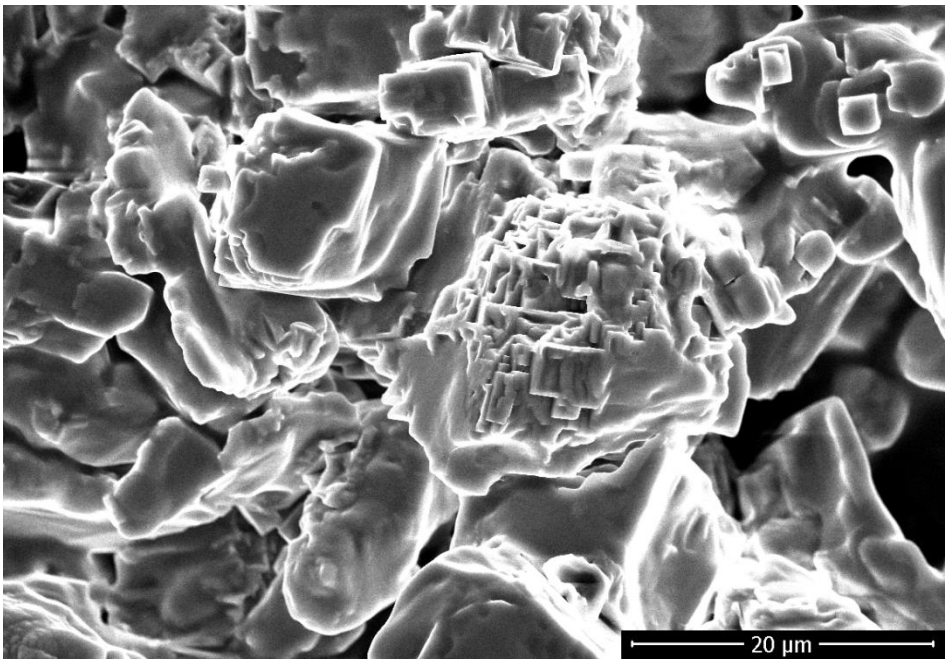

Figure 34 NaCl crystals after the drying

Figure 34a shows as-spun PCL fibres with small (10^1 nm) NaCl crystals inside the fibrous structure. The large NaCl crystals were stuck in the syringe with the un-spun precursor – the crystals were too heavy to be pumped into the emitter. Therefore, the submicroscopic NaCl crystals in the PCL nanofibres did not change the fibres' morphology (the fibres diameter was approximately 170 nm).

In Figure 35b, there are the PCL nanofibres after rinsing in the distilled water. As can be seen, the NaCl crystals present on the fibres' surface were dissolved, creating the nanofibres' wavy surface. However, the desired effect was not achieved – the inter-fibres spaces did not reach dimensions comparable to the size of the cells. The desired effect would be achieved by incorporation of larger NaCl particles into the fibres. However, using our electrospinning setup, there is no possibility of such result – large NaCl crystals would be left in the syringe. A better approach would be spreading of the NaCl particles onto the collector during the electrospinning process. However, the current electrospinning equipment does not allow such workflow (there is no space for the NaCl container). Therefore, a setup modification would be necessary for successful high-porous structure preparation.

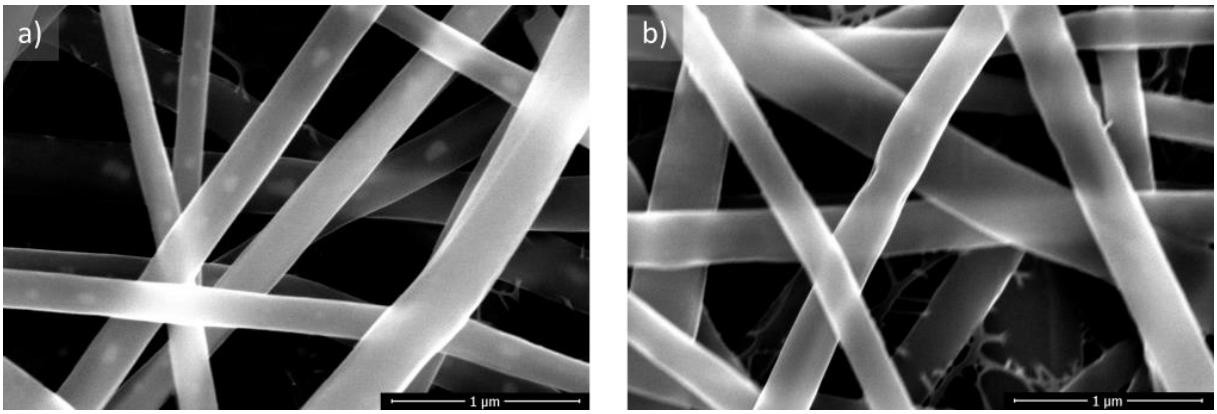

Figure 35 a) As-spun PCL nanofibres with incorporated NaCl crystals; b) PCL nanofibres after dissolution of NaCl crystals in distilled water

5.1.3 Ceramic nanofibres

Results of the approach to neat hydroxyapatite nanofibers preparation are described in this chapter. In Figure 36, there can be seen as-spun hydroxyapatite nanofibres still containing the polymer constituent. Morphology of the fibres differs from the PCL and PCL/HA nanofibres from chapter 5.1.1. The fibres have so-called ribbon morphology – their cross-section is flat, not round. The width of the as-spun fibres was approximately 1.5 µm, the thickness was approximately 0.5 µm. The fibres flat morphology formation can be explained by fast ethanol (solvent) removal from the fibres surface as was described in chapter 2.3.3.

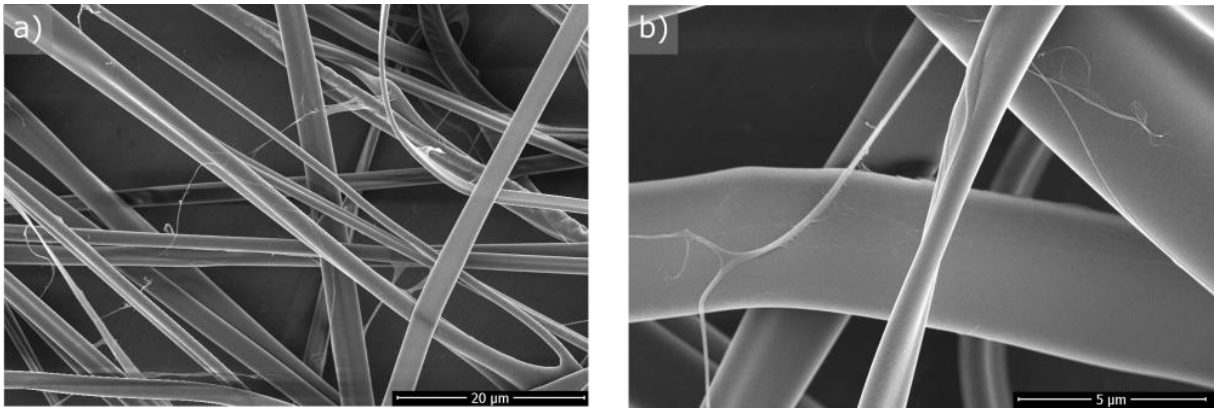

Figure 36 As-spun hydroxyapatite fibres (still containing PVP); a) overview, b) detail

In Figure 37, there is a result of the TGA analysis of neat polyvinyl pyrrolidone. As can be seen, polyvinyl pyrrolidone decomposes completely at 700 °C. Therefore, the as-spun fibres' calcination temperature was set on 750 °C and 1050 °C to map structural changes of the ceramic nanofibres with increasing calcination temperatures. The resulting structures of the calcined nanofibres are in Figure 38. As can be seen in Figure 38a, after calcination at 750 °C the fibres morphology is similar to the as-spun fibres, but there are first calcium phosphate grains precipitating in the fibres (see Figure 38b with a detailed view of the structure calcined at 750 °C). The morphology of the heat treated fibres corresponds to Lee et al. [110], suggesting that the electrospinning process parameters were correctly estimated. However, the begun crystallization considerably decreased toughness of the fibrous structure. The fibres were so brittle that any manipulation with the samples without their damage was prevented.

In Figure 38c there is a structure calcined at 1050 °C. The fibres consist of a chain of small calcium phosphate grains, which is clearly visible in Figure 38d. The structure was again brittle and no manipulation was possible without damaging the structure.

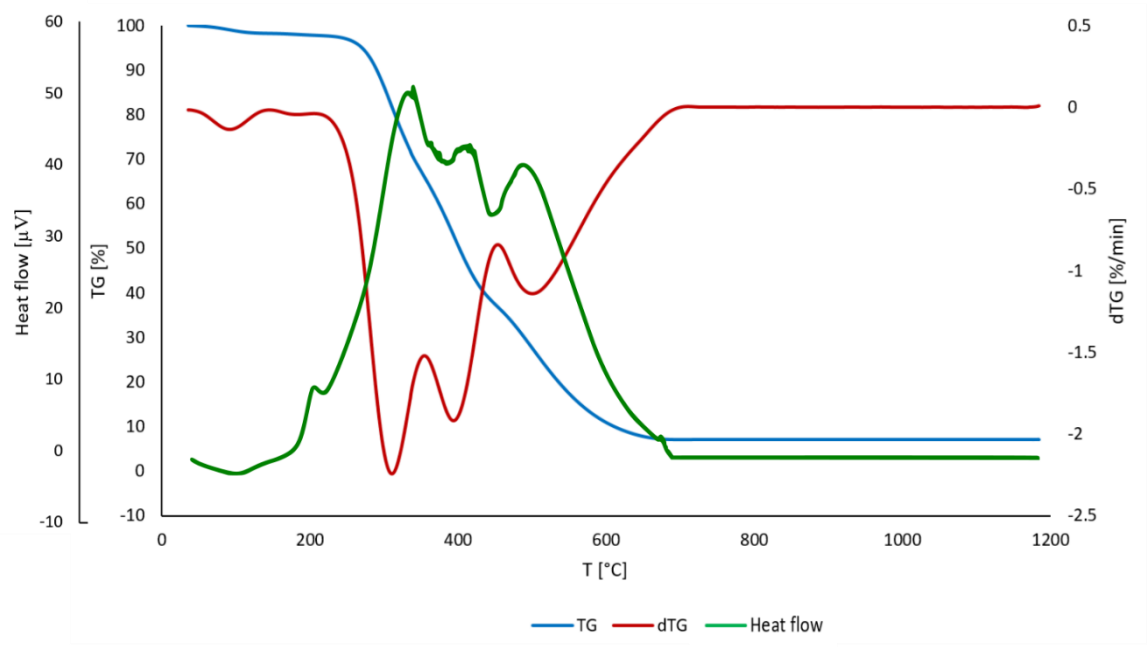

Figure 37 TGA analysis of neat PVP

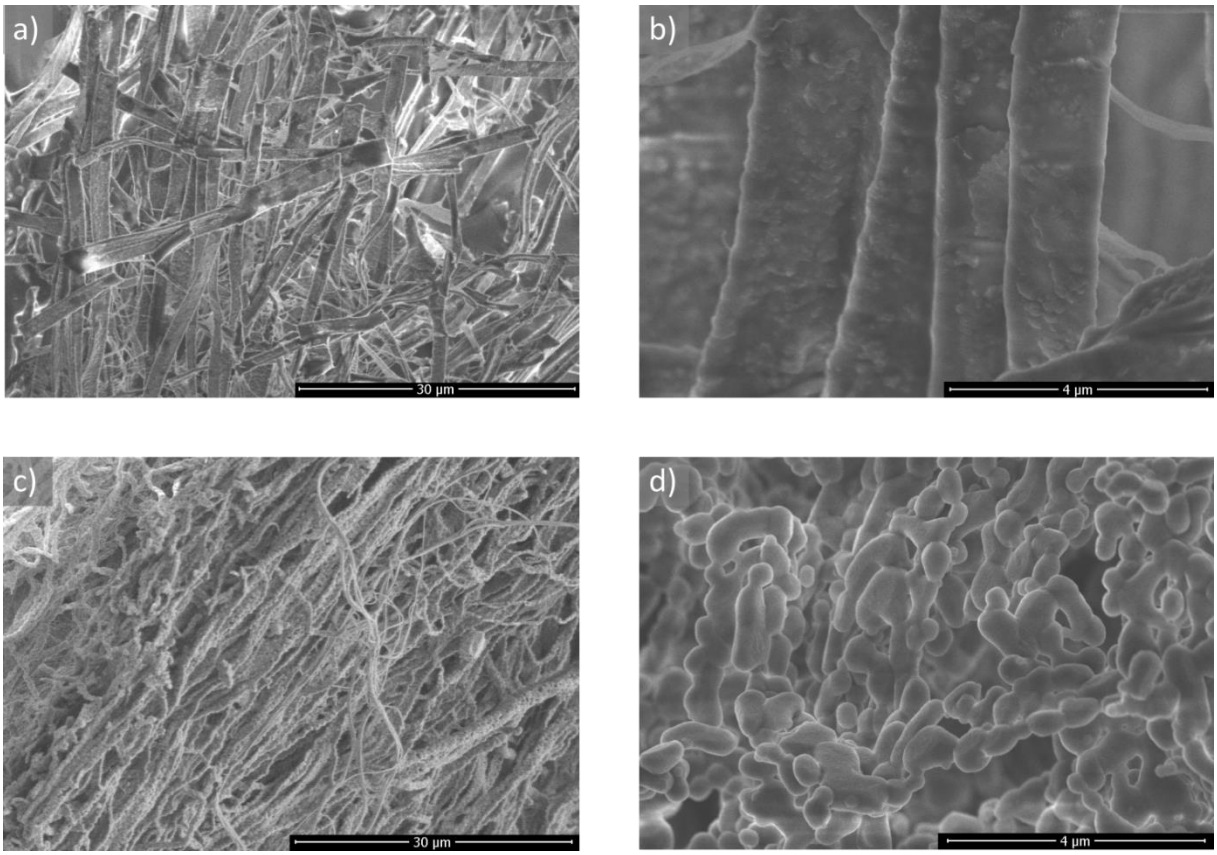

Figure 38 Hydroxyapatite fibres heat treated at a) and b) 750 °C; c) and d) 1050 °C

EDX analysis was done on the calcined samples to confirm chemical composition of the prepared structures. As can be seen from Table 18, the samples calcined at 750 °C contained more calcium than the stoichiometric hydroxyapatite and contrary phosphorus content was lower. The content of

phosphorus was even lower in the sample calcined at 1050 °C. XRD analysis of the sample calcined at 750 °C showed hydroxyapatite-like structure of the fibres, but the structure also contained a considerable (28.9 mol%) amount of calcium oxide, see the XRD spectrum in Figure 39. The sample heat treated at 1050 °C consisted nearly only of the calcium oxide. These results were in contrast to [110], where nearly stoichiometric composition of the hydroxyapatite fibres heat treated at 800 °C (Ca/P = 1.68) was claimed.

Table 18 Chemical composition of calcined hydroxyapatite fibres

Element	HA fibres calcined at 750 °C [at%]	HA fibers calcined at 1050 °C [at%]
Ca	64.9	69.8
P	11.2	1.0
O	24.2	29.2

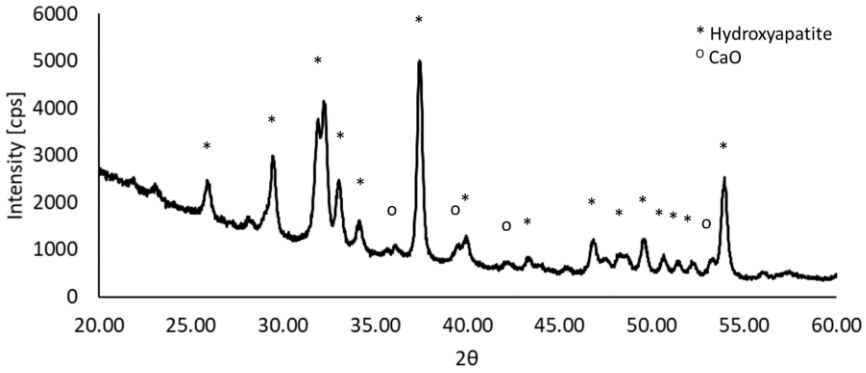

Figure 39 XRD analysis of the ceramic nanofibres calcined at 750 °C

Possibility of ceramic nanofibres preparation via electrospinning process was proven but the data from the XRD and EDX analysis show some imperfections of the resulting chemical and phase composition of the fibres prepared. One of possible reasons is partial phase separation taking place when the hydroxyapatite precursor was mixed with the polymer (PVP) resulting in multiphase composition of the calcined nanofibres. A modification of the precursor preparation process preventing the phase separation would be needed to obtain neat hydroxyapatite fibres. However, considering the ceramic nanofibers' bad mechanical properties, this approach to bone scaffold was abandoned in this work.

5.1.4 Hollow nanofibres

In Figure 40a, there is an example of successfully prepared hollow nanofibres (marked with red arrow) via core-shell electrospinning of the system based on ZrO_2 and PVP solutions. However, not all the fibres were hollow, as can be seen in Figure 40b. The biggest problem lays probably in high demands on the geometrical arrangement of the core-shell setup. The core-shell spinning requires a perfectly concentric alignment of the inner and outer needle to ensure closed outer envelope around the core component, which could not be ensured by commercial needles without guaranteed longitudinal geometry.

The red arrow in Figure 40b shows the consequence of imperfect needles alignment – the inner (polymer) constituent was placed on one side of the electrospun fibre, and after the heat treatment, an “open” fibre was obtained. The green arrow shows a fibre where inner and outer precursors partly mixed and instead of a hollow fibre, a porous structure was prepared. Figure 38a and b show that the

core-shell electrospinning process (with the available setup) is rather unreliable and the resulting structure is highly inhomogeneous, which also suggests low reproducibility of the process. For the mentioned reasons, the hollow fibres were not considered for further utilization and testing in this thesis. However, the experiments proved that it is possible to prepare hollow nanofibers with the core-shell electrospinning setup, but the workflow requires higher geometrical accuracy than the commercially accurate needles can offer. Therefore, to achieve the hollow nanofibers (e.g. for nerve tissue engineering), customized needles with strict geometrical tolerances are crucial.

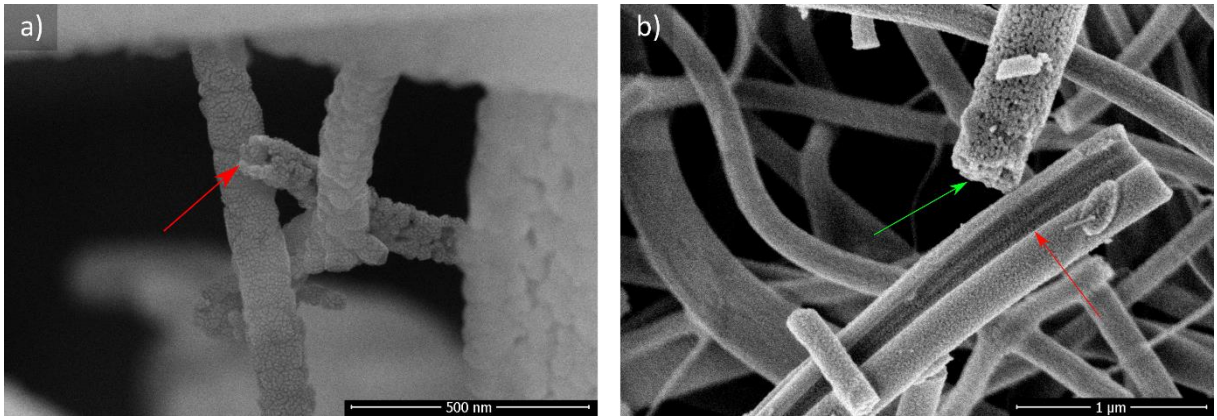

Figure 40 Electrospun hollow nanofibres; a) correct morphology of the hollow nanofibre, b) wrong morphology of the core-shell electrospun nanofibres

5.2 Biological tests

Biological tests are crucial for novel materials and structures to be used in medicine in the future. The biological tests has several steps to evaluate biocompatibility and bioactivity of the structures qualitatively and quantitatively. The SBF test is usually the first test of the structures intended for bone tissue engineering and then follow *in-vitro* cell culture tests. *In-vivo* tests on an animal model are the next important step before the clinical testing.

The neat polycaprolactone and the composite polycaprolactone/hydroxyapatite nanofibres were chosen for the biological testing. They were evaluated as the most promising from all the prepared samples based on their microstructure and mechanical properties.

5.2.1 SBF test

The SBF test proved bioactivity of the electrospun composite structures, whereas neat polycaprolactone fibres remained untouched by rinsing in the SBF. A calcium phosphate phase began to precipitate on the composite fibres (both as-spun and plasma treated) already after one day of the start of the test. The hydroxyapatite nanoparticles' bioactivity was proven by preferred precipitation of the calcium phosphates on the places rich on the ceramic particles, which was noticeable already after the first day of the test, see sample PCL/HA-2 in Figure 41a. It can be noticed that the precipitated structure does not cover the whole surface of the sample. However, the increased amount of the calcium phosphates on the sample surface supported further precipitation of the calcium phosphates, and after seven days of the test, the surface of the sample was covered by submicroscopic crystals (see Figure 41b). The crystalline precipitates layer contained some defect (cracks and dimples), that probably originated during the sample manipulation and preparation for the SEM analysis. The detailed picture of the calcium phosphate precipitates can be seen in in Figure 41c.

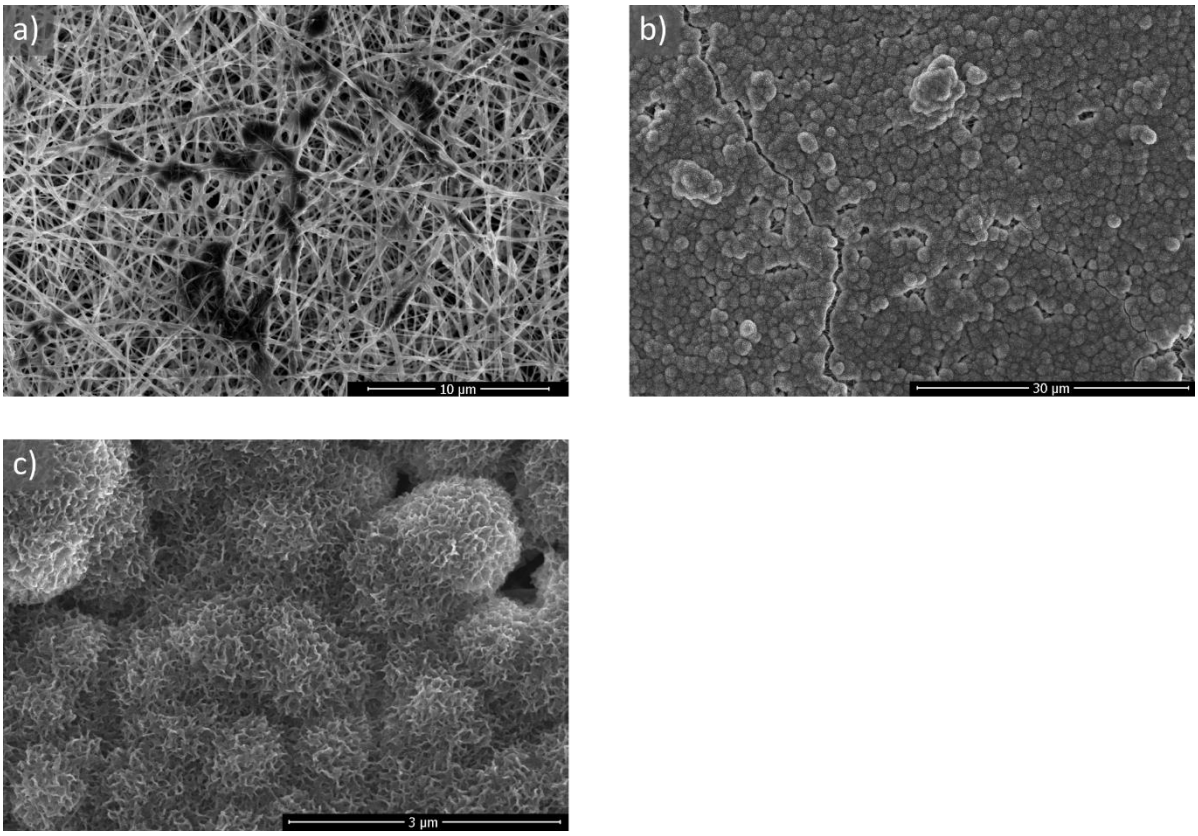

Figure 41 SBF tested sample PCL/HA-2 after a) 1 day, b) 7 days, c) detailed photo of the sample after 7 days of the test

The SBF test of the plasma treated composite fibres showed faster precipitation of the calcium phosphates on the samples surface, as shown in Figure 42. After 1 day of the test, the sample is in Figure 42a – morphology of the precipitate is similar to the as-spun sample after 1 day of the SBF test, but amount of the precipitates is higher on the plasma treated sample. In Figure 42b there is the plasma treated sample after 3 days of the test. The sample's surface is nearly entirely covered by the crystalline precipitates. The precipitated structure contains some defects (cracks and dimples) that probably originated during the sample manipulation before the SEM analysis. The defects were not visible on the sample after 7 day of the test as can be seen in Figure 42c – the precipitated layer was probably thick enough to sustain the manipulation. Figure 42d shows the morphology of the precipitates in detail. It can be noticed that the morphology of the submicroscopic crystals is similar to the precipitates on the as-spun samples. It suggests that the SBF test does not change the type of the precipitated phase but accelerates the precipitation process. Moreover, the higher wettability of the plasma-treated samples allowed the SBF solution to soak into the sample and form the calcium phosphates on the surface of the composite fibrous sample and also inside its microstructure as can be seen in the inset of Figure 42b.

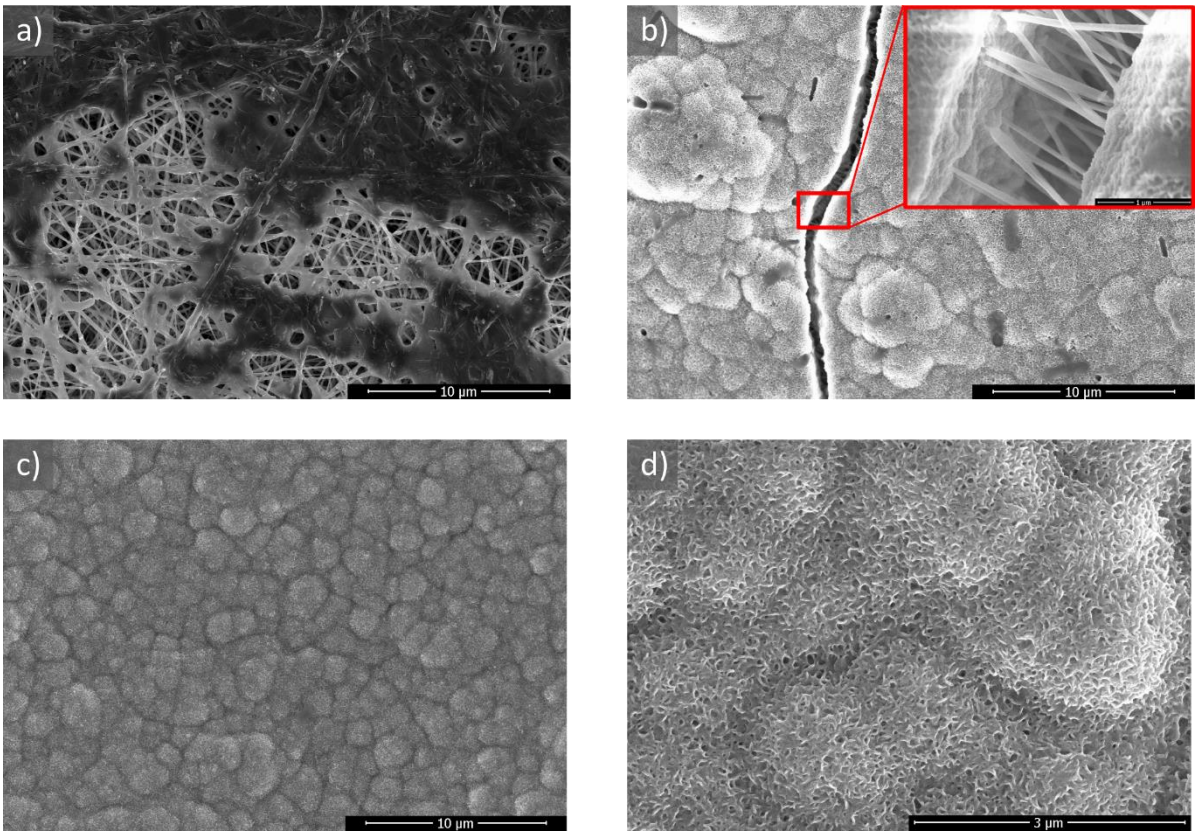

Figure 42 Plasma treated composite fibres after SBF test, a) after 1 day; b) after 3 days; c) after 7 days; d) detail of the precipitates after 7 days of the test

Table 19 shows results of the EDX analysis of the precipitates on the composite plasma-treated sample after 7 days of the SBF test. The precipitated structure's chemical composition shows Ca/P ratio 1.4 which is lower than typical hydroxyapatite composition (1.67). It suggests that the calcium could be substituted by other elements (also listed in Table 19). Unfortunately, XRD analysis could not be provided on the SBF tested composite samples. The precipitated ceramic layer was too thin to obtain representative results.

Table 19 Chemical composition of the precipitates on the composite fibres after 7 days of the SBF test

Element	Weight %	Atomic %
O	35.5	69.3
Na	1.0	1.
Mg	1.0	0.9
Si	0.4	0.3
P	18.0	12.9
Cl	3.2	2.0
Ca	32.4	17.9

5.2.2 *In-vitro* cell culture tests

Next step of the samples biological examination are tests using living cell colonies. The test according to ISO 10993-5 standard was provided. The test showed zero cytotoxicity of the tested materials – no cells mortality was observed. The diagraph in Figure 43 compares the tested structures to the baseline sample (marked as 0 in the diagraph) considered a waterline for the results – the curves above the baseline are supposed to be positive ones. It is important to consider all influences affecting the

specific growth rate – the tested material itself, the structure, the surface treatment, and space availability around the proliferating cells. There are several phenomena visible from the Figure 43. The hydroxyapatite particles increase bioactivity of the tested structure – the most significant contribution to the bioactivity can be seen by the sample PCL/HA-1 (a continuous layer of the polycaprolactone with the hydroxyapatite particles). The measured bioactivity was the highest after 24 hours of the test and then decreased rapidly. The explanation lays in cells giving priority to settle in the places rich on the hydroxyapatite particles where they also proliferate. When all the preferable places are occupied, the proliferation slows down considerably. The specific growth rate of the continuous polycaprolactone layer (the sample PCL-1) was comparable to the other samples after 24 hours of the test, but then it slowed down continuously, suggesting that bulk polycaprolactone is biocompatible but not considerably bioactive.

The fibrous samples' effect was the same for both types of tested materials (neat polycaprolactone and composite) – the specific growth rate was comparable to the baseline after 24 hours of the test, but then it increased above waterline after 48 hours of the test. However, during the next 24 hours the proliferation slowed down and decreased below the waterline in plasma untreated samples (PCL-2, PCL/HA-2). The explanation of the slowed proliferation rate is probably the same as the case of the sample PCL/HA-1 – the cells occupied places stimulating their activity (e.g. crossings of the PCL fibres for the sample PCL-2 and areas rich on hydroxyapatite particles for the sample PCL/HA-2). The situation is different in the case of the plasma treated samples - the samples PCL/HA-4, PCL/HA-5 remained above the baseline for the whole duration of the test, suggesting that increased wettability strongly supports the bioactivity of the composite fibrous structure. However, the proliferation also slowed down during the last 24 hours of the test. To find an explanation for this result, it is necessary to look at the samples after the cultivation test.

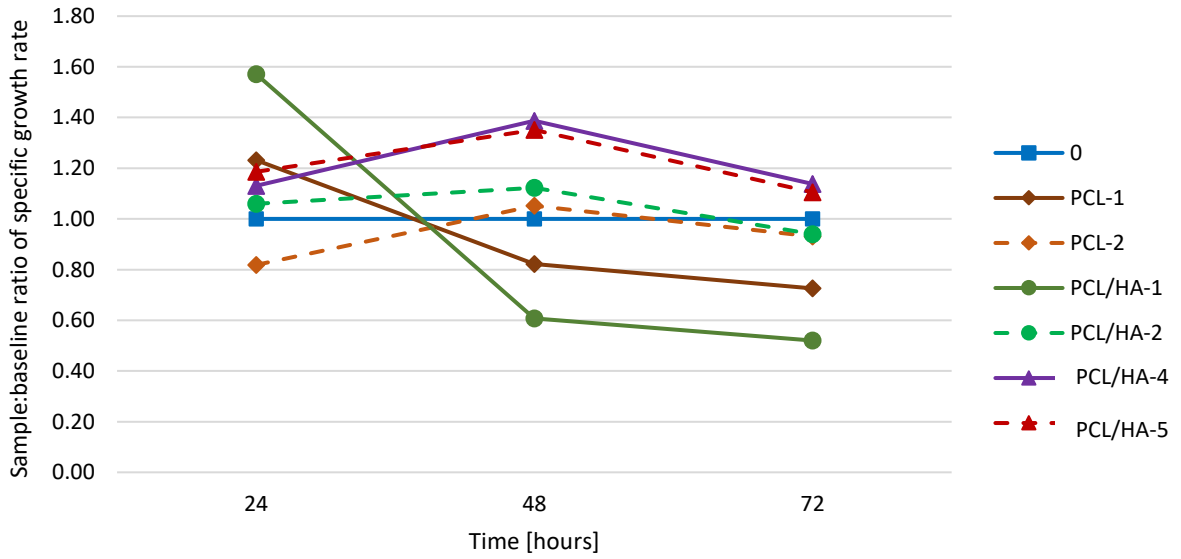

Figure 43 Diagraph comparing the specific growth rate of the samples tested according to ISO 10993-5 standard

Figure 44 shows tested samples after the cell cultivation test. In Figure 44a and b, there is the baseline (0) sample at the beginning of the test and the end of the test. The cells' increased number is obvious, but the sample surface was not entirely covered by the cells. In Figure 44c, there is sample PCL-1 at the end of the test. The cell colony grew during the 72 hours, but the total number of cells was

considerably lower than on the baseline sample, as was already mentioned above. The sample PCL/HA-1 showed much larger cell colony at the end of the test, visually comparable with the baseline sample.

In Figure 44e, there is sample PCL-2 (polycaprolactone random fibres) after 72 hours of the test. Compared to the continuous polycaprolactone layer in Figure 44c, the fibrous morphology's positive influence is visible. However, the sample performance did not reach the baseline level. The hydroxyapatite particles in sample PCL/HA-2 strongly increased the structure's bioactivity and the cell colony after 72 hours of the test was comparable to the baseline – see Figure 44d.

Figure 42g and h shows images of the plasma treated composite samples PCL/HA-4 (random fibres) and PCL/HA-5 (parallel fibres) after 72 hours of the test, respectively. The cells cover entirely the sample surface of both samples. This phenomenon can be called cell monolayer, and it suggests a successful biological test and good bioactivity of the tested structure. [111] It also explains the proliferation rate's deceleration – the cells simply did not have space anymore for colony growth.

According to some literature, the alignment of the fibres has an influence on the morphology of the cells – the cells are prolonged in the direction of the fibres. [112] However, the obtained results of the sample PCL/HA-5 did not show any significant effect of this influence – only roughly 50% of the cells showed the expected elongation. It can be explained by a thin layer of the expected material, which was not stimulating enough for the cells to change their shape.

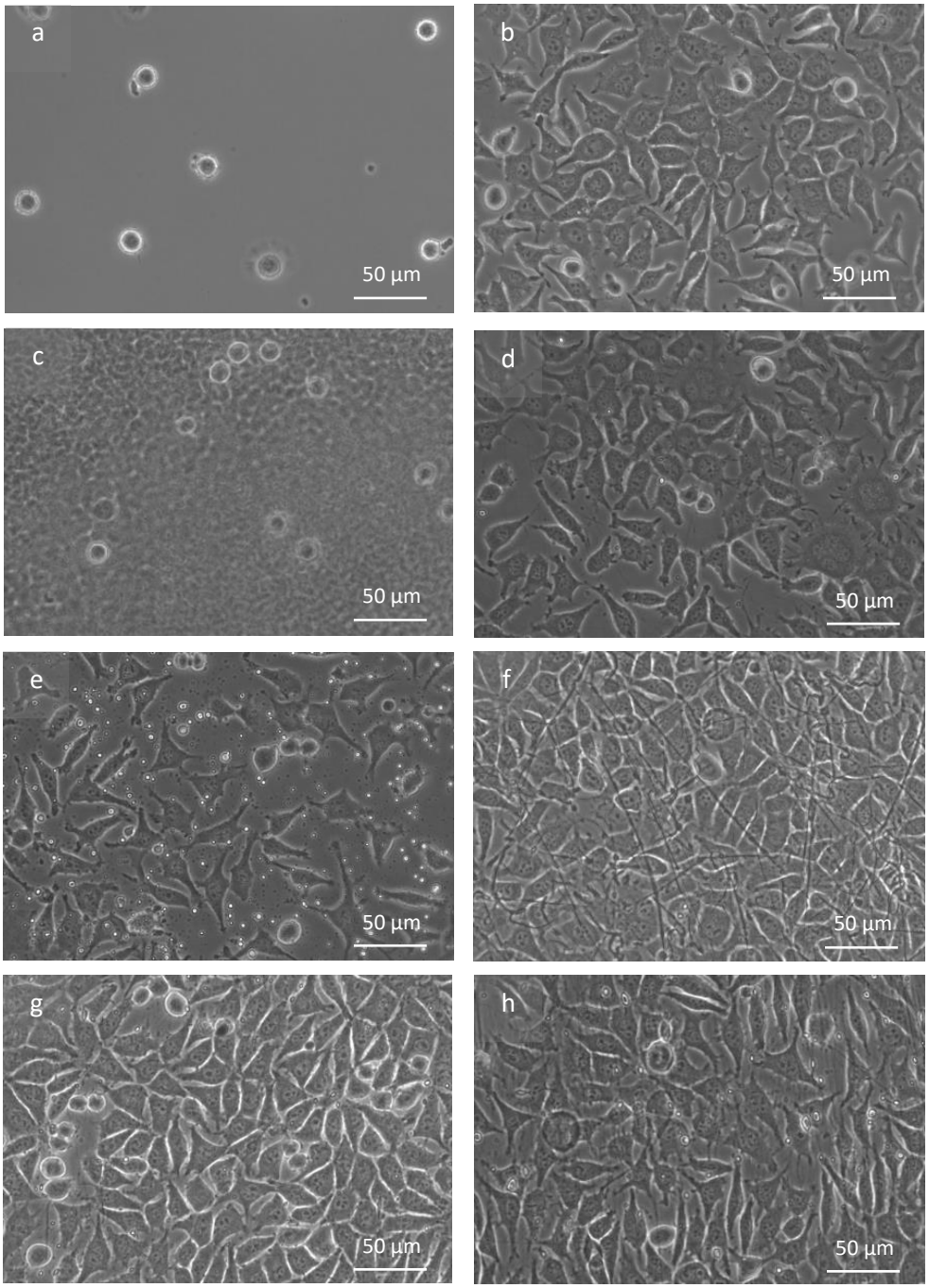

Figure 44 Samples after ISO 10993-5 test a) baseline sample at the beginning of the test, b) baseline sample after 72 hours of the test, c) PCL-1 after 72 hours of the test, d) PCL/HA-1 after 72 hours of the test, e) PCL-2 after 72 hours of the test, f) PCL/HA-2 after 72 hours of the test, g) PCL/HA-4 after 72 hours of the test, h) PCL/HA-5 after 72 hours of the test

In Figure 45 there is colour change during 7 days of the WST-8 test visible by naked eye. The colour changed from pale yellow to orange or deep orange, which is the consequence of the activity of the increasing cells.

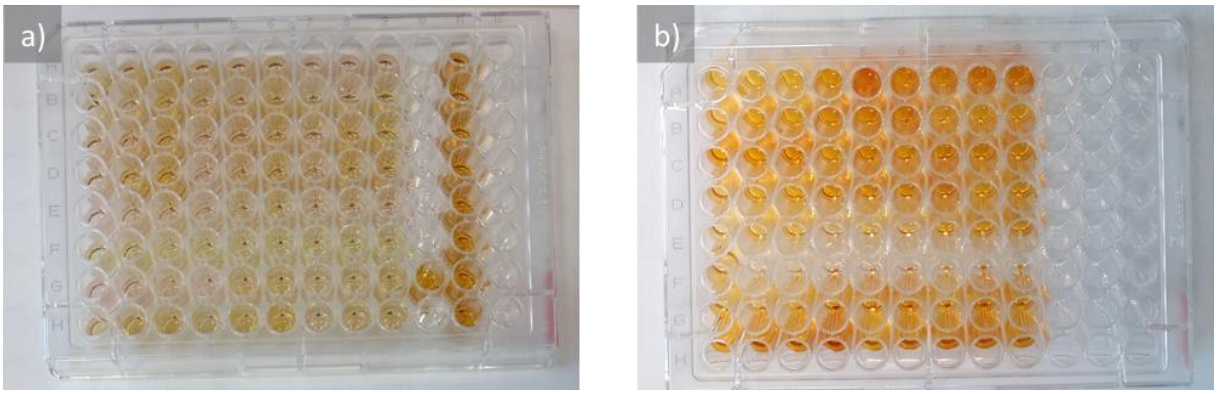

Figure 45 Contrast medium for absorbance measurement after a) 1 day, b) 7 days of the WST-8 test

The quantified results of the absorbance test during the WST-8 test are in Figure 46. The results from day 1 simply show the state of the cell culture after the cell seeding. Most of the samples showed similar absorbance after 1 day of the cultivation. However, absorbance measured on the sample PCL/HA-2 (composite random fibres) was nearly as low as the negative control (well without living cells) showing some mistake during the cell seeding (e.g. low number of the seeded cells) which unfortunately deformed results of this sample for the rest of the test. However, one important information was still obtained from this sample – the cell colony was growing during the test, showing the sample's biocompatibility.

The test results' overall trend is similar to the ISO 10993-5 test – the neat polycaprolactone samples showed the lowest bioactivity at the end of the test, but their biocompatibility was proven. The hydroxyapatite's presence improved the biocompatibility considerably significantly in the second half of the test, which confirms conclusions from the ISO 10993-5 test. The cells proliferation slows down rapidly when all the favorite places are occupied on the neat polycaprolactone samples while the composite fibres offer more places suitable for cells to proliferate as can be seen from the comparison of the samples PCL-2 and PCL/HA-2 in the diagram.

In agreement with the ISO 10993-5 test, the plasma treated samples showed increased bioactivity especially in the second half of the test when they overcome the polycaprolactone as-spun fibres approximately twice and the composite as-spun fibres approximately 1.5 times which is even more significant result than the ISO 10993-5 test showed.

Comparison of polycaprolactone random and parallel fibres (samples PCL-2 and PCL-3, respectively) shows a possible cells stimulation by the fibres direction alignment that contrasts to the ISO 10993-5 test results. However, as has been previously mentioned, the ISO 10993-5 test requires only a thin layer of the tested material, and hence the directional alignment of the fibres could not have an impact. On the other hand, the WST-8 test allows thicker samples and the alignment of the fibres could show some effect. The fibres alignment did not seem to impact the composite as-spun fibres when samples PCL/HA-2 and PCL/HA-3 showed nearly the same results. However, the random and parallel composite samples' difference was more distinct by the plasma treated samples. But considering the standard deviation, the influence of the alignment of the fibres on the structure bioactivity could not be reliably confirmed.

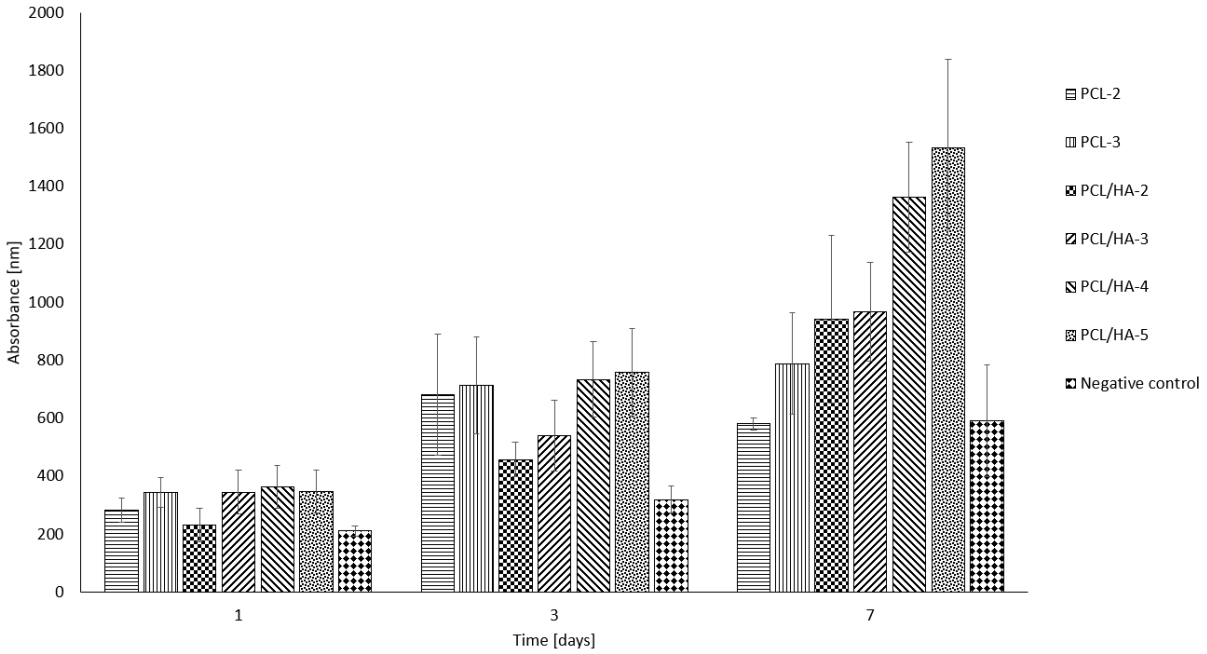

Figure 46 Quantific results of the WST-8 test

After the absorbance measurement and samples fixation, it was possible to compare the samples after the WST-8 test qualitatively. Figure 47 shows a detailed view of the cells after 7 days of the WST-8 test on various samples. There can be seen a different cell morphology between random and parallel samples, regardless of fibres composition. Cells seeded on the randomly organized fibres were spread on the fibres in a round-like shape (see Figure 47a, c, and e where are displayed samples PCL-2, PCL/HA-2 and PCL/HA-4, respectively). The cells on the parallel fibres (Figure 47b, d and f showing samples PCL-3, PCL/HA-3 and PCL/HA-5, respectively) were mostly prolonged along the parallel fibres unlike the cells after the ISO 10993-5 test. The explanation is already mentioned higher "density" of the fibres. Interesting is also Figure 47f (sample PCL/HA-5) where it is visible that the cells were able to move under the fibres, probably thanks to the increased wettability of the structure. It suggests that the cells can move inside the structure and after some longer time they could occupy the inner spaces of the composite fibrous structures.

In Figure 47g there is a detail of the cell attached to the (composite random) fibres. It can be seen that the cell is closely attached to the fibres and it is difficult to distinguish edge of the cells body and the fibres.

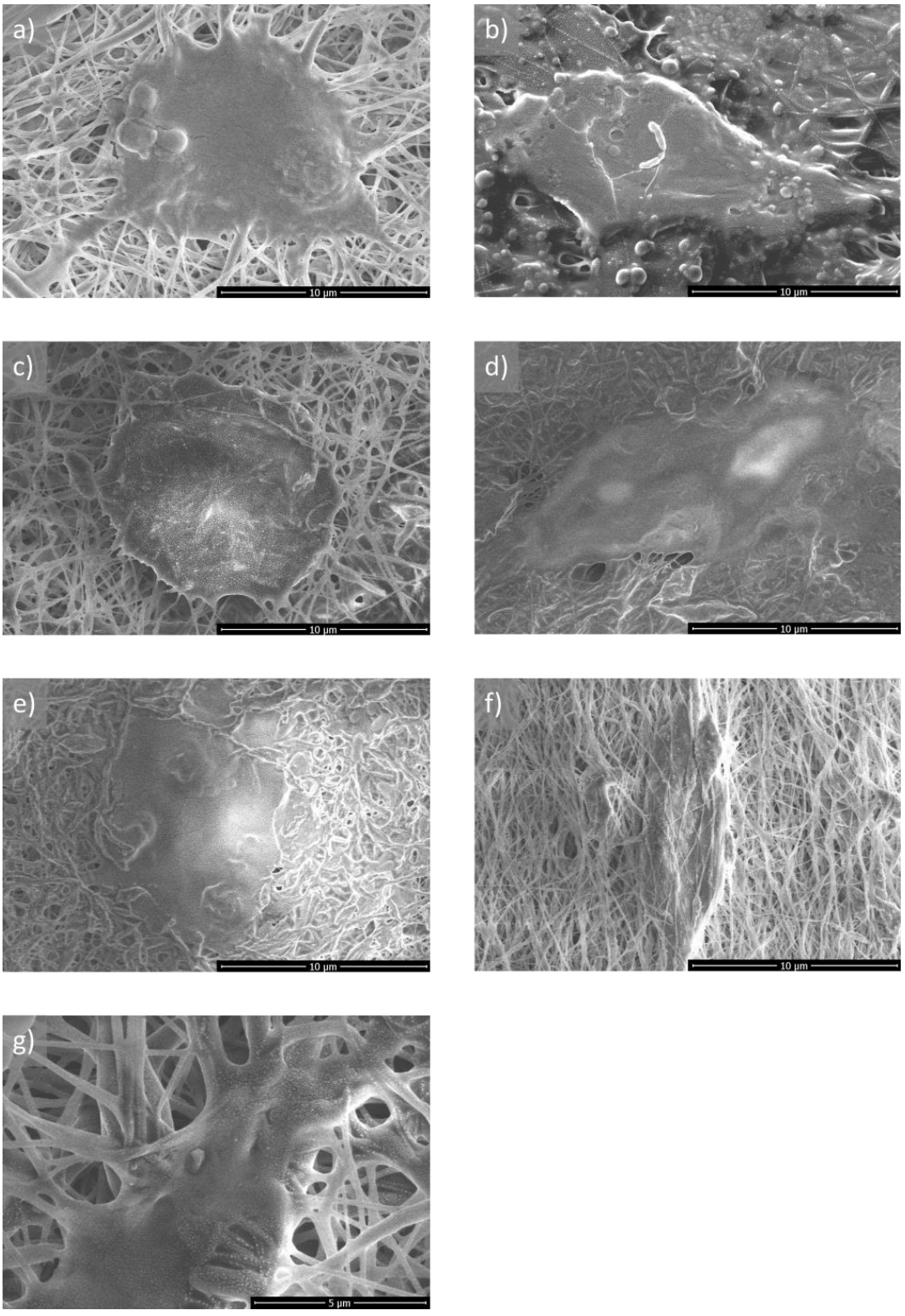

Figure 47 Morphology of the cells cultivated on the samples during the WST-8 test; a) PCL-2, b) PCL-3, c) PCL/HA-2, d) PCL/HA-3, e) PCL/HA-4, f) PCL/HA-5, g) detail of the cell attached onto the composite fibres (PCL/HA-2)

All the biological tests showed corresponding results suggesting the robustness of the testing workflow. The presence of the hydroxyapatite showed two different contributions to the bioactivity of the (composite) structures intended for bone tissue engineering. It induces calcium phosphate (substituted hydroxyapatite) precipitation in the human blood plasma environment and, thanks to its

hydrophilicity, also supports cells adhesion to the structure. The plasma treatment further increases the bioactivity of the structures thanks to increased hydrophilicity of the fibrous meshes. The most significant difference between the ISO 10993-5 test and the WST-8 test lies in the influence of the alignment of the fibres on the cell morphology. Whereas cells did not react to the fibers parallel alignment during the ISO 10993-5 test (probably because of the already mentioned low density of the tested fibrous mesh), the fibre alignment influenced the cell morphology during the WST-8 test. The parallel fibers stimulated the cultured cells prolonged their shape along the fibre direction.

---

6 Conclusions

Polycaprolactone fibres and fibrous structures combining polycaprolactone matrix with hydroxyapatite nanoparticles intended for bone tissue engineering were prepared via electrospinning method. Process obstacles during the electrospinning (needle clogging, hydroxyapatite conglomerates etc.) were overcome, and the optimization led to reliable and repeatable production of the fibrous structures. Random and parallelly aligned nanofibers (both neat polycaprolactone and composite polycaprolactone/hydroxyapatite) were prepared from polycaprolactone solution based precursor by controlling the collector rotation speed. The rotation speed did not influence only direction alignment of the fibres but it also reduced thickness of the electrospun fibres – the diameter of the neat PCL fibres decreased from 172 ± 60 nm at 100 rpm to 124 ± 66 at 2000 rpm. The composite PCL/HA fibres were influenced less by the collector rotation speed – the fibres diameter decreased form 171 ± 107 nm at 100 rpm to 151 ± 75 nm at 2000 rpm.

The as-spun neat polycaprolactone and composite (polycaprolactone/hydroxyapatite) nanofibers were mechanically tested. Both fibres direction alignment and phase composition influenced the nanofibers mechanical properties. The ceramic particles had a large impact on the random nanofibers when the ceramic particles considerably worsened failure stress (from 19 ± 6 MPa to 8 ± 1 MPa for random fibres and from 67 ± 9 to 42 ± 8 for parallel fibres). However, the presence of the ceramic nanoparticles worsened the failure strain only by the random fibres (decrease from 130 ± 19 % to 81 ± 10 %). The elastic modulus was dependent rather on the fibres orientation than on the phase composition – the elastic modulus changed from 20 ± 9 MPa for random neat PCL fibres to 354 ± 47 MPa for parallel PCL fibres. The elastic modulus change was similar for the composite fibres – from 24 ± 5 MPa for random fibres to 307 ± 13 MPa for parallel fibres.

The surface treatment of the electrospun fibres was optimized – a low temperature argon plasma was used to increase the structures' wettability (and hence bioactivity). The structures transformed from highly hydrophobic to rather hydrophilic (the contact angle was unmeasurable after the plasma treatment), and simultaneously the treatment turned to be gentle enough to preserve the sensitive polymer-based structure.

An attempt to prepare hollow nanofibers via core-shell electrospinning method was also made. Some hollow nanofibers were prepared but stability and reliability of the process was rather low. A required geometrical accuracy of the core-shell electrospinning setup was not achieved with commercially available electrospinning needles. However, the experiment design suggests promising approach to the hollow fibres preparation process that can be further improved in the future.

Biological properties of the neat polycaprolactone and composite fibres were analyzed by three different tests: test in simulated body fluid evaluates structures ability to support precipitation of calcium phosphates in environment similar to the human body. Two following in-vitro cell culture tests (ISO standard 10993-5 and WST-8 test) examined living cells response to the tested structures. The SBF test proved bioactivity of the composite structures thanks to the hydroxyapatite nanoparticles incorporated in the structures. Both *in-vitro* tests showed a positive synergic effect of the hydroxyapatite nanoparticles in the polymer matrix, fibrous morphology of the tested structures and surface plasma treatment. The WST-8 test showed 1.5 times higher bioactivity of the plasma-treated composite structures than the neat polycaprolactone fibres, which suggests a promising approach to the structures designed for materials engineering.

7 Literature

1. Park, J. *Bioceramics*; 1 ed.; Springer Science+Business Media, LLC: New York, USA, 2008; p. ; ISBN 978-0-387-09545-5.

2. Hollinger, J.; Einhorn, T.; Doll, B.; Sfeir, C. *Bone Tissue Engineering*; 1 ed.; CRC Press LLC: USA, 2005; p. ; ISBN 0-8493-1621-9.

3. FINKEMEIER, C. BONE-GRAFTING AND BONE-GRAFT SUBSTITUTES. *The Journal of Bone and Joint Surgery-American Volume* 2002, *vol. 84*, 454-464.

4. Denry, I.; Kuhn, L. Design and characterization of calcium phosphate ceramic scaffolds for bone tissue engineering. *Dental Materials* 2016, *vol. 32*, 43-53.

5. Alexander, J. History of the Medical Use of Silver. *Surgical Infections* 2009, *vol. 10*, 289-292.

6. Vacanti, C. The history of tissue engineering. *Journal of Cellular and Molecular Medicine* 2006, *vol. 1*, 569-576.

7. Stock, U.; Vacanti, J. Tissue Engineering: Current State and Prospects. *Annual Review of Medicine* 2001, *vol. 52*, 443-451.

8. Brunette, D.; Tengvall, P.; Textor, M.; Thomsen, O. *Titanium in Medicine: Material Science, Surface Science, Engineering, Biological Responses and Medical Applications*; 1 ed.; Springer-Verlag Berlin Heidelberg: Germany, 2001; p. ; ISBN 978-3-642-56486-4.

9. Dörre, E.; Hübner, H. *Alumina*; 1 ed.; Springer-Verlag Berlin Heidelberg: Germany, 1984; p. ; ISBN 978-3-642-82306-0.

10. Patel, N.; Gohil, P. A Review on Biomaterials: Scope, Applications& Human Anatomy Significance. *International Journal of Emerging Technology and Advanced Engineering* 2012, *2*, 91-101.

11. Denry, I.; Kuhn, L. Design and characterization of calcium phosphate ceramic scaffolds for bone tissue engineering. *Dental Materials* 2016, *vol. 32*, 43-53.

12. Leung, V.; Ko, F. Biomedical applications of nanofibers. *Polymers for Advanced Technologies* 2011, *vol. 22*, 350-365.

13. Rim, N.; Shin, C.; Shin, H. Current approaches to electrospun nanofibers for tissue engineering. *Biomedical Materials* 2013, *vol. 8*, 1-14.

14. Jang, J.; Castano, O.; Kim, H. Electrospun materials as potential platforms for bone tissue engineering. *Advanced Drug Delivery Reviews* 2009, *vol. 61*, 1065-1083.

15. Hutmacher, D. Scaffold design and fabrication technologies for engineering tissues — state of the art and future perspectives. *Journal of Biomaterials Science, Polymer Edition* 2001, *vol. 12*, 107-124.

16. KARAGEORGIOU, V.; KAPLAN, D. Porosity of 3D biomaterial scaffolds and osteogenesis. *Biomaterials* 2005, *vol. 26*, 5474-5491.

17. Sohier, J.; Daculsi, G.; Sourice, S.; de Groot, K.; Layrolle, P. Porous beta tricalcium phosphate scaffolds used as a BMP-2 delivery system for bone tissue engineering. *Journal of Biomedical Materials Research Part A* 2009, *92A*, 1105-1114.

18. Bose, S.; Vahabzadeh, S.; Bandyopadhyay, A. Bone tissue engineering using 3D printing. *Materials Today* 2013, *vol. 16*, 496-504.

19. Sultana, N.; Wang, M. PHBV/PLLA-based composite scaffolds fabricated using an emulsion freezing/freeze-drying technique for bone tissue engineering: surface modification and in vitro biological evaluation. *Biofabrication* 2012, *vol. 4*, 1-14.

20. Kim, H.; Kim, H.; Knowles, J. Production and Potential of Bioactive Glass Nanofibers as a Next-Generation Biomaterial. *Advanced Functional Materials* 2006, *vol. 16*, 1529-1535.

21. Mitchell, G. *Electrospinning: principles, practice and possibilities*; RSC polymer chemistry series; 1 ed.; Royal Society of Chemistry: Cambridge, UK, 2015; p. ; ISBN 978-1-84973-557-5.

22. Ramalingam, M.; Ramakrishna, S. *Nanofiber Composites for Biomedical Applications*; 1 ed.; Elsevier Ltd.: United Kingdom, 2017; p. ; ISBN 978-0-08-100208-7.

23. van de Witte, P.; Dijkstra, P.; van den Berg, J.; Feijen, J. Phase separation processes in polymer solutions in relation to membrane formation. *Journal of Membrane Science* 1996, *vol. 117*, 1-31.

24. Paramonov, S.; Jun, H.; Hartgerink, J. Self-Assembly of Peptide−Amphiphile Nanofibers: The Roles of Hydrogen Bonding and Amphiphilic Packing. *Journal of the American Chemical Society* 2006, *vol. 128*, 7291-7298.

25. Mendes, A.; Strohmenger, T.; Goycoolea, F.; Chronakis, I. Electrostatic self-assembly of polysaccharides into nanofibers. *Colloids and Surfaces A: Physicochemical and Engineering Aspects* 2017, *vol. 531*, 182-188.

26. Alharbi, A.; Alarifi, I.; Khan, W.; Asmatulu, R. Highly Hydrophilic Electrospun Polyacrylonitrile/ Polyvinypyrro-lidone Nanofibers Incorporated with Gentamicin as Filter Medium for Dam Water and Wastewater Treatment. *Journal of Membrane and Separation Technology* 2016, *5*, 38-56.

27. The Difference Between ElectroSpinning and Electrospraying Available online: https://www.azonano.com/article.aspx?ArticleID=5060 (accessed on 2020-10-07).

28. Ramakrishna, S. *An introduction to electrospinning and nanofibers*; 1 ed.; World Scientific: Hackensack, NJ, 2005; p. ; ISBN 98-125-6415-2.

29. Huang, L.; Bui, N.; Manickam, S.; McCutcheon, J. Controlling electrospun nanofiber morphology and mechanical properties using humidity. *Journal of Polymer Science Part B: Polymer Physics* 2011, *vol. 49*, 1734-1744.

30. Koski, A.; Yim, K.; Shivkumar, S. Effect of molecular weight on fibrous PVA produced by electrospinning. *Materials Letters* 2004, *vol. 58*, 493-497.

31. Kessick, R.; Tepper, G. Microscale polymeric helical structures produced by electrospinning. *Applied Physics Letters* 2004, *vol. 84*, 4807-4809.

32. Hou, H.; Jun, Z.; Reuning, A.; Schaper, A.; Wendorff, J.; Greiner, A. Poly(p -xylylene) Nanotubes by Coating and Removal of Ultrathin Polymer Template Fibers. *Macromolecules* 2002, *vol. 35*, 2429-2431.

33. Li, D.; Xia, Y. Direct Fabrication of Composite and Ceramic Hollow Nanofibers by Electrospinning. *Nano Letters* 2004, *vol. 4*, 933-938.

34. Hwang, P.; Murdock, K.; Alexander, G.; Salaam, A.; Ng, J.; Lim, D.; Dean, D.; Jun, H. Poly(ε-caprolactone)/gelatin composite electrospun scaffolds with porous crater-like structures for tissue engineering. *Journal of Biomedical Materials Research Part A* 2016, *vol. 104*, 1017-1029.

35. Wang, Y.; Wang, B.; Wang, G.; Yin, T.; Yu, Q. A novel method for preparing electrospun fibers with nano-/micro-scale porous structures. *Polymer Bulletin* 2009, *vol. 63*, 259-265.

36. Gu, B.; Park, S.; Kim, M.; Kang, C.; Kim, J.; Kim, C. Fabrication of sonicated chitosan nanofiber mat with enlarged porosity for use as hemostatic materials. *Carbohydrate Polymers* 2013, *vol. 97*, 65-73.

37. Lee, J.; Jeong, S.; Bae, M.; Yang, D.; Heo, D.; Kim, C.; Alsberg, E.; Kwon, I. Highly Porous Electrospun Nanofibers Enhanced by Ultrasonication for Improved Cellular Infiltration. *Tissue Engineering Part A* 2011, *vol. 17*, 2695-2702.

38. Pouchlý, V.; Ráheľ, J.; Spusta, T.; Ilčíková, M.; Pavliňák, D.; Morávek, T.; Maca, K. Improved microstructure of alumina ceramics prepared from DBD plasma activated powders. *Journal of the European Ceramic Society* 2019, *vol. 39*, 1297-1303.

39. Ghobeira, R.; Philips, C.; Liefooghe, L.; Verdonck, M.; Asadian, M.; Cools, P.; Declercq, H.; De Vos, W.; De Geyter, N.; Morent, R. Synergetic effect of electrospun PCL fiber size, orientation and plasma-modified surface chemistry on stem cell behavior. *Applied Surface Science* 2019, *vol. 485*, 204-221.

40. Jacobs, T.; De Geyter, N.; Morent, R.; Desmet, T.; Dubruel, P.; Leys, C. Plasma treatment of polycaprolactone at medium pressure. *Surface and Coatings Technology* 2011, *vol. 205*, S543-S547.

41. Khosravi, A.; Ghasemi-Mobarakeh, L.; Mollahosseini, H.; Ajalloueian, F.; Masoudi Rad, M.; Norouzi, M.; Sami Jokandan, M.; Khoddami, A.; Chronakis, I. Immobilization of silk fibroin on the surface of PCL nanofibrous scaffolds for tissue engineering applications. *Journal of Applied Polymer Science* 2018, *vol. 135*, 1-8.

42. Bhattacharjee, P.; Kundu, B.; Naskar, D.; Kim, H.; Maiti, T.; Bhattacharya, D.; Kundu, S. Silk scaffolds in bone tissue engineering: An overview. *Acta Biomaterialia* 2017, *vol. 63*, 1-17.

43. Aragon, J.; Navascues, N.; Mendoza, G.; Irusta, S. Laser-treated electrospun fibers loaded with nano-hydroxyapatite for bone tissue engineering. *International Journal of Pharmaceutics* 2017, *vol. 525*, 112-122.

44. Kokubo, T.; Takadama, H. How useful is SBF in predicting in vivo bone bioactivity?. *Biomaterials* 2006, *vol. 27*, 2907-2915.

45. Tas, A.; Bhaduri, S. Rapid coating of Ti6Al4V at room temperature with a calcium phosphate solution similar to 10× simulated body fluid. *Journal of Materials Research* 2004, *vol. 19*, 2742-2749.

46. Al-Munajjed, A.; Plunkett, N.; Gleeson, J.; Weber, T.; Jungreuthmayer, C.; Levingstone, T.; Hammer, J.; O'Brien, F. Development of a biomimetic collagen-hydroxyapatite scaffold for bone tissue engineering using a SBF immersion technique. *Journal of Biomedical Materials Research Part B: Applied Biomaterials* 2009, *90B*, 584-591.

47. Richbourg, N.; Peppas, N.; Sikavitsas, V. Tuning the biomimetic behavior of scaffolds for regenerative medicine through surface modifications. *Journal of Tissue Engineering and Regenerative Medicine* 2019, *vol. 13*, 1275-1293.

48. Sharif, S.; Ai, J.; Azami, M.; Verdi, J.; Atlasi, M.; Shirian, S.; Samadikuchaksaraei, A. Collagen-coated nano-electrospun PCL seeded with human endometrial stem cells for skin tissue engineering applications. *Journal of Biomedical Materials Research Part B: Applied Biomaterials* 2018, *vol. 106*, 1578-1586.

49. Ferreira, J.; Gomes, S.; Henriques, C.; Borges, J.; Silva, J. Electrospinning polycaprolactone dissolved in glacial acetic acid: Fiber production, nonwoven characterization, and In Vitro evaluation. *Journal of Applied Polymer Science* 2014, *vol. 131*.

50. Yoshimoto, H.; Shin, Y.; Terai, H.; Vacanti, J. A biodegradable nanofiber scaffold by electrospinning and its potential for bone tissue engineering. *Biomaterials* 2003, *vol. 24*, 2077-2082.

51. Sajeev, U.; Anand, K.; Menon, D.; Nair, S. Control of nanostructures in PVA, PVA/chitosan blends and PCL through electrospinning. *Bulletin of Materials Science* 2008, *31*, 343-351.

52. Paneva, D.; Bougard, F.; Manolova, N.; Dubois, P.; Rashkov, I. Novel electrospun poly(ε-caprolactone)-based bicomponent nanofibers possessing surface enriched in tertiary amino groups. *European Polymer Journal* 2008, *vol. 44*, 566-578.

53. Gholipour Kanani, A.; Bahrami, S. Effect of Changing Solvents on Poly(-Caprolactone) Nanofibrous Webs Morphology. *Journal of Nanomaterials* 2011, *vol. 2011*, 1-10.

54. Gomes, S.; Rodrigues, G.; Martins, G.; Roberto, M.; Mafra, M.; Henriques, C.; Silva, J. In vitro and in vivo evaluation of electrospun nanofibers of PCL, chitosan and gelatin: A comparative study. *Materials Science and Engineering: C* 2015, *vol. 46*, 348-358.

55. Van der Schueren, L.; De Meyer, T.; Steyaert, I.; Ceylan, Ö.; Hemelsoet, K.; Van Speybroeck, V.; De Clerck, K. Polycaprolactone and polycaprolactone/chitosan nanofibres functionalised with the pH-sensitive dye Nitrazine Yellow. *Carbohydrate Polymers* 2013, *vol. 91*, 284-293.

56. Nezarati, R.; Eifert, M.; Cosgriff-Hernandez, E. Effects of Humidity and Solution Viscosity on Electrospun Fiber Morphology. *Tissue Engineering Part C: Methods* 2013, *vol. 19*, 810-819.

57. Suwantong, O. Biomedical applications of electrospun polycaprolactone fiber mats. *Polymers for Advanced Technologies* 2016, *vol. 27*, 1264-1273.

58. Groeber, F.; Holeiter, M.; Hampel, M.; Hinderer, S.; Schenke-Layland, K. Skin tissue engineering — In vivo and in vitro applications. *Advanced Drug Delivery Reviews* 2011, *vol. 63*, 352-366.

59. Keirouz, A.; Chung, M.; Kwon, J.; Fortunato, G.; Radacsi, N. 2D and 3D electrospinning technologies for the fabrication of nanofibrous scaffolds for skin tissue engineering: A review. *WIREs Nanomedicine and Nanobiotechnology* 2020, *vol. 12*.

60. Park, Y.; Ju, H.; Lee, J.; Kim, D.; Lee, O.; Moon, B.; Park, H.; Jeong, J.; Yeon, Y.; Park, C. Three-dimensional electrospun silk-fibroin nanofiber for skin tissue engineering. *International Journal of Biological Macromolecules* 2016, *vol. 93*, 1567-1574.

61. Bakhsheshi-Rad, H.; Hadisi, Z.; Ismail, A.; Aziz, M.; Akbari, M.; Berto, F.; Chen, X. In vitro and in vivo evaluation of chitosan-alginate/gentamicin wound dressing nanofibrous with high antibacterial performance. *Polymer Testing* 2020, *vol. 82*.

62. Yao, C.; Yeh, J.; Chen, Y.; Li, M.; Huang, C. Wound-healing effect of electrospun gelatin nanofibres containing Centella asiatica extract in a rat model. *Journal of Tissue Engineering and Regenerative Medicine* 2017, *vol. 11*, 905-915.

63. Shin, Y.; Shin, D.; Lee, E.; Lee, J.; Kim, J.; Song, S.; Hwang, D.; Lee, J.; Kim, B.; Lim, D. et al. Hyaluronic Acid/PLGA Core/Shell Fiber Matrices Loaded with EGCG Beneficial to Diabetic Wound Healing: A review. *Advanced Healthcare Materials* 2016, *vol. 5*, 3035-3045.

64. Zhang, Q.; Du, Q.; Zhao, Y.; Chen, F.; Wang, Z.; Zhang, Y.; Ni, H.; Deng, H.; Li, Y.; Chen, Y. Graphene oxide-modified electrospun polyvinyl alcohol nanofibrous scaffolds with potential as skin wound dressings. *RSC Advances* 2017, *vol. 7*, 28826-28836.

65. Agnes Mary, S.; Giri Dev, V. Electrospun herbal nanofibrous wound dressings for skin tissue engineering. *The Journal of The Textile Institute* 2014, *vol. 106*, 886-895.

66. Augustine, R.; Dominic, E.; Reju, I.; Kaimal, B.; Kalarikkal, N.; Thomas, S. Electrospun polycaprolactone membranes incorporated with ZnO nanoparticles as skin substitutes with enhanced fibroblast proliferation and wound healing. *RSC Advances* 2014, *vol. 4*.

67. Kim, B.; Cheong, H.; Choi, E.; Yun, S.; Choi, B.; Park, K.; Kim, I.; Park, D.; Cha, H. Accelerated skin wound healing using electrospun nanofibrous mats blended with mussel adhesive protein and polycaprolactone. *Journal of Biomedical Materials Research Part A* 2017, *vol. 105*, 218-225.

68. Chahal, S.; Kumar, A.; Hussian, F. Development of biomimetic electrospun polymeric biomaterials for bone tissue engineering. A review. *Journal of Biomaterials Science, Polymer Edition* 2019, *vol. 30*, 1308-1355.

69. Khajavi, R.; Abbasipour, M.; Bahador, A. Electrospun biodegradable nanofibers scaffolds for bone tissue engineering. *Journal of Applied Polymer Science* 2016, *vol. 133*, n/a-n/a.

70. Patlolla, A.; Arinzeh, T. Evaluating apatite formation and osteogenic activity of electrospun composites for bone tissue engineering. *Biotechnology and Bioengineering* 2014, *vol. 111*, 1000-1017.

71. Suganya, S.; Venugopal, J.; Ramakrishna, S.; Lakshmi, B.; Giri Dev, V. Herbally derived polymeric nanofibrous scaffolds for bone tissue regeneration. *Journal of Applied Polymer Science* 2014, *vol. 131*, n/a-n/a.

72. Binulal, N.; Natarajan, A.; Menon, D.; Bhaskaran, V.; Mony, U.; Nair, S. PCL–gelatin composite nanofibers electrospun using diluted acetic acid–ethyl acetate solvent system for stem cell-based bone tissue engineering. *Journal of Biomaterials Science, Polymer Edition* 2013, *vol. 25*, 325-340.

73. Pereira, I.; Ayres, E.; Averous, L.; Schlatter, G.; Hebraud, A.; de Paula, A.; Viana, P.; Goes, A.; Oréfice, R. Differentiation of human adipose-derived stem cells seeded on mineralized electrospun co-axial poly(ε-caprolactone) (PCL)/gelatin nanofibers. *Journal of Materials Science: Materials in Medicine* 2014, *vol. 25*, 1137-1148.

74. Cai, Y.; Zhang, G.; Wang, L.; Jiang, Y.; Ouyang, H.; Zou, X. Novel biodegradable three-dimensional macroporous scaffold using aligned electrospun nanofibrous yarns for bone tissue engineering. *Journal of Biomedical Materials Research Part A* 2012, *100A*, 1187-1194.

75. Moradi, S.; Golchin, A.; Hajishafieeha, Z.; Khani, M.; Ardeshirylajimi, A. Bone tissue engineering: Adult stem cells in combination with electrospun nanofibrous scaffolds. *Journal of Cellular Physiology* 2018, *vol. 233*, 6509-6522.

76. Ardeshirylajimi, A.; Mossahebi-Mohammadi, M.; Vakilian, S.; Langroudi, L.; Seyedjafari, E.; Atashi, A.; Soleimani, M. Comparison of osteogenic differentiation potential of human adult stem cells loaded on bioceramic-coated electrospun poly (L-lactide) nanofibres. *Cell Proliferation* 2015, *vol. 48*, 47-58.

77. Hasan, A.; Memic, A.; Annabi, N.; Hossain, M.; Paul, A.; Dokmeci, M.; Dehghani, F.; Khademhosseini, A. Electrospun scaffolds for tissue engineering of vascular grafts. *Acta Biomaterialia* 2014, *vol. 10*, 11-25.

78. Abdal-hay, A.; Bartnikowski, M.; Hamlet, S.; Ivanovski, S. Electrospun biphasic tubular scaffold with enhanced mechanical properties for vascular tissue engineering. *Materials Science and Engineering: C* 2018, *vol. 82*, 10-18.

79. Zhu, Y.; Cao, Y.; Pan, J.; Liu, Y. Macro-alignment of electrospun fibers for vascular tissue engineering. *Journal of Biomedical Materials Research Part B: Applied Biomaterials* 2009, *92B*, 1-9.

80. Vaz, C.; van Tuijl, S.; Bouten, C.; Baaijens, F. Design of scaffolds for blood vessel tissue engineering using a multi-layering electrospinning technique. *Acta Biomaterialia* 2005, *vol. 1*, 575-582.

81. Tan, Z.; Gao, X.; Liu, T.; Yang, Y.; Zhong, J.; Tong, C.; Tan, Y. Electrospun vein grafts with high cell infiltration for vascular tissue engineering. *Materials Science and Engineering: C* 2017, *vol. 81*, 407-415.

82. Gaudin, R.; Knipfer, C.; Henningsen, A.; Smeets, R.; Heiland, M.; Hadlock, T. Approaches to Peripheral Nerve Repair: Generations of Biomaterial Conduits Yielding to Replacing Autologous Nerve Grafts in Craniomaxillofacial Surgery. *BioMed Research International* 2016, *vol. 2016*, 1-18.

83. Bozkurt, A.; Lassner, F.; O'Dey, D.; Deumens, R.; Böcker, A.; Schwendt, T.; Janzen, C.; Suschek, C.; Tolba, R.; Kobayashi, E. et al. The role of microstructured and interconnected pore channels in a collagen-based nerve guide on axonal regeneration in peripheral nerves. *Biomaterials* 2012, *vol. 33*, 1363-1375.

84. Lohmeyer, J.; Siemers, F.; Machens, H.; Mailänder, P. The Clinical Use of Artificial Nerve Conduits for Digital Nerve Repair: A Prospective Cohort Study and Literature Review. *Journal of Reconstructive Microsurgery* 2009, *vol. 25*, 055-061.

85. Beachley, V.; Wen, X. Polymer nanofibrous structures: Fabrication, biofunctionalization, and cell interactions. *Progress in Polymer Science* 2010, *vol. 35*, 868-892.

86. Chew, S.; Mi, R.; Hoke, A.; Leong, K. Aligned Protein-Polymer Composite Fibers Enhance Nerve Regeneration: A Potential Tissue-Engineering Platform. *Advanced Functional Materials* 2007, *vol. 17*, 1288-1296.

87. Neal, R.; Tholpady, S.; Foley, P.; Swami, N.; Ogle, R.; Botchwey, E. Alignment and composition of laminin-polycaprolactone nanofiber blends enhance peripheral nerve regeneration. *Journal of Biomedical Materials Research Part A* 2012, *100A*, 406-423.

88. Costa, H.; Ferreira Bento, R.; Salomone, R.; Azzi-Nogueira, D.; Zanatta, D.; Paulino Costa, M.; da Silva, C.; Strauss, B.; Haddad, L. Mesenchymal bone marrow stem cells within polyglycolic acid tube observed in vivo after six weeks enhance facial nerve regeneration. *Brain Research* 2013, *vol. 1510*, 10-21.

89. Thakkar, S.; Misra, M. Electrospun polymeric nanofibers: New horizons in drug delivery. *European Journal of Pharmaceutical Sciences* 2017, *vol. 107*, 148-167.

90. Jiang, H.; Hu, Y.; Zhao, P.; Li, Y.; Zhu, K. Modulation of protein release from biodegradable core–shell structured fibers prepared by coaxial electrospinning. *Journal of Biomedical Materials Research Part B: Applied Biomaterials* 2006, *79B*, 50-57.

91. Yang, Y.; Li, X.; Qi, M.; Zhou, S.; Weng, J. Release pattern and structural integrity of lysozyme encapsulated in core–sheath structured poly(dl-lactide) ultrafine fibers prepared by emulsion electrospinning. *European Journal of Pharmaceutics and Biopharmaceutics* 2008, *vol. 69*, 106-116.

92. Zeng, J.; Aigner, A.; Czubayko, F.; Kissel, T.; Wendorff, J.; Greiner, A. Poly(vinyl alcohol) Nanofibers by Electrospinning as a Protein Delivery System and the Retardation of Enzyme Release by Additional Polymer Coatings. *Biomacromolecules* 2005, *vol. 6*, 1484-1488.

93. Sulejczak, D.; Andrychowski, J.; Kowalczyk, T.; Nakielski, P.; Frontczak-Baniewicz, M.; Kowalewski, T. Electrospun nanofiber mat as a protector against the consequences of brain injury. *Folia Neuropathologica* 2014, *vol. 1*, 56-69.

94. Jang, C.; Cho, Y.; Jang, Y.; Kim, M.; Kim, G. Antibacterial effect of electrospun polycaprolactone/polyethylene oxide/vancomycin nanofiber mat for prevention of periprosthetic infection and biofilm formation. *International Journal of Pediatric Otorhinolaryngology* 2015, *vol. 79*, 1299-1305.

95. Vellayappan, M.; Venugopal, J.; Ramakrishna, S.; Ray, S.; Ismail, A.; Mandal, M.; Manikandan, A.; Seal, S.; Jaganathan, S. Electrospinning applications from diagnosis to treatment of diabetes. *RSC Advances* 2016, *vol. 6*, 83638-83655.

96. Xu, L.; Sheybani, N.; Ren, S.; Bowlin, G.; Yeudall, W.; Yang, H. Semi-Interpenetrating Network (sIPN) Co-Electrospun Gelatin/Insulin Fiber Formulation for Transbuccal Insulin Delivery. *Pharmaceutical Research* 2015, *vol. 32*, 275-285.

97. Wang, X.; Dong, Z.; Cheng, H.; Wan, S.; Chen, W.; Zou, M.; Huo, J.; Deng, H.; Zhang, X. A multifunctional metal–organic framework based tumor targeting drug delivery system for cancer therapy. *Nanoscale* 2015, *vol. 7*, 16061-16070.

98. Zong, S.; Wang, X.; Yang, Y.; Wu, W.; Li, H.; Ma, Y.; Lin, W.; Sun, T.; Huang, Y.; Xie, Z. et al. The use of cisplatin-loaded mucoadhesive nanofibers for local chemotherapy of cervical cancers in mice. *European Journal of Pharmaceutics and Biopharmaceutics* 2015, *vol. 93*, 127-135.

99. EN ISO 10993-5. *Biological evaluation of medical devices: Tests for in vitro cytotoxicity.* London: BSI Group, 2009, 34 p.

100. van Meerloo, J.; Kaspers, G.; Cloos, J. Cell Sensitivity Assays: The MTT Assay. *Cancer Cell Culture* 2011, *731*, 237-245.

101. Colorimetric Cell Viability Kit I (WST-8). *PromoCell|Human Centered Science* 2016.

102. Castkova, K.; Hadraba, H.; Matousek, A.; Roupcova, P.; Chlup, Z.; Novotna, L.; Cihlar, J. Synthesis of Ca,Y-zirconia/hydroxyapatite nanoparticles and composites. *Journal of the European Ceramic Society* 2016, *vol. 36*, 2903-2912.

103. Wang, X.; Zhao, H.; Turng, L.; Li, Q. Crystalline Morphology of Electrospun Poly(ε-caprolactone) (PCL) Nanofibers. *Industrial & Engineering Chemistry Research* 2013, *vol. 52*, 4939-4949.

104. Bergström, L. Shear thinning and shear thickening of concentrated ceramic suspensions. *Colloids and Surfaces A: Physicochemical and Engineering Aspects* 1998, *vol. 133*, 151-155.

105. Mubyana, K.; Koppes, R.; Lee, K.; Cooper, J.; Corr, D. The influence of specimen thickness and alignment on the material and failure properties of electrospun polycaprolactone nanofiber mats. *Journal of Biomedical Materials Research Part A* 2016, *vol. 104*, 2794-2800.

106. Ebert, D.; Bhushan, B. Durable Lotus-effect surfaces with hierarchical structure using micro- and nanosized hydrophobic silica particles. *Journal of Colloid and Interface Science* 2012, *vol. 368*, 584-591.

107. Aronov, D.; Rosen, R.; Ron, E.; Rosenman, G. Tunable hydroxyapatite wettability: Effect on adhesion of biological molecules. *Process Biochemistry* 2006, *vol. 41*, 2367-2372.

108. Alemán-Domínguez, M.; Ortega, Z.; Benítez, A.; Vilariño-Feltrer, G.; Gómez-Tejedor, J.; Vallés-Lluch, A. Tunability of polycaprolactone hydrophilicity by carboxymethyl cellulose loading. *Journal of Applied Polymer Science* 2018, *vol. 135*.

109. Shahmoradi, S.; Yazdian, F.; Tabandeh, F.; Soheili, Z.; Hatamian Zarami, A.; Navaei-Nigjeh, M. Controlled surface morphology and hydrophilicity of polycaprolactone toward human retinal pigment epithelium cells. *Materials Science and Engineering: C* 2017, *vol. 73*, 300-309.

110. Lee, J.; Kim, Y. Hydroxyapatite nanofibers fabricated through electrospinning and sol–gel process. *Ceramics International* 2014, *vol. 40*, 3361-3369.

111. Bhatia, S.; Yetter, A. Correlation of visual in vitro cytotoxicity ratings of biomaterials with quantitative in vitro cell viability measurements. *Cell Biology and Toxicology* 2008, *vol. 24*, 315-319.

112. Cao, H.; Mchugh, K.; Chew, S.; Anderson, J. The topographical effect of electrospun nanofibrous scaffolds on the in vivo and in vitro foreign body reaction. *Journal of Biomedical Materials Research Part A* 2009, *93*, 1151-1159.

8 List of abbreviations

AA	Acetic acid
FA	Formic acid
EDX	Energy dispersive X-ray analysis
HA	Hydroxyapatite
PCL	Polycaprolactone
PVA	Polyvinyl alcohol
SBF	Sinulated body fluid
SEM	Scanning electron microscopy
wt.%	Weight %
XPS	X-ray photoelectron spectroscopy
XRD	X-ray diffraction analysis

9 Authors publications and other outputs

Publications

Kaspar, P.; Sobola, D.; Částková, K.; Dallaev, R.; Šťastná, E.; Sedlák, P.; Knápek, A.; Trčka, T.; Holcman, V. Case Study of Polyvinylidene Fluoride Doping by Carbon Nanotubes. *Materials* **2021**, *14*.

Stastna, E.; Castkova, K.; Rahel, J. Influence of Hydroxyapatite Nanoparticles and Surface Plasma Treatment on Bioactivity of Polycaprolactone Nanofibers. *Polymers* **2020**, *12*.

Castkova, K.; Kastyl, J.; Sobola, D.; Petrus, J.; Stastna, E.; Riha, D.; Tofel, P. Structure–Properties Relationship of Electrospun PVDF Fibers. *Nanomaterials* **2020**, *10*.

Conferences

Workshop for young ceramists, Bologna, Italy, 2018; oral presentation – *Influence of ceramic particles on bioactivity of the ceramic-polymer biocomposites*

NANOCON, Brno, Czech Republic, 2018; poster presentation – *Electrospinning and biocompatibility of polymer-ceramic nanofibers for tissue engineering*

CEITEC PhD Retreat II, Telč, Czech Republic, 2017; poster presentation - *Electrospinning and thermal treatment of titania nanofibers*

Conference for Young Scientists in Ceramics, Novi Sad, Serbia; oral presentation – *Preparation of biocompatible and bioresorbable fibrous structures*

NANOCON, Brno, Czech Republic, 2016; poster presentation: *Electrospinning and Thermal Treatment of Yttria Doped Zirconia Fibers*

Research internships

Friedrich-Alexander Universität Erlangen-Nürenberg, Germany, October – November 2019. The internship focused mainly on mechanical and biological (WST-8) tests of the polycaprolactone and polycaprolactone/hydroxyapatite nanofibres.